# Spatio-spectral Analysis on the Unit Sphere

**Zubair Khalid**

August 2013

A thesis submitted for the degree of Doctor of Philosophy
of The Australian National University


Australian National University

Research School of Engineering
College of Engineering and Computer Science
The Australian National University

# Declaration

The contents of this thesis are the results of original research and have not been submitted for a higher degree to any other university or institution.

Much of the work in this thesis has been published for publication as journal papers or conference proceedings. These papers are:

Journal articles

J1. **Z. Khalid**, S. Durrani, P. Sadeghi, and R. A. Kennedy, "Spatio-spectral Analysis on the Sphere using Spatially Localized Spherical Harmonics Transform," *IEEE Trans. Signal Process.*, vol. 60, no. 3, pp. 1487–1492, Mar. 2012.

J2. P. Sadeghi, R. A. Kennedy, and **Z. Khalid**, "Commutative Anisotropic Convolution on the 2-Sphere," *IEEE Trans. Signal Process.*, vol. 60, no. 12, pp. 6697–6703, Dec. 2012.

J3. **Z. Khalid**, P. Sadeghi, R. A. Kennedy, and S. Durrani, "Spatially Varying Spectral Filtering of Signals on the Unit Sphere," *IEEE Trans. Signal Process.*, vol. 61, no. 3, pp. 530–544, Feb. 2013.

J4. **Z. Khalid**, R. A. Kennedy, S. Durrani, P. Sadeghi, Y. Wiaux, and J. D. McEwen, "Fast Directional Spatially Localized Spherical Harmonic Transform," *IEEE Trans. Signal Process.*, vol. 61, no. 9, pp. 2192-2203, May 2013.

Conference papers

C1. **Z. Khalid**, S. Durrani, R. A. Kennedy, and P. Sadeghi, "Concentration Uncertainty Principles for Signals on the Unit Sphere," in *Proc. IEEE Int. Conf. Acoust., Speech, Signal Process., ICASSP'2012*, Kyoto, Japan, Mar. 2012.

C2. **Z. Khalid**, R. A. Kennedy, and P. Sadeghi, "Efficient Computation of Commutative Anisotropic Convolution on the 2-Sphere," in *5th International Conference on Signal Processing and Communication Systems, ICSPCS'2011*, Gold Coast, Australia, Dec. 2012.

The following publications are also the results from my Ph.D. study but not included in this thesis:

Journal articles

J5. **Z. Khalid** and S. Durrani, "Distance Distributions in Regular Polygons," *IEEE Veh. Tech.*, vol. 62, no. 5, pp. 2363-2368, June 2013.

J6. S. Durrani, **Z. Khalid**, and J. Guo, "A Tractable Framework for Exact Probability of Node Isolation and Minimum Node Degree Distribution in Finite Multi-hop Network," *IEEE Veh. Tech.*, Jun. 2013. (Submitted)

Conference papers

C3. **Z. Khalid**, S. Durrani, R. A. Kennedy, and P. Sadeghi, "Revisiting Slepian Concentration Problem on the Sphere for Azimuthally Non-symmetric Regions," in *5th International Conference on Signal Processing and Communication Systems, ICSPCS'2011*, Honolulu, HI, Dec. 2011.

C4. **Z. Khalid**, S. Durrani, P. Sadeghi, and R. A. Kennedy, "On the Construction of Low-pass Filters on the Unit Sphere," in *Proc. IEEE Int. Conf. Acoust., Speech, Signal Process., ICASSP'2011*, Prague, Czech Republic, May. 2011.

C5. W. Huang, **Z. Khalid**, and R. A. Kennedy, "Efficient Computation of Spherical Harmonics Transform using CUDA," in *5th International Conference on Signal Processing and Communication Systems, ICSPCS'2011*, Honolulu, HI, Dec. 2011.

C6. **Z. Khalid**, R. A. Kennedy, S. Durrani, and P. Sadeghi, "Conjugate Gradient Algorithm for Extrapolation of Sampled Bandlimited Signals on the 2-Sphere," in *Proc. IEEE Int. Conf. Acoust., Speech, Signal Process., ICASSP'2012*, Kyoto, Japan, Mar. 2012.

C7. **Z. Khalid**, S. Durrani, R. A. Kennedy, and P. Sadeghi, "Ambiguity Function and Wigner Distribution on the Sphere," in *Proc. IEEE Int. Conf. Acoust., Speech, Signal Process., ICASSP'2012*, Kyoto, Japan, Mar. 2012.

C8. **Z. Khalid** and S. Durrani,"Connectivity of Three Dimensional Wireless Sensor Networks Using Geometrical Probability," in *Proc. AusCTW*, Adelaide, Feb. 2013.

The research work presented in this thesis has been performed jointly with Dr. Salman Durrani (The Australian National University, Australia), Dr. Parastoo Sadeghi (The Australian National University, Australia), Prof. Rodney A. Kennedy (The Australian National University, Australia), Dr. Yves Wiaux (Ecole Polytechnique Fédérale de Lausanne (EPFL), Switzerland) and Dr. Jason D. McEwen (University College London, UK). The substantial majority of this work was my own.

Zubair Khalid
Research School of Engineering,
The Australian National University,
Canberra,
ACT 0200,
Australia.

اپنے من میں ڈوب کر پا جا سراغِ زندگی

*Delve into your soul to find the secrets of life;*

**Sir Dr. Allama Muhammad Iqbal** (Poet and Philospher), 1877-1938 A.D.

# Acknowledgements

The work presented in this thesis would not have been possible without the support of a number of individuals and organizations and they are gratefully acknowledged below:

- First and the foremost, I would like to thank Almighty Allah for bestowing His countless blessings upon me and giving me the strength and directions to carry out and complete this work.

- I would like to express my sincere and very special thanks to my supervisors and friends Drs. Salman Durrani, Parastoo Sadeghi and Prof. Rodney A. Kennedy for their guidance, support and encouragement throughout my PhD studies. They have granted me freedom and flexibility in my research, which enabled me to explore new ideas. They are always willing to have in-depth discussion whenever I approach them for help. Their continuous appreciation for the research ideas fueled my interest in the work and helped me to develop focussed research work. I cannot express the eternal gratitude I feel towards them. I also thank them for carefully going through my publication drafts, and helping me in learning the various skills of academic research. Apart from my research studies, they have also given me great support in obtaining teaching and supervision experiences. They have been also extremely helpful in all matters other than academics.

- Special thanks to Dr. Jason McEwen for supervising me in one of the projects covered in this thesis. I would also like to thank him for his hospitality during my two months visit to UCL in the winter of 2012-2013. It was a valuable experience in my PhD, where I learnt about the applications of signal processing in astrophysics and cosmology. Jason has been very helpful during my visit to UCL and helped me to strengthen my research skills. Most

of the discussions with Jason have been invaluable in finding new research direction.

- I also wish to thank Dr. Yves Wiaux at Ecole Polytechnique Fédérale de Lausanne (EPFL), Switzerland for providing remote supervision and guidance.

- I would also like to thank my undergraduate teachers and Profs. Asim Loan, Zubair A. Khan and Haroon A. Babri, back in Pakistan, for encouraging me to commence higher studies.

- It is my great pleasure to study in the applied signal processing (ASP) group at the Research School of Engineering. I would like to thank everyone for making ASP group a friendly and relaxing research environment. Special thanks to my friends and colleagues Ali Nasir, Usman Qayyum, Asim Khawaja, Yibeltal Alem and Daniel Chae for providing friendly environment and stimulating company.

- I would also like to acknowledge the assistance of administrative staff at the college of engineering and computer. I am especially thankful to our school administrators Ms. Lesley Goldburg and Ms. Elspeth Davies.

- Thanks must go to the Department of Employment Educations and Work Relations of Australian Government for providing me with the PhD scholarship and stipend. I would like to thank The Australian National University for providing 2010 ANU Vice Chancellors Travel Grant for supporting my visit to attend ICASSP in Prague, Czech Republic and providing me with 2012 Dean's Travel Grant to fund my visit to UCL. I would also like to acknowledge the support provided by the Australian Research Council's Discovery Projects funding scheme (Project No. DP1094350).

- I thank my parents for providing me with lots of love and prayers. My every little success would not have been possible without their support and prayers. The integral decision of my father to leave the village for the sake of our education has been an inspiration for me throughout my life. I also convey my thanks to my brothers and sister for taking care of everything back home during my absence.

- I would like to give my affectionate thanks to my wife, Saba and my daughter, Maryam for their constant support, understanding, and prayers. I thank my wife for accepting the hardships of student life. I appreciate her for providing me with great companionship.

# Abstract

This thesis is focussed on the development of new signal processing techniques to analyse signals defined on the sphere. Analysis and processing of signals defined on the sphere find applications in various fields of science and engineering, such as cosmology, geophysics and medical imaging. The objective to develop new signal processing methods is served by formulating, extending and tailoring existing Euclidean domain signal processing theories in ways that they become suitable for analysis of signals defined on the sphere.

The first part of this thesis develops a new type of convolution between two signals on the sphere. This is the first type of convolution on the sphere which is commutative. Two other advantages, in comparison with existing definitions in the literature, are that the new convolution admits anisotropic filters and signals and the domain of the output remains on the sphere. The spectral analysis of the convolution is provided and a fast algorithm for efficient computation of convolution output is developed.

The second part of the thesis is focused on the development of signal processing techniques to analyse signals on the sphere in joint spatio-spectral (spatial-spectral) domain. A transform analogous to short-time Fourier transform (STFT) in time-frequency analysis is formulated for signals defined on the sphere, in order to devise a spatio-spectral representation of a signal. The proposed transform is referred as the spatially localized spherical harmonic transform (SLSHT) and is defined as windowed spherical harmonic transform, resulting in the SLSHT distribution. The properties of the SLSHT distribution and its analysis in the spherical harmonic domain are also provided. Furthermore, examples are provided to demonstrate the capability of SLSHT to reveal spatially localized spectral contents in a signal that were not obtainable from traditional spherical harmonics analysis. With the consideration that data-sets on the sphere can be of considerable size and the SLSHT is intrinsically computationally demanding depending on the band-limits

of the signal and window, a fast algorithm for the efficient computation of the transform is developed. The floating point precision numerical accuracy of the fast algorithm is demonstrated and a full numerical complexity analysis is presented.

A general framework for spatially-varying spectral filtering of signals defined on the unit sphere is also developed, as an analogy to joint time-frequency filtering. For spatio-spectral filtering, the spherical signals are first mapped from the spatial domain into a joint spatio-spectral domain using SLSHT, where a spatio-spectral signal transformation or modification is introduced. Next, a suitable scheme to transform the modified signal from the spatio-spectral domain back to an admissible signal in the spatial domain using the least squares approach is proposed. It is shown that the overall action of the SLSHT and spatio-spectral signal modification can be described through a single transformation matrix, which is useful in practice. Finally, two specific and useful instances of spatially-varying spectral filtering are presented, defined through multiplicative and convolutive modification of the SLSHT distribution. The proposed framework enables filtering or modification in the spatio-spectral domain which cannot be carried out in either the spatial or spectral domain.

# List of Acronyms

| | |
|---|---|
| CMB | cosmic microwave background |
| STFT | short-time Fourier transform |
| SLSHT | spatially localized spherical harmonic transform |
| FFT | fast Fourier transform |
| MMD | multiplicative modified distribution |
| CMD | convolutive modified distribution |
| WMAP | Wilkinson microwave anisotropy probe |
| 3D | 3 dimensional |
| DC | Direct current (average value) |

# Notations

| | |
|---|---|
| $x$ | scalar variable |
| $\boldsymbol{x}$ | vector variable |
| $\hat{\boldsymbol{x}}$ | unit vector |
| $\mathbf{X}$ | matrix variable |
| $X_{x,y}$ | element in row $x$ and column $y$ of $\mathbf{X}$ |
| $\langle f, g \rangle$ | inner product of two variables $f$ and $g$ |
| $\|(\cdot)\|_p$ | $L_p$ norm |
| $\|(\cdot)\|$ | $L_2$ norm |
| $\|(\cdot)\|_{HS}$ | Hilbert-Schmidt norm |
| $\|(\cdot)\|$ | absolute value of parameter $(\cdot)$ |
| $\overline{(\cdot)}$ | conjugate operation |
| $(\cdot)'$ | transpose operation on vector |
| $(\cdot)^T$ | transpose operation on vector |
| $(\cdot)^H$ | Hermitian (conjugate transpose) operation |
| $\lfloor(\cdot)\rfloor$ | floor function |
| $\delta_{p,q}$ | Kronecker delta |
| $\delta()$ | Dirac delta |
| $\mathfrak{S}(L)$ | Equiangular tessellation on the sphere |
| $\mathfrak{C}(L)$ | Equiangular tessellation on SO(3) |
| $(\ell, m) \leftrightarrow n$ | mapping of two variables $(\ell, m)$ to single variable $n$ using rule c.f. (2.17) |
| $(f)_\ell^m$ | spherical harmonic transform of degree $\ell$ and order $m$ |
| $\frac{d}{dx}$ | derivative with respect to $x$ |
| $\star$ | Anisotropic convolution operand |
| $\circledcirc$ | Isotropic convolution operand |
| max() | maximum of the parameters |
| min() | minimum of the parameters |
| diag($\boldsymbol{x}$) | a diagonal matrix with diagonal elements given by vector $\boldsymbol{x}$ |
| $\lceil(\cdot)\rceil$ | Integer ceiling function |

# Contents

# List of Figures

# Chapter 1

# Introduction

## 1.1 Motivation and Background

The main focus of this thesis is to develop novel signal processing techniques for the analysis of data and signals defined on the unit sphere (or 2-sphere[1]), denoted by $\mathbb{S}^2$. The analysis and processing of signals defined on the sphere has been an active area of research in the past two decades. Signals that are inherently defined on the sphere appear in many applications found in various fields of science and engineering. These applications include surface analysis in medical imaging [2, 3], geodesy and planetary studies [1,4,5], computer graphics and computer vision [6–9], planetary science [5], electromagnetic inverse problems [10], study and analysis of cosmic microwave background (CMB) in cosmology [11–17], 3D beamforming [18] and wireless channel modeling in communication systems [19].

The essence of signal processing embeds the notions of signals and linear systems; filtering, smoothing; prediction; detection and estimation in the presence of noise; feature extraction. Signal processing techniques and theories have been thoroughly investigated and explored, primarily based on the assumption that signals are defined on the real line, which is conventionally identified with time. Further, conventional multidimensional signal processing, where signals are defined on a multidimensional Euclidean domain, is a natural generalization that has also been extensively researched.

For the processing of signals on the sphere, the mapping of the data on the sphere to a two dimensional plane, enables the use of signal processing methods

[1]In the sequel, "unit sphere", "2-sphere" or simply "sphere" refer to the same thing.

developed for Euclidean domain, but this procedure introduces errors. This is due to the fact that the modeling of the signal defined on the sphere in the Euclidean domain is not suitable. For example, the curvature needs to be taken into account in planetary studies, especially for small heavenly bodies such as the Earth and the Mars [20]. Therefore it is often required that signal processing techniques developed for the Euclidean domain be extended and reformulated in non-trivial ways so that they are suitable and well-defined for the spherical domain.

Extension of signal processing techniques developed for Euclidean signals is a natural and sensible approach to analyze the signals inherently defined on the sphere. In this context, many signal processing techniques have been tailored and extended from the Euclidean domain to the spherical domain [4, 15, 16, 21–30]. These include convolution [31–33], filtering [25, 30, 34], feature extraction [5, 24] and spectrum estimation [1,20], finite-impulse-response (FIR) filtering [26], Slepian concentration problem [35–38] on the sphere [1,27,39], to name a few. Among these developments, the most fundamental notion is the analog of Fourier transform, which corresponds to spherical harmonic transform [10,31,40,41] for signals on the sphere. By definition of the spherical harmonic transform, any signal on the sphere can be expanded in terms of spherical harmonic functions (or spherical harmonics for short), and therefore, the spherical harmonic coefficients constitute the spectral domain representation of any signal defined on the sphere. We also note the work in the mathematical literature (e.g., [42, 43]) providing algebraic view of the signal processing methods, based on which a group theoretic formulation of continuous spherical wavelets is proposed in [21, 44].

This thesis is predominantly focussed on the formulation and the development of signal processing techniques to analyze signals defined on the sphere. In the remainder of this chapter, we first review the previous work on development of signal processing techniques on the sphere. Then we discuss the research problems, which are to be investigated in this thesis. Finally, we provide the summary of our contributions and outline of thesis.

### 1.1.1 Convolution on the Sphere

One important signal processing tool is convolution between two signals defined on the unit sphere, which is fundamental for filtering applications. While there are various formulations of convolution on the sphere [28, 30, 31, 45–47], these do not

serve as an analog of the Euclidean-domain convolution as they lack some desired or expected properties as we explain below.

One well-known and widely-used definition for convolution on the unit sphere appears in [31], which has been generalized for the $n$-sphere and applied for estimation of probability density functions in [48]. The advantage of this convolution is that it results in a simple multiplication of the spectral (spherical harmonic) coefficients of the signal and the filter in the Fourier domain. However, the convolution involves full rotation of the filter by all independent Euler angles which includes an extra averaging over the first rotation about the $z-$axis. This is presumably done to ensure that the output domain of convolution is $\mathbb{S}^2$, but it results in smoothing the filter by projecting it into the subspace of azimuthally symmetric signals. Consequently, this convolution becomes identical to a simpler isotropic convolution [46, 47] as shown in [32]. In contrast to conventional convolution in the Euclidean domain, due to excessive smoothing, convolution in [31,46,47] is not commutative and discards information.

Another definition of convolution for signals on the unit sphere can be found in [30,45] and has been referred to as directional correlation in [28], since it preserves the directional features of both the signal and filter. The convolution involves full rotation of the filter by all independent Euler angles and a double integration over the points on the unit sphere. While this results in a desired directional or anisotropic convolution, the output remains a function of the three rotations applied to the filter and consequently, the output domain is not $\mathbb{S}^2$. Moreover, the convolution is not commutative. From the discussion above, it becomes clear that existing definitions of the convolution do not serve as direct analog of the convolution definition in Euclidean domain.

### 1.1.2 Spatially Localized Spherical Harmonic Transform and Spatio-spectral Analysis on the Sphere

For analysis of signals on the sphere, many signal processing techniques have been developed and extended from the Euclidean domain to the spherical domain [4, 15, 16, 21–25, 27–30]. At their core, most of these techniques process the signal directly either in the spatial spherical domain or in the spectral domain, formed by spherical harmonic coefficients. Since the spherical harmonic functions are not spatially concentrated functions on the sphere, spherical harmonic coef-

ficients provide information about *global* contribution of spherical harmonics in the signal and do not convey any insight about the localized contribution of the spherical harmonics. Therefore, in addition to the information given by spherical harmonic transform, the signal analysis techniques are essentially required to reveal the localization of features in the signal.

In order to obtain and analyze the localized spectral contents of signals defined on the sphere, wavelets have been extensively investigated and explored due to their ability to resolve localized signal content in both space and scale. Wavelet techniques for signals on the sphere were originally established in a group theoretic framework [21, 44, 49–51]. Inspired from this original work and following the formulation of wavelets on Euclidean domain, more practical and different notions of wavelets have been developed in recent works [15, 16, 22–24, 28–30, 49], These developed wavelet techniques have been utilized in various applications (e.g., in astrophysics [13, 14, 52–55] and geophysics [5, 56, 57]). Some of the wavelet techniques on the sphere also incorporate directional phenomena in the spatial-scale decomposition of a signal (e.g., [5, 28–30]).

An alternative to the wavelet (i.e., spatial-scale) approach is a "spatio-spectral" (spatial-spectral) approach, where the goal is to obtain a joint spatio-spectral representation of signals defined on the sphere. Analogous to windowed Fourier transform in the Euclidean domain, the localized spectral analysis, composed of spatial windowing followed by spherical harmonic transform, was first devised in [4], and was used to interpret global estimates of the gravity and topography of Venus in the context of geodynamical models. It is also shown that the localized transform is invertible by spatial averaging of the transform. The effectiveness of the transform to reveal the localized spectral contents of a signal, however, depends on the chosen window function. The authors in [4] use azimuthally symmetric spectrally truncated window function which is concentrated in the spectral domain, but exhibits sidelobes in the spatial domain. Since the simultaneous localization of a window in spatial and spectral domains determines the quality of the global estimates of topography and gravity, the eigenfunctions obtained from Slepian concentration problem on the sphere [27] are used as window functions in [1, 20, 58], where again azimuthally symmetric window functions have been used for windowing in the spatial domain. In these investigations, the localized spectral analysis has been carried

out with an objective to estimate the spectrum[2] of the signal. However, it can also be used to obtain the spatio-spectral representation of the signal that reveals the contribution of spectral contents in any spatially localized region. The domain of such representation is jointly spatial and spectral, or spatio-spectral for short.

The localized spectral analysis method, composed of windowing in the spatial domain followed by the spherical harmonic transform, is analogous in nature and spirit to the short-time Fourier transform (STFT) in time-frequency analysis. In time-frequency analysis, STFT has been under exploration for the last half of the century (e.g. [59–68]). The absence of cross terms in the STFT representation of a signal, which appear in quadratic distributions like Wigner, makes the STFT a more attractive choice to study signals in time-frequency domain than using quadratic type distributions [65, 69]. In addition, the magnitude-wise shift invariance property of the STFT in both time and frequency domains simplifies the interpretation of the time-frequency representation of the signal [69]. Since STFT reveals the time dependence and evolution of the signal spectrum, it has been used in many applications. These include obtaining of localized frequency contents and spectral estimation of non-stationary signals [61], analysis of speech signals [70], radar applications [71] and time-varying filtering [72–74].

### 1.1.3 Filtering in the Spatio-spectral Domain

Representation of a signal in the spatio-spectral domain depicts how its spectral contents are changing with space, that is, it provides information about spatially varying spectral components in a signal. Moreover, the spatio-spectral representation gives an indication as to which spectral components of the signal are present at a given spatial position and their relative amplitude, thus it reveals the localized spectral contents. Consider an analogy in time-frequency domain: the time frequency representation of a signal is conceptually a musical score with frequency running along one axis and time along the other, and the time-frequency representation indicates the frequency content, the timing information, and the duration of various dominant signal components [75]. Such representations are useful for the analysis, modification, synthesis, and detection of a variety of non-stationary signals with time-varying spectral content [76].

[2]It must be noted here that the word spectrum refers to normalized energy of the signal per spherical harmonic degree [1, 4, 20], and must not be confused with the spectral domain representation of the signal.

Most of the existing signal processing techniques developed on the sphere either process the signal directly either in the spatial (spherical) domain or in the spectral domain. However, there are situations where analysis and modification of spherical signals jointly or simultaneously in spatial and spectral domains is required. This is particularly important when we wish to reveal and modify *spatially-varying* spectral contents of signals. For this purpose, the spherical harmonic transform is not adequate because it cannot directly enlighten the "localized" spatial contributions of a signal in the spectral domain. For example, consider the convolutive smoothing in the spatial domain [31,77], which is equivalent to the multiplication of the signal and filter spherical harmonic coefficients in spectral domain. Therefore, the same filter is used for smoothing the signal at all spatial positions and it is not possible to apply a spatially-varying operation in the spectral domain and vice versa. This motivates the need to look for suitable joint *spatio-spectral* signal transformations on the unit sphere.

The closest class of related work is the extension of Euclidean wavelets to spherical wavelets, which enables filtering at different scales [5, 15, 21, 22, 24, 29, 78]. The theoretical conditions on the invertibility of spherical wavelet transform are presented in [30] and the proposed framework is illustrated using wavelets that provide space-scale decomposition. However, to the best of our knowledge, there exists no framework that directly deals with signal transformations and modifications in joint spatio-spectral domain rather than in joint spatial and scale (wavelet) domains.

Interestingly the Euclidean counterpart, namely joint time-frequency signal analysis and filtering, has been well established for several decades [73, 74, 79–81]. In particular, the short-time Fourier transform (STFT) and its variations [64, 66, 67,73,74,80,81] have triggered research to generalize the concepts of filtering theory to joint time-frequency domain. Saleh and Subotic presented an interesting and novel approach of time-frequency filtering in [74], where they devised the modification of the STFT representation of signal as masking with the filter function in the time-frequency domain. A similar concept is also adopted in [72] for discrete-time signals and is generalized in [73] for different operations in time-frequency domain.

### 1.1.4 Directional Localized Spherical Harmonic Transform and Fast Algorithms for Spatio-spectral Analysis

The use of an azimuthally symmetric window function in obtaining the spatio-spectral representation of a signal provides mathematical simplifications, however, such an approach cannot discriminate localized directional features in the spatio-spectral domain. This motivates the use of *asymmetric* window functions in the spatio-spectral transformation of a signal using the spatially localized spherical harmonic transform. Analogous to the STFT representation in time-frequency analysis, the definition of the localized spherical harmonic transform in [4] can be employed to define the spatio-spectral representation of a signal using azimuthally asymmetric window functions for spatial localization. The use of an asymmetric window function enables the transform to reveal directional features in the spatio-spectral domain.

Furthermore we note that the development of fast algorithms for the computation of spatio-spectral representation of signal is of considerable importance. This is due to the fact that the data-sets on the sphere can be of considerable size (e.g., three million samples on the sphere for current data-sets [82] and fifty million samples for forthcoming data-sets [83]), for which the computation of the spatio-spectral representation of a signal becomes computationally challenging.

## 1.2 Overview and Contribution of Thesis

The focus of this thesis is to revisit existing signal processing theories on the sphere and develop new techniques which enable the analysis of signals in spatio-spectral domain. Moreover, the problem of developing fast algorithms for the proposed techniques is also addressed.

### 1.2.1 Questions to be Answered

Following the literature review presented in Section 1.1, we pose the following questions that are answered in this thesis:

Q1. How should the convolution be defined on the sphere such that it serves as counterpart of Euclidean convolution and satisfies the properties like commutativity and being anisotropic in nature? If such a convolution can be defined,

how can we evaluate the convolution output in computationally efficient manner?

Q2. How can we develop a tool, analogous to STFT in time-frequency analysis, for signals on the sphere to obtain such a representation of a signal in joint spatio-spectral domain, which can reveal the localized contribution of spectral contents in a signal?

Q3. How should we suitable window function for spatial localization in obtaining localized spherical harmonic transform?

Q4. For signals on the sphere, how can we formulate the concentration uncertainty principle that relates the signal concentration in spatial and spectral domains?

Q5. Given the spatio-spectral representation of a signal on the sphere, how can we perform filtering operations on the signal in spatio-spectral domain?

Q6. Once the spatio-spectral representation of a signal is modified as a result of processing or filtering in the spatio-spectral domain, how can we obtain a physically valid signal on the sphere that "best" corresponds to the modified spatio-spectral representation?

Q7. What are the potential candidates for spatio-spectral filtering operations and how can these joint-domain operations be formulated as linear transformations of the signal in spatial or spectral domain?

Q8. How can we obtain the information about the directional features of the signal in the spatio-spectral domain?

Q9. How can we efficiently compute the spatio-spectral representation of a signal?

### 1.2.2 Thesis Contributions and Organization

Fig. 1.1 depicts the flowchart of the thesis. The mathematical background is presented in Chapter 2. The first original contribution in this thesis (Chapter 3) is based on finding the counterpart of Euclidean convolution on the unit sphere. The second part of the thesis (Chapters 4-6) develops signal analysis in the spatio-spectral domain. The second part can be further categorized into development of

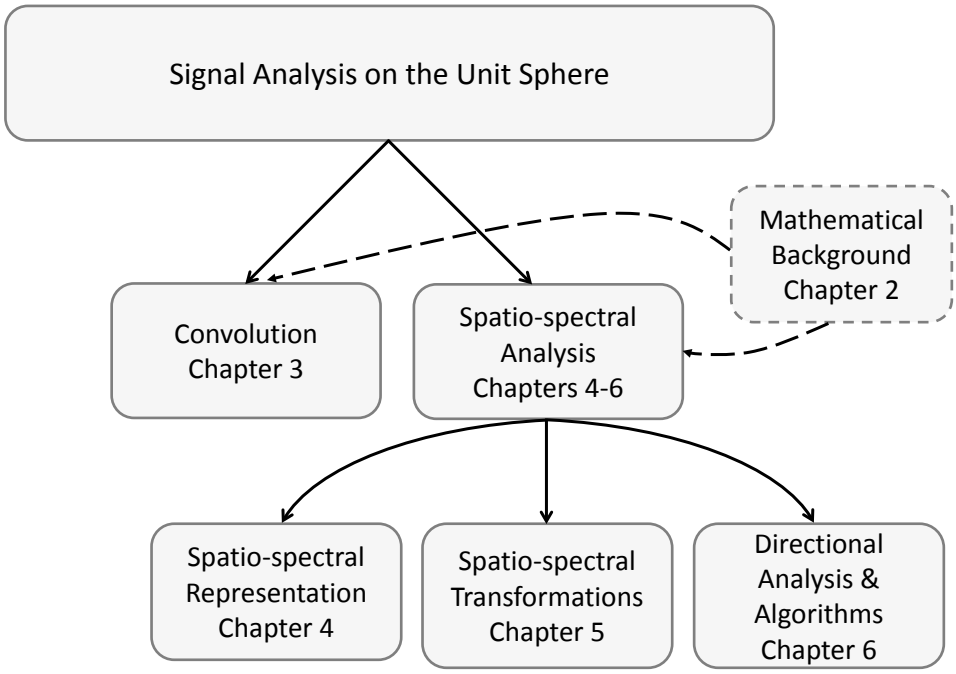


Figure 1.1: Thesis Flow Chart.

techniques to obtain spatio-spectral representation (Chapter 4), signal transformations in the spatio-spectral domain (Chapter 5), and incorporating directional phenomena in the spatio-spectral domain and development of fast algorithms (Chapter 6).

The summary of the contributions in each chapter is as follows:

**Chapter 3 - Commutative Anisotropic Convolution**

In Chapter 3, we consider the problem of defining convolution on the sphere that is analogous to the familiar Euclidean-domain $\mathbb{R}^2$ convolution in many ways. We first revisit the existing definitions of convolution on the sphere and then propose a new definition of convolution. Following the discussion in Section 1.1.1, we note that the existing definitions in the literature are not analogous in nature to the Euclidean domain convolution. The new contributions in this chapter are

1. We prove that, in order to obtain desired properties, not all independent Euler rotations should be involved in the definition of convolution. Instead, we introduce a controlled dependency between the two rotations of the filter about the $z-$axis. Therefore, there are only two degrees of freedom in the convolution. We highlight that the same philosophy has been rightfully applied to convolution in the 2-dimensional Euclidean space, $\mathbb{R}^2$, where not all

three proper "isometries" of the space (2 translations and one rotation) are involved in convolution.

2. We propose a new definition of convolution on the sphere with the following desired properties:
   - In contrast to the averaging over all possible rotations, it is formulated considering the rotations characterized by two parameters, which agrees with the fact that $\mathbb{S}^2$ is two dimensional;
   - It generates an output whose domain remains in $\mathbb{S}^2$;
   - It is anisotropic in nature, i.e., the directional features of both filter and signal contribute towards the output of convolution;
   - It is commutative, that is, changing the roles of filter and signal does not change the outcome of convolution.
3. We formulate and analyze the proposed convolution in the spectral (spherical harmonic) domain.
4. We also present a fast algorithm for the efficient computation of the proposed convolution. In the development of a fast algorithm, we employ the factoring of rotation approach followed by separation of variables technique.

The results in Chapter 3 have been presented in the following publications which are listed again for ease of reference:

J2. P. Sadeghi, R. A. Kennedy, and **Z. Khalid**, "Commutative Anisotropic Convolution on the 2-Sphere," *IEEE Trans. Signal Process.*, vol. 60, no. 12, pp. 6697–6703, Dec. 2012.

C2. **Z. Khalid**, R. A. Kennedy, and P. Sadeghi, "Efficient Computation of Commutative Anisotropic Convolution on the 2-Sphere," in *5th International Conference on Signal Processing and Communication Systems, ICSPCS'2011*, Gold Coast, Australia, Dec. 2012.

**Chapter 4 - Spatially Localized Spherical Harmonic Transform for Spatio-spectral Analysis**

In Chapter 4, we consider the development of a tool for signals on the sphere, analogous to STFT in time-frequency analysis, to obtain the signal representation

in spatio-spectral domain. We use the definition of a spatially localized transform in [1, 4] to obtain the spatio-spectral representation of a signal. Later, we analyze different window functions from the perspective of an uncertainty principle. The concentration uncertainty principles that relate the simultaneous concentration of a signal in the spatial and spectral domain are also derived in Chapter 3. The main contributions in Chapter 3 are summarized below:

1. We develop a tool called the *spatially localized spherical harmonic transform (SLSHT)* to represent a signal on the unit sphere in a joint spatio-spectral domain. We give a matrix representation of this transform operation, resulting in the spatio-spectral representation which we call the *SLSHT distribution*. The SLSHT is defined as spherical harmonic transform of the spatially localized signal, where spatial localization is achieved using a window function. Applying the SLSHT distribution to the example of the Mars topographic map shows the ability of the transform to reveal spatially-localized spectral contributions.

2. We introduce a transform operation inspired by the characteristic function in time-frequency analysis [65]. This transform operation results in a new spatio-spectral distribution, which we call complementary distribution. We investigate the properties of complementary distribution and derive the results that relate the signal, the window function and the complementary distribution.

3. We discuss the inherent trade-off between the spatial and spectral resolution of the window function from the perspective of the uncertainty principle.

4. Finally, we present a concentration uncertainty principles for signals on the sphere which relate the localization of the concentration of a signal in spatial and spectral domains.

The results in Chapter 4 have been presented in the following publications which are listed again for ease of reference:

J1. **Z. Khalid**, S. Durrani, P. Sadeghi, and R. A. Kennedy, "Spatio-spectral Analysis on the Sphere using Spatially Localized Spherical Harmonics Transform," *IEEE Trans. Signal Process.*, vol. 60, no. 3, pp. 1487–1492, Mar. 2012.

C1. **Z. Khalid**, S. Durrani, R. A. Kennedy, and P. Sadeghi, "Concentration Uncertainty Principles for Signals on the Unit Sphere," in *Proc. IEEE Int. Conf. Acoust., Speech, Signal Process., ICASSP'2012*, Kyoto, Japan, Mar. 2012.

**Chapter 5 - Spatially Localized Spherical Harmonic Transform for Spatio-spectral Analysis**

In Chapter 5, we present a framework for filtering and modification of signals in the joint spatio-spectral domain. The SLSHT distribution of a signal presented in Chapter 4 is processed in the joint spatio-spectral domain to yield the modified distribution and transformed back to the spatial domain using a suitably devised inverse operation. Due to the modification of the SLSHT distribution, there is a possibility that there exists no physical signal which corresponds to the modified distribution—an analogous problem is well known in time-frequency analysis [73, 74, 79–81]. Therefore, there is a need to find the signal that best approximates the modified distribution. The main contributions in this chapter are:

1. We present a general formulation of an integral operator that transforms the SLSHT distribution of a signal to a modified spatio-spectral distribution. We also formulate this spatio-spectral modification as a linear transformation of the signal in the spectral domain.

2. For the case when the modified spatio-spectral distribution is not a valid SLSHT distribution, we devise a suitable inverse spatio-spectral transform, which finds a signal whose distribution best approximates the modified distribution in the least squares sense.

3. Using the proposed paradigm of signal transformation, we investigate two types of filtering operations in spatio-spectral domain. First we consider filtering as multiplication of the filter function defined in spatio-spectral domain and the given SLSHT distribution. Next, we perform filtering as convolution of the filter function and the SLSHT distribution of a signal. In contrast to the conventional *spatially-invariant spectral filtering*, these types of filtering operations can be thought as *spatially-varying spectral filtering* of signals in the spatio-spectral domain.

The results in Chapter 5 have been presented in the following publication which is listed again for ease of reference:

J3. **Z. Khalid**, P. Sadeghi, R. A. Kennedy, and S. Durrani, "Spatially Varying Spectral Filtering of Signals on the Unit Sphere," *IEEE Trans. Signal Process.*, vol. 61, no. 3, pp. 530–544, Feb. 2013.

**Chapter 6 - Spatially Localized Spherical Harmonic Transform for Spatio-spectral Analysis**

In Chapter 4, the SLSHT distribution for spatio-spectral representation of a signal is defined as localized spherical harmonic transform, where we use an azimuthally symmetric window function. The transformation of the signal in the spatio-spectral domain using the SLSHT distribution is explored and investigated in Chapter 5. The use of an azimuthally symmetric window function provides mathematical simplifications in obtaining the spatio-spectral representation of the signal, however, the use of a symmetric function may not be able to discriminate localized directional features in the spatio-spectral domain. This motivates us to use asymmetric window functions for spatial localization in the spatio-spectral transformation of a signal. In order to serve this objective, we define the SLSHT and the SLSHT distributions using azimuthally asymmetric window functions for spatial localization. Since the use of an asymmetric window function enables the transform to reveal directional features in the spatio-spectral domain, we call the proposed transform the directional SLSHT and the spatio-spectral representation as directional SLSHT distribution. We also provide a harmonic analysis of the proposed transform and present an inversion relation to recover the signal from its directional SLSHT distribution. Furthermore, we develop fast algorithms for the evaluation of directional SLSHT distribution. The main contributions in this chapter are:

1. We present the directional SLSHT to transform a signal on the sphere onto its joint spatio-spectral domain as a directional SLSHT distribution. The directional SLSHT is composed of SO(3) spatial localization followed by the spherical harmonic transform.

2. We propose the use of an azimuthally asymmetric window function to obtain spatial localization, which enables the transform to resolve directional features in the spatio-spectral domain. We also present an inversion relation to synthesize the original signal from its directional SLSHT distribution using our formulation.

3. Since data-sets on the sphere arising in applications are of considerable size, we develop a fast algorithm for the efficient computation of the directional SLSHT distribution of a signal. The computational complexity of computing the directional SLSHT is reduced by providing an alternative harmonic formulation of the transform and then exploiting the factoring of rotation approach [84] and the fast Fourier transform. We also study the numerical accuracy and the speed of our fast algorithm.

4. Since the directional SLSHT distribution relies on a window function for spatial localization, we analyze the band-limited window function obtained from the Slepian concentration problem on the sphere, with nominal concentration in an elliptical region around the north pole. We also provide an illustration that highlights the capability of the directional SLSHT to reveal directional features in the spatio-spectral domain. This capacility is likely to be of use in many applications.

The results in Chapter 6 have been presented in the following publication which is listed again for ease of reference:

J4. **Z. Khalid**, R. A. Kennedy, S. Durrani, P. Sadeghi, Y. Wiaux, and J. D. McEwen, "Fast Directional Spatially Localized Spherical Harmonic Transform," *IEEE Trans. Signal Process.*, 2013. (Accepted)

Finally, Chapter 7 gives a summary of the thesis results and provides suggestions for future research work.

# Chapter 2

# Signals on the Sphere and Mathematical Background

In this chapter, we introduce important concepts related to signals defined on the unit sphere, in order to provide mathematical background and to clarify the adopted notation used in later chapters.

## 2.1 Hilbert Space $L^2(\mathbb{S}^2)$

### 2.1.1 Unit Sphere Domain

Let $\mathbb{S}^2$ denote the 2-sphere or unit sphere domain, which is defined as

$$\mathbb{S}^2 \triangleq \{\boldsymbol{x} \in \mathbb{R}^3 \colon \|\boldsymbol{x}\| = 1\} \tag{2.1}$$

where $\boldsymbol{x}$ denotes the vector in 3-dimensional Euclidean or Cartesian domain $\mathbb{R}^3$ and $\|\boldsymbol{x}\|$ denotes the Euclidean norm. The points on the $\mathbb{S}^2$ belong to $\mathbb{R}^3$ but the unit sphere is different from $\mathbb{R}^3$ in a way that it is bounded and has a constant non-zero curvature.

By definition, a vector representing a point on the sphere is a unit vector, and is parameterized in terms of spherical coordinates. We define two such unit-norm vectors, $\hat{\boldsymbol{x}}$ and $\hat{\boldsymbol{y}}$, represented in the spherical coordinates as $\hat{\boldsymbol{x}} \equiv \hat{\boldsymbol{x}}(\theta, \phi) \triangleq (\sin\theta\cos\phi,\, \sin\theta\sin\phi,\, \cos\theta)' \in \mathbb{S}^2$ and $\hat{\boldsymbol{y}} \equiv \hat{\boldsymbol{y}}(\vartheta, \varphi) \triangleq (\sin\vartheta\cos\varphi,\, \sin\vartheta\sin\varphi,\, \cos\vartheta)' \in \mathbb{S}^2$, respectively, where $(\cdot)'$ denotes matrix or vector transpose. $\theta, \vartheta \in [0, \pi]$ represent the co-latitude or elevation measured with respect to the positive $z-$axis and

$\phi, \varphi \in [0, 2\pi)$ represent the longitude or azimuth and are measured with respect to the positive $x-$axis in the $x-y$ plane. The dot product between two vectors $\hat{\boldsymbol{x}}$ and $\hat{\boldsymbol{y}}$, representing two points on the sphere, is related to the the central angle $\Delta_s$ between the vectors $\hat{\boldsymbol{x}}$ and $\hat{\boldsymbol{y}}$,

$$\hat{\boldsymbol{x}} \cdot \hat{\boldsymbol{y}} = \cos \triangle_s\big((\theta, \phi), (\vartheta, \varphi)\big) = \sin\theta \sin\vartheta \cos(\phi - \varphi) + \cos\theta \cos\vartheta. \tag{2.2}$$

### 2.1.2 Signals on the Sphere - Hilbert Space $L^2(\mathbb{S}^2)$

We consider complex-valued functions, such as $f(\theta, \phi) = f(\hat{\boldsymbol{x}})$ and $h(\theta, \phi) = h(\hat{\boldsymbol{x}})$, defined on the unit sphere. Define the inner product

$$\big\langle f, h \big\rangle \triangleq \int_{\mathbb{S}^2} f(\hat{\boldsymbol{x}})\, \overline{h(\hat{\boldsymbol{x}})}\, ds(\hat{\boldsymbol{x}}), \tag{2.3}$$

where $ds(\hat{\boldsymbol{x}}) = \sin\theta\, d\theta\, d\phi$ is the area element, $\overline{(\cdot)}$ denotes complex conjugate and the integration is carried out over the whole unit sphere. The inner product in (2.3) induces a norm $\|f\| \triangleq \langle f, f\rangle^{1/2}$. Finite energy functions defined on the unit sphere, such that $\|f\| < \infty$, are referred as "signals on the unit sphere". Signals on the sphere form a Hilbert space $L^2(\mathbb{S}^2)$ under the inner product defined in (2.3). Throughout this thesis, functions with finite induced norm belonging to $L^2(\mathbb{S}^2)$ are referred as signals on the sphere or signals for short.

### 2.1.3 Spherical Harmonics

The Hilbert space $L^2(\mathbb{S}^2)$ is separable and the spherical harmonic functions (or spherical harmonics for short) form the archetype complete orthonormal set of basis functions. The spherical harmonic, $Y_\ell^m(\hat{\boldsymbol{x}}) = Y_\ell^m(\theta, \phi)$, for degree $\ell \geq 0$ and order $|m| \leq \ell$ is defined as [40]

$$Y_\ell^m(\theta, \phi) = N_\ell^m P_\ell^m(\cos\theta)\, e^{im\phi}, \tag{2.4}$$

where $N_\ell^m$ is the normalization factor given by

$$N_\ell^m \triangleq \sqrt{\frac{2\ell + 1}{4\pi} \frac{(\ell - m)!}{(\ell + m)!}}, \tag{2.5}$$

which ensures that $\|Y_\ell^m\| = 1$. $P_\ell^m(x)$ in (2.4) is the associated Legendre function defined for degree $\ell$ and order $0 \leq m \leq \ell$ as [40, 85]

$$P_\ell^m(x) = \frac{(-1)^m}{2^\ell \ell!}(1-x^2)^{m/2}\frac{d^{\ell+m}}{dx^{\ell+m}}(x^2-1)^\ell \tag{2.6}$$

$$P_\ell^{-m}(x) = (-1)^m \frac{(\ell-m)!}{(\ell+m)!}P_\ell^m(x), \tag{2.7}$$

for $|x| \leq 1$. The zero order associated Legendre polynomials are referred as Legendre polynomials ($P_\ell(x)$), that is, $P_\ell^0(x) = P_\ell(x)$.

### 2.1.4 Properties of Spherical Harmonics

#### Orthonormality

With the definition of spherical harmonic functions in (2.4), they satisfy the orthonormality condition

$$\left\langle Y_\ell^m, Y_p^q \right\rangle = \delta_{\ell,p}\delta_{m,q}, \tag{2.8}$$

where $\delta_{m,q}$ is the Kronecker delta function: $\delta_{m,q} = 1$ for $m = q$ and is zero otherwise.

#### Spherical Harmonics Addition Theorem

We also note one of the important property of spherical harmonics, known as spherical harmonics addition theorem [85]

$$\sum_{m=-\ell}^{\ell} Y_\ell^m(\hat{\boldsymbol{x}})\,\overline{Y_\ell^m(\hat{\boldsymbol{y}})} = \frac{2\ell+1}{4\pi}P_\ell^0(\cos\Delta_s) \tag{2.9}$$

where $\cos\Delta_s = \hat{\boldsymbol{x}}\cdot\hat{\boldsymbol{y}}$ is defined in (2.2). Furthermore, the completeness relation on the sphere is given by [85]

$$\sum_{\ell=0}^{\infty}\sum_{m=-\ell}^{\ell} Y_\ell^m(\hat{\boldsymbol{x}})\,\overline{Y_\ell^m(\hat{\boldsymbol{y}})} = (\sin\theta)^{-1}\delta(\theta-\vartheta)\,\delta(\phi-\varphi). \tag{2.10}$$

**Complex Conjugate Property**

We also note the following relation between $Y_\ell^m(\hat{\boldsymbol{x}})$ and $Y_\ell^{-m}(\hat{\boldsymbol{x}})$

$$\overline{Y_\ell^m(\hat{\boldsymbol{x}})} = (-1)^m Y_\ell^{-m}(\hat{\boldsymbol{x}}). \tag{2.11}$$

### 2.1.5 Spherical Harmonic (Fourier) Transform

By completeness of spherical harmonics [10], any signal $f \in L^2(\mathbb{S}^2)$ can be expanded as

$$f(\hat{\boldsymbol{x}}) = \sum_{\ell=0}^{\infty} \sum_{m=-\ell}^{\ell} (f)_\ell^m Y_\ell^m(\hat{\boldsymbol{x}}), \tag{2.12}$$

where

$$(f)_\ell^m \triangleq \left\langle f, Y_\ell^m \right\rangle = \int_{\mathbb{S}^2} f(\hat{\boldsymbol{x}}) \overline{Y_\ell^m(\hat{\boldsymbol{x}})}\, ds(\hat{\boldsymbol{x}}), \tag{2.13}$$

is the spherical harmonic Fourier coefficient (or spherical harmonic coefficient for short) of degree $\ell$ and order $m$. The equality in (2.12) is understood in terms of convergence in the mean (strong convergence in the norm)

$$\lim_{L\to\infty} \| f(\hat{\boldsymbol{x}}) - \sum_{\ell=0}^{L} \sum_{m=-\ell}^{\ell} (f)_\ell^m Y_\ell^m(\hat{\boldsymbol{x}}) \| = 0. \tag{2.14}$$

The signal $f \in L^2(\mathbb{S}^2)$ is said to be band-limited with maximum spherical harmonic degree or spectral degree or band-limit $L_f$ if $(f)_\ell^m = 0$ for $\ell > L_f$.

The signal $f \in L^2(\mathbb{S}^2)$ is said to be azimuthally symmetric if all of the non-zero order spherical harmonic coefficients are zero, that is, if $(f)_\ell^m = 0$ for $m \neq 0$.

Using (2.12) and employing the orthonormality of spherical harmonics, we can obtain the following Parseval relation

$$\|f\|^2 = \left\langle f, f \right\rangle = \sum_{\ell=0}^{\infty} \sum_{m=-\ell}^{\ell} |(f)_\ell^m|^2. \tag{2.15}$$

#### 2.1.5.1 Shorthand Notations and Vector Notation

In the following we may use the following shorthand notations

$$\sum_{\ell=0}^{\infty} \sum_{m=-\ell}^{\ell} \triangleq \sum_{\ell,m}^{\infty}, \qquad \sum_{\ell=0}^{L} \sum_{m=-\ell}^{\ell} \triangleq \sum_{\ell,m}^{L} \tag{2.16}$$

for brevity. For notational simplifications, we may also express the spherical harmonic $Y_\ell^m$ as $Y_n$ and the spherical harmonic coefficient $(f)_\ell^m$ as $(f)_n$. That is, as a function of a single integer index $n$ instead of two integer indices $\ell$ and $m$, using the *one-to-one* mapping

$$(\ell, m) \leftrightarrow n, \quad n = \ell^2 + \ell + m, \quad \ell = \lfloor \sqrt{n} \rfloor, \quad m = n - \lfloor \sqrt{n} \rfloor (\lfloor \sqrt{n} \rfloor - 1), \quad (2.17)$$

where $\lfloor \cdot \rfloor$ denotes the integer floor function. We will also deal with the spherical harmonic coefficients in vector form. Using the mapping defined in (2.17), we define

$$\boldsymbol{f} = \big((f)_0, (f)_1, (f)_2, \cdots\big)' = \big((f)_0^0, (f)_1^{-1}, (f)_1^0, (f)_1^1, \cdots\big)' \quad (2.18)$$

as the *spectral response* of the signal $f$. For a band-limited signal $f$ with band-limit $L_f$, $\boldsymbol{f} = \big((f)_0, (f)_1, (f)_2, \cdots, (f)_{N_f}\big)'$, where $N_f = L_f^2 + 2L_f$. For an azimuthally symmetric signal $f$, define $\boldsymbol{f}^0 = \big((f)_0^0, (f)_1^0, (f)_2^0, \cdots\big)'$.

#### 2.1.5.2 Spherical Harmonic (Fourier) Transform Operator

Define the operator $\mathcal{F}$, which transforms the signal $f(\hat{\boldsymbol{x}})$ into its spectral response $\boldsymbol{f}$ as

$$\boldsymbol{f} = \big(\mathcal{F} f\big)(\hat{\boldsymbol{x}}). \quad (2.19)$$

Also the inverse spherical harmonic transform $\mathcal{F}^{-1}$ is well-defined such that $\mathcal{F}^{-1}\boldsymbol{f} = f(\hat{\boldsymbol{x}})$.

### 2.1.6 Spherical Dirac Delta Function

The Dirac delta function $\delta(\hat{\boldsymbol{x}}, \hat{\boldsymbol{y}})$ on the sphere with the sifting property

$$f(\hat{\boldsymbol{x}}) = \int_{\mathbb{S}^2} \delta(\hat{\boldsymbol{x}}, \hat{\boldsymbol{y}}) f(\hat{\boldsymbol{y}})\, ds(\hat{\boldsymbol{y}}), \quad (2.20)$$

has following expansion in spherical harmonic domain (see completeness relation in (2.10))

$$\delta(\hat{\boldsymbol{x}}, \hat{\boldsymbol{y}}) = \sum_{\ell,m}^{\infty} Y_\ell^m(\hat{\boldsymbol{x}}) \overline{Y_\ell^m(\hat{\boldsymbol{y}})}. \quad (2.21)$$

Note that $\delta(\hat{\boldsymbol{x}}, \hat{\boldsymbol{y}}) \notin L^2(\mathbb{S}^2)$.

### 2.1.7 Useful Subspaces of $L^2(\mathbb{S}^2)$

The set of *band-limited* signals, such as $f(\hat{\boldsymbol{x}}) \in L^2(\mathbb{S}^2)$, with the maximum spectral degree $L_f$ such that $(f)_\ell^m = 0$ for $\ell > L_f$ forms a $(L_f+1)^2$ dimensional closeed subspace of $L^2(\mathbb{S}^2)$ and is denoted by $\mathcal{H}_{L_f}$.

The set of azimuthally symmetric functions which are independent of the azimuth angle (such that $f(\hat{\boldsymbol{x}}) = f(\theta,\phi) = f(\theta)$) forms a subspace of $L^2(\mathbb{S}^2)$ and is denoted by $\mathcal{H}^0$. In this case, only the zero-order spherical harmonic coefficients of $f$ are non-zero. That is $(f)_\ell^m = 0$ for all $m \neq 0$. Mathematically, any signal $f \in \mathcal{H}^0$ can be expressed as

$$\begin{aligned} f(\theta,\phi) = f(\theta) &= \sum_{\ell=0}^{\infty} (f)_\ell^0 Y_\ell^0 \\ &= \sqrt{\frac{2\ell+1}{4\pi}} (f)_\ell^0 P_\ell(\cos\theta). \end{aligned} \tag{2.22}$$

Completeness of $\mathcal{H}^0$ follows from the completeness of Legendre polynomials [85].

### 2.1.8 Spherical Harmonics Triple Product

The spherical harmonics triple product is given by

$$T(u;r;n) = T(s,t;p,q;\ell,m) = \triangleq \int_{\mathbb{S}^2} Y_r(\hat{\boldsymbol{x}}) Y_u(\hat{\boldsymbol{x}}) \overline{Y_n(\hat{\boldsymbol{x}})}\, ds(\hat{\boldsymbol{x}}) \tag{2.23}$$

with mappings $(s,t) \leftrightarrow u$, $(p,q) \leftrightarrow r$ and $(\ell,m) \leftrightarrow n$. The triple product can be expressed in terms of Wigner-3$j$ symbols [40] as

$$\begin{aligned} T(u;r;n) = T(s,t;p,q;\ell,m) = (-1)^m \sqrt{\frac{(2s+1)(2p+1)(2\ell+1)}{4\pi}} \\ \begin{pmatrix} s & p & \ell \\ 0 & 0 & 0 \end{pmatrix} \begin{pmatrix} s & p & \ell \\ t & q & -m \end{pmatrix}. \end{aligned} \tag{2.24}$$

We note that $T(u;r;n) = T(r;u;n)$. We further note that the Wigner-3$j$ symbols [40] are real-valued. Therefore, $\overline{T(u;r;n)} = T(u;r;n)$, which can also be directly proven using (2.23), symmetry relations of Wigner-3$j$ symbols and the fact that $T(u;r;n)$ is non-zero only when $s+p+\ell$ is even.

## 2.2 Rotations on the Sphere

Rotations on the sphere serve as counterparts of translations of the Euclidean domain. We define the effect of rotations on the signal defined on the sphere as an operator. We first define the rotation operator and later we note the effect of rotation in spectral domain.

### 2.2.1 Rotation Operator

Rotations on the sphere are often parameterized using Euler angles $(\varphi, \vartheta, \omega) \in \mathrm{SO}(3)$, where $\varphi \in [0,\, 2\pi)$, $\vartheta \in [0,\, \pi]$ and $\omega \in [0,\, 2\pi)$ [40]. Using the '$zyz$' Euler convention, we define the rotation operator $\mathcal{D}_\rho = \mathcal{D}(\varphi, \vartheta, \omega)$, which rotates a function on a sphere in the sequence of $\omega$ rotation around the $z$-axis, then $\vartheta$ rotation about the $y$-axis followed by a $\varphi$ rotation around the $z$-axis. If a function $f(\theta, \phi)$ is rotated on the sphere, then

$$\big(\mathcal{D}_\rho f\big)(\hat{\boldsymbol{x}}) = \big(\mathcal{D}(\varphi, \vartheta, \omega) f\big)(\hat{\boldsymbol{x}}) \triangleq f(\boldsymbol{R}^{-1}\hat{\boldsymbol{x}}), \tag{2.25}$$

where $\boldsymbol{R}$ is the $3 \times 3$ rotation matrix corresponding to the rotation operator $\mathcal{D}(\varphi, \vartheta, \omega)$ and is given by [85]

$$\boldsymbol{R} = \begin{pmatrix} \cos\varphi\cos\vartheta\cos\omega - \sin\varphi\sin\omega & -\cos\varphi\cos\vartheta\sin\omega - \sin\varphi\cos\omega & \cos\varphi\sin\vartheta \\ \sin\varphi\cos\vartheta\cos\omega - \cos\varphi\sin\omega & -\sin\varphi\cos\vartheta\sin\omega + \cos\varphi\cos\omega & \sin\varphi\sin\vartheta \\ \sin\vartheta\cos\omega & \sin\vartheta\sin\omega & \cos\vartheta \end{pmatrix}. \tag{2.26}$$

The inverse of $\mathcal{D}(\varphi, \vartheta, \omega)$ denoted by $\mathcal{D}(\varphi, \vartheta, \omega)^{-1}$ is $\mathcal{D}(-\omega, -\vartheta, -\varphi)$.

### 2.2.2 Effect of Rotation in Spectral Domain

If a signal $f(\theta, \phi)$ is rotated on the sphere under rotation operator $\mathcal{D}(\varphi, \vartheta, \omega)$, the spherical harmonic coefficient, of degree $\ell$ and order $m$, of the rotated signal is a linear combination of different order spherical harmonic coefficients of the original signal of the *same* degree $\ell$ as [40]

$$\big(\mathcal{D}(\varphi, \vartheta, \omega) f\big)_\ell^m \triangleq \big\langle \mathcal{D}(\varphi, \vartheta, \omega) f, Y_\ell^m \big\rangle = \sum_{m'=-\ell}^{\ell} D_\ell^{m,m'}(\varphi, \vartheta, \omega)(f)_\ell^{m'}, \tag{2.27}$$

where $D_\ell^{m,m'}(\varphi,\vartheta,\omega) = D_\ell^{m,m'}(\rho)$ is the Wigner-$D$ function defined in next subsection.

### 2.2.3 Wigner-$D$ Function

The Wigner-$D$ function is defined as

$$D_\ell^{m,m'}(\rho) = D_\ell^{m,m'}(\varphi,\vartheta,\omega) = e^{-im\varphi} d_\ell^{m,m'}(\vartheta) e^{-im'\omega}, \quad \rho = (\varphi,\vartheta,\omega) \in \mathrm{SO}(3) \tag{2.28}$$

where $|m|$, $|m'| \leq \ell$ and $d_\ell^{mm'}(\vartheta)$ is the Wigner-$d$ function [40] given by

$$d_\ell^{m,m'}(\theta) = \sum_n (-1)^{n-m'+m} \times \frac{\sqrt{(\ell+m')!(\ell-m')!(\ell+m)!(\ell-m)!}}{(\ell+m'-n)!(n)!(\ell-n-m)!(n-m'+m)!} \times \cos\left(\frac{\theta}{2}\right)^{2\ell-2n+m'-m} \sin\left(\frac{\theta}{2}\right)^{2n-m'+m}, \tag{2.29}$$

We note the following relation between spherical harmonic function and Wigner-$D$ function

$$D_\ell^{m,0}(\varphi,\vartheta,0) = \sqrt{\frac{4\pi}{2\ell+1}} \overline{Y_\ell^m(\vartheta,\varphi)}. \tag{2.30}$$

### 2.2.4 Rotation of Azimuthally Symmetric Function

For the azimuthally symmetric functions $h(\hat{\boldsymbol{x}}) \in \mathcal{H}^0$, the $\omega$ rotation around $z-$axis becomes ineffective and can be set to $\omega = 0$. Hence, the expression in (2.27) simplifies to

$$\big(\mathcal{D}(\varphi,\vartheta,0)h\big)_\ell^m = D_\ell^{m,0}(\varphi,\vartheta,0)(h)_\ell^0 = \sqrt{\frac{4\pi}{2\ell+1}} \overline{Y_\ell^m(\vartheta,\varphi)}(h)_\ell^0, \tag{2.31}$$

where the second equality follows from the relation between spherical harmonic and Wigner-$D$ function given in (2.30).

## 2.3 Signals on the Rotation Group SO(3)

For $\ell \geq 0$ and $m, m' \in \mathbb{Z}$ such that $|m|, |m'| \leq \ell$, the Wigner-$D$ functions in (2.28) form a complete set of orthogonal functions for the space $L^2(\mathrm{SO}(3))$ of functions

defined on the rotation group SO(3) and follow the orthogonality relation

$$\int_{\mathrm{SO}(3)} D_{\ell}^{m,m'}(\rho)\overline{D_{p}^{q,q'}(\rho)}\,d\rho = \frac{8\pi^2}{2\ell+1}\,\delta_{\ell p}\delta_{mq}\delta_{m'q'}, \tag{2.32}$$

where $d\rho = d\varphi \sin\vartheta d\vartheta d\omega$ and the integral is a triple integral over all rotations $(\varphi, \vartheta, \omega) \in \mathrm{SO}(3)$ [40]. Thus, any function $f \in L^2(\mathrm{SO}(3))$ may be expressed as

$$f(\rho) = \sum_{\ell=0}^{\infty} \sum_{m=-\ell}^{\ell} \sum_{m=-\ell'}^{\ell'} \left(f\right)_{\ell}^{m,m'} D_{\ell}^{m,m'}(\rho), \tag{2.33}$$

where

$$\left(f\right)_{\ell}^{m,m'} = \frac{2\ell+1}{8\pi^2} \int_{\mathrm{SO}(3)} f(\rho)\overline{D_{\ell}^{m,m'}(\rho)}\,d\rho. \tag{2.34}$$

The signal $f$ is said to be band-limited with maximum degree $L_f$ if $\left(f\right)_{\ell}^{m,m'} = 0$, $\forall \ell > L_f$.

## 2.4 Summary

In this chapter, we have introduced the required mathematical background. The notation adopted in this chapter is used throughout this thesis. However, the new notation or formulation, if required, will be defined in later chapters.

# Chapter 3

# Commutative Anisotropic Convolution

In this chapter, we propose a new definition of convolution on the 2-sphere that is analogous to the familiar Euclidean-domain convolution in many ways. The proposed convolution is the first type of convolution on the 2-sphere which is commutative. Two other advantages, in comparison with existing definitions in the literature, are that 1) the new convolution admits anisotropic filters and signals and 2) the domain of the output remains on the sphere. Therefore, the new convolution well emulates the conventional Euclidean convolution. In addition to providing the new definition of convolution and discussing its properties, we provide the spectral analysis of the convolution output. We also develop a fast algorithm for efficient computation of proposed convolution. This convolutional framework can be useful in filtering applications for signals defined on the 2-sphere.

This chapter is organized as follows. We review the existing definitions in the literature, which leads to our problem formulation in Section 3.1. In Section 3.2, we establish a commutative anisotropic convolution and provide some graphical depiction of the proposed approach. In Section 3.3, we present the spectral analysis of the proposed convolution. Finally, in order to efficiently compute the commutative anisotropic convolution, we develop a fast algorithm in Section 3.4.

## 3.1 Existing Formulations of Convolution

The conventional convolution between two functions on 2-dimensional Euclidean space, $\mathbb{R}^2$ is

$$\big(f \star h\big)(\boldsymbol{x}) \triangleq \int_{\mathbb{R}^2} f(\boldsymbol{x}-\boldsymbol{y})h(\boldsymbol{y})\,d\boldsymbol{y}, \tag{3.1}$$

where $\boldsymbol{x}$, $\boldsymbol{y} \in \mathbb{R}^2$. It is easy to verify that the convolution is commutative, $f \star h = h \star f$.

On the premise that rotations on the sphere are counterparts of translations in the Euclidean domain, the following definitions of convolution on $\mathbb{S}^2$ in the literature involve all three independent rotations in the rotation group SO(3). The aim of the next two subsections is to formally, albeit briefly, introduce these definitions and point out the differences in their characterizations. We then pose a set of questions in search for a counterpart of Euclidean convolution on the 2-sphere.

### 3.1.1 Type 1 (Anisotropic) Convolution

The following definition has appeared in [30, 45]

$$g(\varphi,\vartheta,\omega) = h \star f \triangleq \int_{\mathbb{S}^2} \big(\mathcal{D}(\varphi,\vartheta,\omega)h\big)(\hat{\boldsymbol{x}})\, f(\hat{\boldsymbol{x}})\, ds(\hat{\boldsymbol{x}}). \tag{3.2}$$

By this definition, the domain of convolution output does not belong to $\mathbb{S}^2$. Instead, as it is clear from above, $g$ is a function of three independent Euler rotation angles $\varphi, \vartheta, \omega$. Since a proper rotation on the 2-sphere is an isometry, we can apply the inverse of rotation operator to both parts of the integrand in (3.2) and leave the integral unchanged, as follows:

$$\begin{aligned} h \star f &= \int_{\mathbb{S}^2} \big(\mathcal{D}(\varphi,\vartheta,\omega)^{-1}\,\mathcal{D}(\varphi,\vartheta,\omega)h\big)(\hat{\boldsymbol{x}})\,\big(\mathcal{D}(\varphi,\vartheta,\omega)^{-1} f\big)(\hat{\boldsymbol{x}})\, ds(\hat{\boldsymbol{x}}) \\ &= \int_{\mathbb{S}^2} h(\hat{\boldsymbol{x}})\,\big(\mathcal{D}(\varphi,\vartheta,\omega)^{-1} f\big)(\hat{\boldsymbol{x}})\, ds(\hat{\boldsymbol{x}}) = \int_{\mathbb{S}^2} h(\hat{\boldsymbol{x}})\,\big(\mathcal{D}(-\omega,-\vartheta,-\varphi)\, f\big)(\hat{\boldsymbol{x}})\, ds(\hat{\boldsymbol{x}}). \end{aligned} \tag{3.3}$$

However, since $\mathcal{D}(\varphi,\vartheta,\omega) \neq \mathcal{D}(-\omega,-\vartheta,-\varphi)$ in general, this convolution is not commutative.

### 3.1.2 Type 2 (Isotropic) Convolution

The following definition is adapted from [31]

$$\big(h \circledcirc f\big)(\hat{\boldsymbol{x}}) \triangleq \frac{1}{2\pi}\int_0^{2\pi}\int_0^{\pi}\int_0^{2\pi} h(\boldsymbol{R}^{-1}\hat{\boldsymbol{x}})\, f(\boldsymbol{R}\,\hat{\boldsymbol{\eta}})\, d\omega\, \sin\vartheta\, d\vartheta\, d\varphi, \tag{3.4}$$

where $\hat{\boldsymbol{\eta}} = (1,0,0)' \in \mathbb{S}^2$ is the north pole. Noting that in $f(\boldsymbol{R}\,\hat{\boldsymbol{\eta}})$, the first rotation by $\omega$ of the north pole around the $z-$axis is ineffectual, we can rewrite the above convolution as

$$\big(h \circledcirc f\big)(\hat{\boldsymbol{x}}) = \frac{1}{2\pi}\int_0^{2\pi}\int_0^{\pi}\int_0^{2\pi} \big(\mathcal{D}(\varphi,\vartheta,\omega)h\big)(\hat{\boldsymbol{x}})\, f(\vartheta,\varphi)\, d\omega\, \sin\vartheta\, d\vartheta\, d\varphi. \tag{3.5}$$

Compared to (3.2), (3.5) has a somewhat similar spirit with the difference that an extra averaging over the first rotation $\omega$ is performed which turns the filter $h$ into an azimuthally symmetric kernel $h_0 \triangleq \mathcal{P}^0 h$, where $\mathcal{P}^0$ is the projection operator which projects a signal belonging to $L^2(\mathbb{S}^2)$ into the subspace $\mathcal{H}^0 \subset L^2(\mathbb{S}^2)$. This will bring the output of the convolution back to $\mathbb{S}^2$. However, as shown in [32] this definition is identical to the isotropic convolution [46, 47]

$$(h_0 \circledast f)(\hat{\boldsymbol{x}}) \triangleq \int_{\mathbb{S}^2} h_0(\hat{\boldsymbol{x}}\cdot\hat{\boldsymbol{y}})\, f(\hat{\boldsymbol{y}})\, ds(\hat{\boldsymbol{y}}), \quad \hat{\boldsymbol{x}} \in \mathbb{S}^2, \tag{3.6}$$

and the extra averaging over $\omega$ "kills" any directional azimuthal component of the filter.

This convolution, when evaluated in the spherical harmonic domain is given by

$$\big\langle h \circledcirc f, Y_\ell^m \big\rangle = \big\langle h_0 \circledast f, Y_\ell^m \big\rangle = \sqrt{\frac{4\pi}{2\ell+1}}\big(h\big)_\ell^0\big(f\big)_\ell^m, \tag{3.7}$$

which has a desirable multiplicative property between spherical harmonic coefficients of the filter and signal. However, as expected, only the zero-order spherical harmonic coefficients of the filter are present, which makes this definition not commutative in general, and information is discarded.

### 3.1.3 Problem Statement

From the discussion above, it becomes clear that existing definitions are either anisotropic, but with an output whose domain is not in $\mathbb{S}^2$, or their output domain

is $\mathbb{S}^2$, but can only accommodate isotropic filters. Neither of the convolutions are commutative.

Motivated by the differences in the characterization of convolution on the sphere, we define a convolution on $\mathbb{S}^2$, which simultaneously satisfies the following requirements: 1) the domain of its output is $\mathbb{S}^2$, 2) involves an integral over points on $\mathbb{S}^2$, 3) is anisotropic, and 4) is commutative.

## 3.2 Commutative Anisotropic Convolution on the 2-Sphere

The Euclidean convolution in (3.1) forms an implicit prescription for constructing a suitable notion of convolution on $\mathbb{S}^2$. In particular, we are guided by the fact that in $\mathbb{R}^2$, not all three isometries are involved in the convolution. Only two translations and not the rotation are used. Hence, it is natural to think that only two degrees of freedom in the rotations on $\mathbb{S}^2$ should be used to define the convolution, because $\mathbb{S}^2$ is a 2-dimensional, albeit curved, surface. Therefore, we propose the following formulation as the initial candidate for our convolution

$$g_\omega(\vartheta, \varphi) \triangleq \int_{\mathbb{S}^2} \big(\mathcal{D}(\varphi, \vartheta, \omega)h\big)(\hat{\boldsymbol{x}}) f(\hat{\boldsymbol{x}})\, ds(\hat{\boldsymbol{x}}). \tag{3.8}$$

This candidate appears to be somewhat similar to the anisotropic convolution in (3.2), but it differs in philosophy and actual content. For example, in (3.2), the left hand side is a function of $\varphi, \vartheta, \omega$ or the convolution results in a function whose domain is not $\mathbb{S}^2$. Here, on the other hand, the output should be understood as a function of $\vartheta$ and $\varphi$ only. The initial rotation angle $\omega$ in (3.8) is unspecified at this point. It might be a constant or a function of $\vartheta$ and $\varphi$. Our initial candidate satisfies the first three requirements in Section 3.1.3. However, it is still lacking the commutative property, which will be dealt with below.

### 3.2.1 Commutative Anisotropic Convolution

Our aim here is to constrain the rotation operator in (3.8) such that the definition of convolution becomes commutative. We present the result in the following theorem.

**Theorem 3.1** *A necessary and sufficient condition for the anisotropic convolution in* (3.8) *to be commutative is* $\omega = \pi - \varphi$.

**Proof**

We first prove the necessary condition and show that for the convolution to be commutative, $\omega$ has to be $\pi - \varphi$. Following similar reasoning as in (3.3), we can write (3.8) as

$$\begin{aligned} g_\omega(\vartheta, \varphi) &= \int_{\mathbb{S}^2} \big(\mathcal{D}(\varphi, \vartheta, \omega)\, h\big)(\hat{\boldsymbol{x}})\, f(\hat{\boldsymbol{x}})\, ds(\hat{\boldsymbol{x}}) \\ &= \int_{\mathbb{S}^2} h(\hat{\boldsymbol{x}})\, \big(\mathcal{D}(-\omega, -\vartheta, -\varphi) f\big)(\hat{\boldsymbol{x}})\, ds(\hat{\boldsymbol{x}}). \end{aligned} \tag{3.9}$$

Our objective is to select $\omega$ such that

$$\mathcal{D}(\varphi, \vartheta, \omega) = \mathcal{D}(-\omega, -\vartheta, -\varphi), \tag{3.10}$$

so that the convolution becomes commutative. The negative rotation $-\vartheta$ around the $y-$axis appears to be out of range of permissible co-latitude rotations ($[0, \pi]$), which is resolved through the following identity [85]

$$\mathcal{D}(\varphi, \vartheta, \omega) = \mathcal{D}(\pi + \varphi, -\vartheta, \pi + \omega), \tag{3.11}$$

where the $z-$axis rotations have $(\mathrm{mod}\, 2\pi)$ been omitted to avoid clutter. Now by equating (3.10) and (3.11), we obtain two equations $-\varphi = \pi + \omega$ and $-\omega = \pi + \varphi$, which give the value of $\omega$

$$\omega \equiv -\pi - \varphi \equiv \pi - \varphi \pmod{2\pi}, \tag{3.12}$$

that makes the rotation operator $\mathcal{D}(\varphi, \vartheta, \omega)$ satisfy the "involution" property

$$\mathcal{D}(\varphi, \vartheta, \pi - \varphi) = \mathcal{D}(\varphi, \vartheta, \pi - \varphi)^{-1}.$$

Due to this involution of the rotation operator for $w = \pi - \varphi$, the anisotropic convolution in (3.9) becomes commutative. In fact, using a new operator $\odot$ for such a commutative convolution

$$\big(h \odot f\big)(\vartheta, \varphi) \triangleq g_\omega(\vartheta, \varphi)\big|_{\omega = \pi - \varphi} = g_{\pi - \varphi}(\vartheta, \varphi), \tag{3.13}$$

we conclude that

$$\begin{aligned}\big(h \odot f\big)(\vartheta,\varphi) &= \int_{\mathbb{S}^2} \big(\mathcal{D}(\varphi,\vartheta,\pi-\varphi)\,h\big)(\hat{\boldsymbol{x}})\,f(\hat{\boldsymbol{x}})\,ds(\hat{\boldsymbol{x}}) \\ &= \int_{\mathbb{S}^2} h(\hat{\boldsymbol{x}})\,\big(\mathcal{D}(\varphi,\vartheta,\pi-\varphi)^{-1}\,f\big)(\hat{\boldsymbol{x}})\,ds(\hat{\boldsymbol{x}}) \\ &= \int_{\mathbb{S}^2} h(\hat{\boldsymbol{x}})\,\big(\mathcal{D}(\varphi,\vartheta,\pi-\varphi)\,f\big)(\hat{\boldsymbol{x}})\,ds(\hat{\boldsymbol{x}}) = \big(f \odot h\big)(\vartheta,\varphi). \qquad \square\end{aligned}$$

The sufficient condition is proven by inserting $\omega = \pi - \varphi$ in $\mathcal{D}(\varphi,\vartheta,\omega)$ and verifying using (3.11) that $\mathcal{D}(\varphi,\vartheta,\pi-\varphi)^{-1} = \mathcal{D}(-\pi+\varphi,-\vartheta,-\varphi) = \mathcal{D}(\varphi,\vartheta,\pi-\varphi)$, which results in a commutative convolution.

**Remark 3.1** *The proposed convolution can be interpreted as a mapping of anisotropic convolution defined on* $\mathrm{SO}(3)$ *in* (3.2) *to* $\mathbb{S}^2$ *with the constraint that* $\omega$ *varies with the longitude* $\varphi$ *given by* (3.12)*. Since,* $\omega$ *must be chosen as a function of* $\varphi$*, it cannot be freely controlled at each spatial position.*

In summary, we began with (3.8) with $\omega$ unspecified and have shown that it must be chosen to be a function of $\varphi$ (and not $\vartheta$) according to (3.12) for the overall rotation operation to be an involution, which yields the desired commutativity. We now provide a geometric interpretation of this definition and later we present an example to illustrate the proposed convolution.

### 3.2.2 Graphical Depiction

In Fig. 3.1 we present a sequence of images to depict the commutative convolution in action. Fig. 3.1a depicts a simplified filter signal indicated by an asymmetric region on the 2-sphere. The filter, of course, in general has support on the whole 2-sphere. The first portion of the $\omega$ rotation (by $\pi$) is shown in Fig. 3.1b and may be associated with flipping or "reversing" the filter (similar to Euclidean convolution). Fig. 3.1c is the $\omega = \pi - \varphi$ rotation; Fig. 3.1d shows the $\vartheta$ rotation and, finally, Fig. 3.1e shows the filter after the $\varphi$ rotation. Fig. 3.2 shows an intrinsic rotation along axis $\hat{\boldsymbol{w}} = (\,\cos(\pi+\varphi),\ \sin(\pi+\varphi),\ 0\,)'$ by a single rotation $\vartheta$, which effects the same rotation of Fig. 3.1b to Fig. 3.1e.

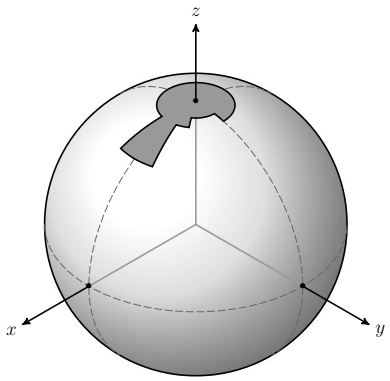


(a) $\mathcal{D}(0,0,0)$ – initial position.

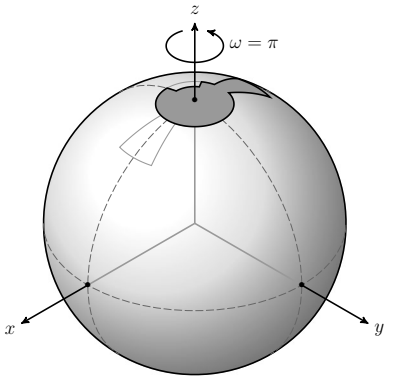


(b) $\mathcal{D}(0,0,\pi)$ – $\pi$ about $z-$axis.

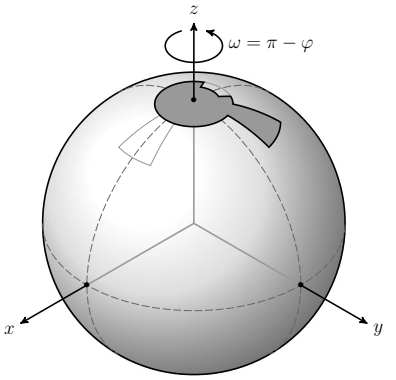


(c) $\mathcal{D}(0,0,\pi-\varphi)$ – $\pi-\varphi$ about $z-$axis

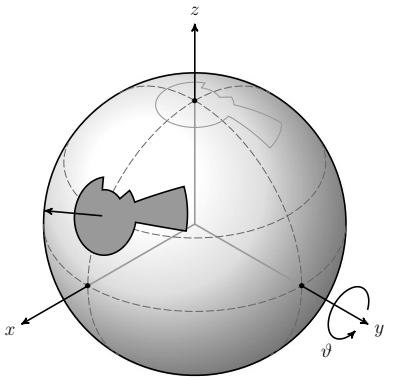


(d) $\mathcal{D}(0,\vartheta,\pi-\varphi)$ – $\vartheta$ about $y-$axis.

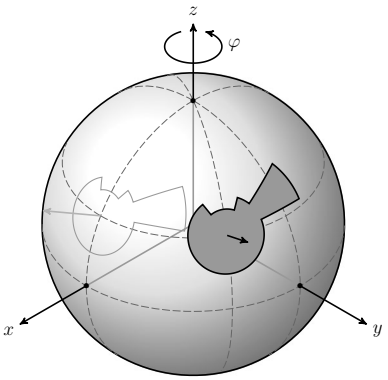


(e) $\mathcal{D}(\varphi,\vartheta,\pi-\varphi)$ – $\varphi$ about $z-$axis

Figure 3.1: Action of the commutative convolution kernel. A nominal asymmetrical support region for the kernel is transformed under the action of operator $\mathcal{D}(\varphi,\vartheta,\pi-\varphi)$ according to its component rotations.

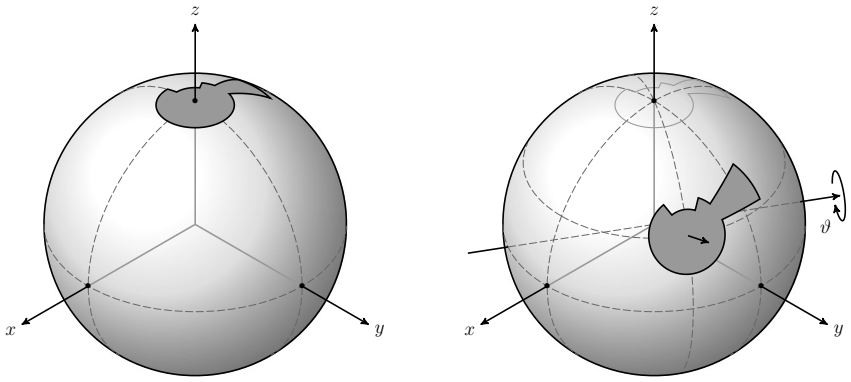


(a) $f(\hat{\boldsymbol{x}})$. (b) $\big(\mathcal{D}(\varphi,\vartheta,-\varphi)f\big)(\hat{\boldsymbol{x}})$.

Figure 3.2: Single intrinsic rotation version of $\mathcal{D}(\varphi,\vartheta,-\varphi)$.

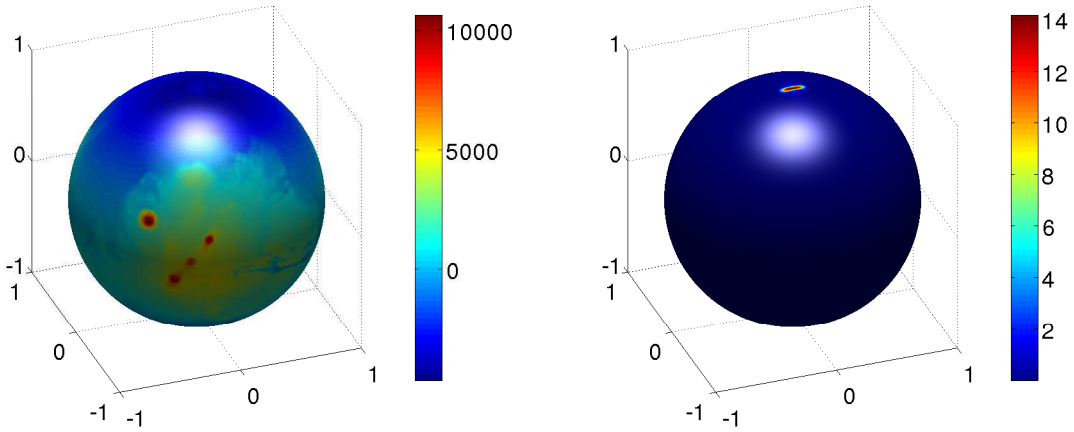


(a) Mars signal. (b) Asymmetric filter function.

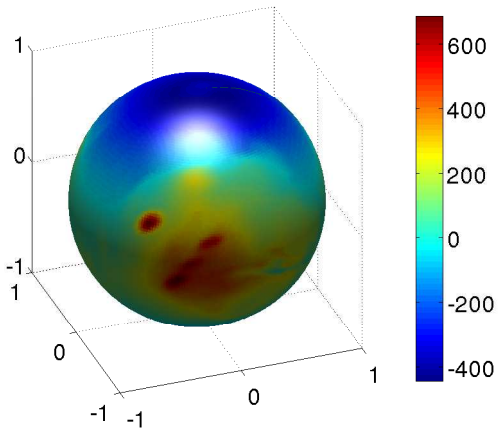


(c) Filtered signal.

Figure 3.3: Illustration of the commutative convolution. (a) Mars signal is convolved with (b) asymmetric spatially concentrated bandlimited filter kernel to obtain (c) smoothed (low-pass filtered) Mars signal.

### 3.2.3 Illustration of the Proposed Convolution

As an illustration of the proposed convolution, we consider the filtering of a signal using a filter kernel, which is spatially concentrated in an asymmetric region around north pole. We consider the Mars topographical map as a signal on the sphere which is obtained by using a spherical harmonic model for the topography of Mars[1] up to a maximum spherical harmonic degree 150 and is shown in Fig. 3.3a. We use a bandlimited filter kernel with the maximum spherical harmonic degree 80 and spatial concentration in a strip region around north pole, bounded by co-latitude $\theta = \frac{\pi}{128}$ and the planes $|y| = \arcsin\frac{9\pi}{256}$ [86]. The filter kernel is obtained as a solution of Slepian concentration problem on the sphere and is shown in Fig. 3.3b, which is convolved with the signal (Mars topographic map) to obtain the filtered signal shown in Fig. 3.3c. This filtering is equivalent to directional smoothing of the Mars signal using asymmetric smoothing function where the direction of the smoothing function at each spatial position $(\vartheta, \varphi)$ is $\pi - \varphi$.

### 3.2.4 Alternative Characterization of Anisotropic Convolution

The expression in (3.8) represents the convolution in the spatial domain based on the spatial-domain representations of filter and signal. Before concluding this section, we give an alternative form expressed in terms of the spherical harmonic coefficients of $h(\hat{\boldsymbol{x}})$, denoted by $\big(h\big)_s^t$, and those of $f(\hat{\boldsymbol{x}})$, denoted by $\big(f\big)_p^q$. Using the spherical harmonic coefficient expansion of $f$ and $h$ in (2.12) and the effect of rotation operator on spherical harmonic coefficients in (2.27), we can write (3.8) as

$$\begin{aligned} g_\omega(\vartheta,\varphi) &= \int_{\mathbb{S}^2} \sum_{s,t} Y_s^t(\hat{\boldsymbol{x}}) \sum_{t'=-s}^{s} D_s^{t,t'}(\varphi,\vartheta,\omega) \big(h\big)_s^{t'} \sum_{p,q} \big(f\big)_p^q Y_p^q(\hat{\boldsymbol{x}})\, ds(\hat{\boldsymbol{x}}) \\ &= \sum_{s,t} \sum_{p,q} (-1)^q \big(f\big)_p^{-q} \delta_{s,p} \delta_{t,q} \sum_{t'=-s}^{s} D_s^{t,t'}(\varphi,\vartheta,\omega) \big(h\big)_s^{t'}, \end{aligned} \tag{3.14}$$

where $\delta_{s,p}$ is the Kronecker delta function and is equal to one only when $s = p$ and zero otherwise. We have also employed the conjugate symmetry property of spherical harmonics and the orthonormal property of spherical harmonics. Simplifying

[1] `http://www.ipgp.fr/~wieczor/SH/`

the expression in (3.14) yields the sought result

$$g_\omega(\vartheta,\varphi) = \sum_{s,t}(-1)^t \big(f\big)_s^{-t} \sum_{t'=-s}^{s} D_s^{t,t'}(\varphi,\vartheta,\omega)\,\big(h\big)_s^{t'}. \tag{3.15}$$

We note that the expression in (3.15) is valid for any $\omega$ (a constant or a function of $\vartheta$ and $\varphi$). The corresponding expression for commutative anisotropic convolution can be obtained by setting $\omega = \pi - \varphi$.

## 3.3 Spectral Analysis of Commutative Anisotropic Convolution

We now analyze the result of commutative anisotropic convolution in the spherical harmonic domain. That is, we want to evaluate $\big(g\big)_\ell^m = \langle g_{\pi-\varphi}, Y_\ell^m\rangle$. We start with the expression of $g_\omega$ in (3.15), which specifies the anisotropic convolution output function in terms of Wigner-$D$ functions and the spherical harmonic coefficients $\big(f\big)_s^{-t}$ and $\big(h\big)_s^t$. The spherical harmonic coefficient of the convolution output is then

$$\langle g_{\pi-\varphi}, Y_\ell^m\rangle = \sum_{s,t}(-1)^t \big(f\big)_s^{-t} \sum_{t'=-s}^{s} \big(h\big)_s^{t'} \langle D_s^{t,t'}, Y_\ell^m\rangle_{\mathbb{S}}^2, \tag{3.16}$$

where the notation $\langle D_s^{t,t'}, Y_\ell^m\rangle_{\mathbb{S}}^2$ is used to emphasize that the inner product is taken over 2 rotation angles characterizing $\mathbb{S}^2$ and not over all three rotation angles that specify SO(3). Now, using the Wigner-$D$ function expression in (2.28) and its relation with spherical harmonics in (2.30), we can write $\langle D_s^{t,t'}, Y_\ell^m\rangle$ as

$$\begin{aligned}\langle D_s^{t,t'}, Y_\ell^m\rangle &= \int_0^\pi \int_0^{2\pi} D_s^{t,t'}(\varphi,\vartheta,\pi-\varphi)\overline{Y_\ell^m(\vartheta,\varphi)}\,d\varphi\,\sin\vartheta\,d\vartheta \\ &= \sqrt{\frac{2\ell+1}{4\pi}} \int_0^\pi d_s^{t,t'}(\vartheta)\,d_\ell^{m,0}(\vartheta) \int_0^{2\pi} e^{-i(t-t'+m)\varphi}\,e^{-it'\pi}\,d\varphi\,\sin\vartheta\,d\vartheta, \end{aligned} \tag{3.17}$$

where, by orthogonality of exponentials over $[0, 2\pi]$, the inner integral is non-zero only when $t - t' + m = 0$ or only when $t' = t + m$. In this case, the expression in (3.16) can be written as

$$\langle g_{\pi-\varphi}, Y_\ell^m\rangle = (-1)^m 2\pi \sqrt{\frac{2\ell+1}{4\pi}} \sum_{s=0}^{\infty} \sum_{t=-K_1}^{K_2} \big(f\big)_s^{-t} \big(h\big)_s^{t+m} \int_0^\pi d_s^{t,t+m}(\vartheta) d_\ell^{m,0}(\vartheta) \sin\vartheta d\vartheta, \tag{3.18}$$

where $K_1 = \max(-s, -s-m)$ and $K_2 = \min(s, s-m)$, which ensure $|m+t| \leq s$. The integral in (3.18) that involves the inner product of Wigner-$d$ functions can be solved using two approaches. The first approach is based on using the following expansion of product of Wigner-$d$ functions [87]

$$\int_0^\pi d_s^{t,t+m}(\vartheta)\, d_\ell^{m,0}(\vartheta) \sin\vartheta\, d\vartheta = \sum_{j=|s-\ell|}^{s+\ell} C_1(j,s,t,\ell,m) \int_0^\pi d_j^{t+m,t+m}(\vartheta)\, \sin\vartheta\, d\vartheta, \tag{3.19}$$

where $C_1(j,s,t,\ell,m)$ is given using Wigner-3$j$ symbols as

$$C_1(j,s,t,\ell,m) = 2j+1 \begin{pmatrix} s & \ell & j \\ t+m & 0 & -(t+m) \end{pmatrix} \begin{pmatrix} s & \ell & j \\ t & m & -(t+m) \end{pmatrix}. \tag{3.20}$$

Using the expression of Wigner-$d$ function in (2.29), the integral in (3.19) simplifies to

$$\begin{aligned} \int d_j^{t+m,t+m}(\vartheta)\, \sin\vartheta\, d\vartheta = 2 \sum_{n=0}^{\substack{\min(j+t+m,\\ j-t-m)}} (-1)^n \\ \times \frac{(j+t+m-n+1)!(j-t-m-n+1)!(j-n)!}{n!(j+1)!}. \end{aligned} \tag{3.21}$$

Another approach to solve the integral in (3.18) is to directly use Wigner-$d$ function in (2.29) to obtain

$$\begin{aligned} \int_0^\pi d_s^{t,t+m}(\vartheta)\, d_\ell^{m,0}(\vartheta)\, \sin\vartheta\, d\vartheta = \sum_n \sum_{n'} (-1)^{(n+n')} \\ \times C_2(s,t,m,n)\, C_3(\ell,m,n')\, C_4(s,\ell,n,n'), \end{aligned} \tag{3.22}$$

with

$$\begin{aligned} C_2(s,t,m,n) &\triangleq \frac{\sqrt{(s+t+m)!(s-t-m)!(s+t)!(s-t)!}}{(s+t+m-n)!(n)!(s-n-t)!(n-m)!}, \\ C_3(\ell,m,n') &\triangleq \frac{\sqrt{(\ell)!(\ell)!(\ell+m)!(\ell-m)!}}{(\ell-n')!(n')!(\ell-n'-m)!(n'+m)!}, \\ C_4(s,\ell,n,n') &\triangleq 2\frac{(s+\ell-n-n')!(n+n')!}{(s+\ell+1)!}, \end{aligned}$$

where the range of summations over $n$ and $n'$ are given by $\max(0, m) \leq n \leq \min(s - t, s - t + m)$ and $\max(0, -m) \leq n' \leq \min(\ell, \ell - m)$ with the further condition that $n + n' \leq s + \ell$. The expression in (3.22) allows us to explicitly evaluate the integral involved in (3.18) without using Wigner-3$j$ symbols.

### 3.3.1 Special Case – One Function is Azimuthally Symmetric

Let $h(\hat{\boldsymbol{x}})$ be an azimuthally symmetric function, which implies $\big(h\big)_s^t = \langle h, Y_s^t \rangle = 0$ for $t \neq 0$. For this special case, we can write (3.15) with $\omega = \pi - \varphi$ as

$$\big(h \odot f\big)(\vartheta, \varphi) = g_{\pi-\varphi}(\vartheta, \varphi) = \sum_{s,t} (-1)^t d_s^{t,0}(\vartheta)\, e^{-it\varphi} \,\big(f\big)_s^{-t}\, \big(h\big)_s^0, \tag{3.23}$$

which can be expressed using relation (2.30) as

$$\big(h \odot f\big)(\vartheta, \varphi) = \sum_{s,t} (-1)^t \sqrt{\frac{4\pi}{2s+1}}\, \overline{Y_s^t(\vartheta, \varphi)}\, \big(f\big)_s^{-t}\, \big(h\big)_s^0. \tag{3.24}$$

Using conjugate symmetry and orthonormal property of spherical harmonics, we obtain

$$\langle h \odot f, Y_\ell^m \rangle = \sqrt{\frac{4\pi}{2\ell+1}}\, \big(h\big)_\ell^0\, \big(f\big)_\ell^m, \tag{3.25}$$

which is also equal to $\langle f \odot h, Y_\ell^m \rangle$. By commutativity, a simplified form of multiplication in the spherical harmonic domain results if either the signal (nominally $f$) or filter (nominally $h$) is azimuthally symmetric.

In comparison, the convolution in [31] is not commutative and we observe

$$\begin{aligned}
\langle h \circledcirc f, Y_\ell^m \rangle &= \sqrt{\frac{4\pi}{2\ell+1}}\, \big(h\big)_\ell^0\, \big(f\big)_\ell^m, \\
\langle f \circledcirc h, Y_\ell^m \rangle &= \sqrt{\frac{4\pi}{2\ell+1}}\, \big(f\big)_\ell^0\, \big(h\big)_\ell^0 \delta_{m,0},
\end{aligned}$$

where $h(\hat{\boldsymbol{x}})$ is an azimuthally symmetric function.

## 3.4 Efficient Computation

In this section, we consider the problem of efficiently evaluating the commutative anisotropic convolution in (3.13). Since the commutative anisotropic convolution is a special case of SO(3) convolution, it can be computed efficiently by employing the existing efficient algorithms [45] for SO(3) convolution to compute $g(\varphi, \vartheta, \omega)$ in (3.8) and then mapping $g(\varphi, \vartheta, \omega)$ to the $g_{\pi-\varphi}(\vartheta, \varphi)$, whose domain is $\mathbb{S}^2$, with a constrain $\omega = \pi - \phi$. However, this method of computation of $g_{\pi-\varphi}(\vartheta, \varphi)$ involves redundancy as we do not need to compute the SO(3) convolution for all values of $\omega$, instead, we need to compute for only $\omega = \pi - \varphi$. In order to avoid this redundancy, we present fast algorithm for the efficient computation of commutative anisotropic convolution. Following the spectral analysis of the commutative anisotropic convolution given in Section 3.3, we note that the convolution output $g_{\pi-\varphi}(\vartheta, \varphi)$ is not a band-limited function on the sphere, even when both signal $f(\theta, \phi)$ and filter $h(\theta, \phi)$ are band-limited functions. Therefore, we further note that the convolution output cannot be defined using fixed number of samples on the sphere.

For the computation of commutative anisotropic convolution given in (3.13), we present here a range of algorithms, from the direct quadrature evaluation, to the semi-fast algorithm that employs the existing efficient methods for SO(3) convolution, to the proposed fast algorithm where we use the factoring of rotation approach [84] and employ FFT for efficient computation. We show that the proposed fast algorithm is more computationally efficient than the direct quadrature evaluation and semi-fast algorithm. In terms of computational complexity, our proposed fast algorithm provides a saving of $O(N)$ over existing efficient techniques, when the convolution output is defined on $O(N^2)$ number of samples on the sphere. Later, through numerical experiments, we verify the computational complexity of the proposed fast algorithm.

### 3.4.1 Discretization of $\mathbb{S}^2$ and SO(3)

For representation of a signal on the sphere, it is required to define discretization of both the spherical coordinates of the unit sphere and the Euler angle representation of SO(3). We consider the equiangular sampling tessellation schemes, which support the computation of exact quadrature for band-limited signals.

For the unit sphere domain, we use the equiangular sampling scheme [41]

$\mathfrak{S}(L) = \{\theta_{n_\theta} = 2\pi n_\theta/(2L+1),\, \phi_{n_\phi} = 2\pi n_\phi/(2L+1) : 0 \leq n_\theta \leq L,\, 0 \leq n_\phi \leq 2L\}$ as a grid of $(L+1) \times (2L+1)$ sample points on the sphere. Using the quadrature weights derived in [41], the integral of a band-limited function $f$ with band-limit $L_f$ over the sphere can be computed exactly as quadrature using the sampling scheme $\mathfrak{S}(L_f)$. Since the commutative convolution output $g_{\pi-\varphi}(\vartheta, \varphi)$ is not a band-limited function, therefore we cannot associate the size of the sampling grid for output with the band-limit of the output. The larger the size of the grid, the better is the resolution of the convolution output. We use $N$ to characterize the sampling grid $\mathfrak{S}(N)$ for the commutative anisotropic convolution output.

For the discretization of Euler angle representation of SO(3), we consider equiangular tessellation scheme $\mathfrak{C}(L) = \{\varphi_{n_\varphi} = 2\pi n_\varphi/(2L+1),\, \vartheta_{n_\vartheta} = 2\pi n_\vartheta/(2L+1),\, \omega_{n_\omega} = \pi(2n_\omega+1)/(2L+1) : 0 \leq n_\vartheta \leq L,\, 0 \leq n_\varphi, n_\omega \leq 2L\}$ as a grid of $(2L+1) \times (L+1) \times (2L+1)$ sample points.

### 3.4.2 Direct Quadrature Evaluation

Here, we discuss computation of the commutative convolution by evaluating the integral in (3.8), with $\omega = \pi - \varphi$, directly using a quadrature rule on the sphere. If the output is required to be computed on the equiangular grid $\mathfrak{S}(N)$ on the sphere, the signals $f$ and $h$ are required to be sampled on the same grid. By virtue of the sampling theorem for band-limited signals on the sphere [41], if $N \geq \max(L_f, L_h)$, the integral can be computed *exactly* as summation over the spatial domain samples by employing the quadrature weights associated with the sampling scheme. Since the integral is computed as a two dimensional summation over the grid $\mathfrak{S}(N)$, evaluated for each sample point on the two dimensional grid $\mathfrak{S}(N)$ of the output, the computational complexity to obtain the convolution output $g_{\pi-\varphi}(\vartheta, \varphi)$ on the grid $\mathfrak{S}(N)$ is $O(N^4)$.

### 3.4.3 Semi-Fast Algorithm - SO(3) Convolution Case

Here, we present the computation of commutative convolution using the fast algorithm for SO(3) convolution described in [45] to obtain the convolution output $g(\varphi, \vartheta, \omega)$ given in (3.2) and defined on SO(3), followed by the mapping along

$\omega = \pi - \varphi$ to obtain $g_{\pi-\varphi}(\vartheta, \varphi)$ as

$$g_{\pi-\varphi}(\vartheta, \varphi) = g(\varphi, \vartheta, \omega)\Big|_{w=\pi-\varphi}. \tag{3.26}$$

Following (3.14), we rewrite (3.15) as

$$\begin{aligned} g(\varphi, \vartheta, \omega) &= \sum_{s=0}^{L} \sum_{t=-s}^{s} \sum_{t'=-s}^{s} (-1)^t \big(f\big)_s^{-t} \big(h\big)_s^{t'} D_s^{t,t'}(\varphi, \vartheta, \omega) \\ &= \sum_{s=0}^{L} \sum_{t=-s}^{s} \sum_{t'=-s}^{s} (-1)^t \big(f\big)_s^{-t} \big(h\big)_s^{t'} \\ &\qquad \times e^{-it\varphi} d_s^{t,t'}(\vartheta) e^{-it'\omega}, \end{aligned} \tag{3.27}$$

where $L = \min(L_f, L_h)$. The direct computation of (3.27) involves three summations for sample points defined on a three dimensional grid and therefore has complexity $O(L^3 N^3)$. We note that the summations over $t$ and $t'$ involve complex exponentials and therefore can be computed efficiently by using FFT, reducing the overall complexity to $O(LN^3 \log_2 N)$, which is not better than the complexity of the direct quadrature case if $L \log_2 N > N$. However, it can be further lowered by using the factoring of rotation approach, originally presented in [84] and then applied for fast computation of SO(3) convolution [45].

By factoring the single rotation $\vartheta$ around $y$-axis as

$$\mathcal{D}(0, \vartheta, 0) = \mathcal{D}(-\pi/2, -\pi/2, \vartheta)\, \mathcal{D}(0, \pi/2, \pi/2) \tag{3.28}$$

and again incorporating the effect of rotation on spherical harmonic coefficients given in (2.27) and the definition of Wigner-$D$ function in (2.28), we can write the Wigner-$d$ function in (3.27) as

$$d_s^{t,t'}(\vartheta) = i^{t-t'} \sum_{t''=-s}^{s} d_s^{t'',t}(\pi/2)\, d_s^{t'',t'}(\pi/2)\, e^{-it''\vartheta}, \tag{3.29}$$

which is used to express the SO(3) convolution formulated in (3.27) as

$$\begin{aligned} g(\varphi, \vartheta, \omega) = \sum_{s=0}^{L} \sum_{t=-s}^{s} \sum_{t'=-s}^{s} \sum_{t''=-s}^{s} & i^{3t-t'} \big(f\big)_s^{-t} \big(h\big)_s^{t'} \\ & \times d_s^{t'',t}(\pi/2)\, d_s^{t'',t'}(\pi/2)\, e^{-it\varphi - it''\vartheta - it'\omega}, \end{aligned} \tag{3.30}$$

and rearrangement of the terms yields

$$g(\varphi,\vartheta,\omega) = \sum_{t=-s}^{s} \sum_{t'=-s}^{s} \sum_{t''=-s}^{s} e^{-it\varphi - it''\vartheta - it'\omega},$$
$$\times \underbrace{\sum_{s=\max(|t|,|t'|,|t''|)}^{L} i^{3t-t'} \big(f\big)_s^{-t} \big(h\big)_s^{t'} d_s^{t''t}(\pi/2)\, d_s^{t''t'}(\pi/2)}_{I(t,t',t'')}. \tag{3.31}$$

We note that the convolution output in (3.31) is a 3-dimensional FFT of $I(t,t',t'')$. The rotation $\vartheta$, which accounts for the computation of the Wigner-$d$ function for all $\vartheta$, can be performed as a rotation around the $z$-axis by employing the factoring of rotation given in (3.28), the effect of which can be expressed using complex exponential and Wigner-$d$ functions evaluated at $\pi/2$ only.

The evaluation of $I(t,t',t'')$ involves the summation over $s$ for three dimensions $t$, $t'$, $t''$ and therefore has complexity $O(L^4)$. Using $I(t,t',t'')$, the SO(3) convolution output $g(\varphi,\vartheta,\omega)$ in (3.31) on the grid $\mathfrak{C}(N)$ can be computed in $O(N^3 \log_2 N)$. The overall complexity to evaluate SO(3) convolution is therefore $O(L^4 + N^3 \log_2 N)$ which is better than the complexity of the exact quadrature case.

As we mentioned earlier, once the SO(3) convolution output $g(\varphi,\vartheta,\omega)$ is obtained, it can be used to determine the commutative convolution output $g_{\pi-\varphi}(\vartheta,\varphi)$ using (3.26). This method of using existing fast algorithms for SO(3) convolution to evaluate the commutative convolution enables the efficient computation in the harmonic space, however it involves redundancy in the computation as the current efficient method evaluates the SO(3) convolution output for all $\omega \in [0, 2\pi)$. Instead, we only need the SO(3) convolution output for $\omega = \pi - \varphi$. We remove this redundancy in the computation and propose fast algorithm in the next subsection.

**Remark 3.2** *Although both $\varphi$ and $\omega$ are defined for $[0, 2\pi)$, we have deliberately chosen different sampling criterion along $\varphi$ and $\omega$ in the definition of our adopted* SO(3) *sampling scheme $\mathfrak{C}(N)$ (see Section 3.4.1). Specifically we have considered $2N+1$ (an odd number) samples along both $\varphi$ and $\omega$, but the sampling points along $\varphi$ are symmetric around $\varphi = 0$ and the sampling points along $\omega$ are symmetric around $\omega = \pi$. This is in contrast to the conventional* SO(3) *sampling [24]. However, it is necessary here as we are evaluating the commutative convolution $g_{\pi-\varphi}(\vartheta,\varphi)$ using* SO(3) *convolution $g(\varphi,\vartheta,\omega)$ with the constraint $\omega = \pi - \phi$, which can only be applied if the proposed sampling $\mathfrak{C}(N)$ for* SO(3) *is used.*

### 3.4.4 Proposed Fast Algorithm

Here, we propose a fast algorithm for the evaluation of commutative convolution on the sphere. Following the harmonic domain formulation of SO(3) convolution in (3.30) and using the relation between the convolution output on SO(3) and the commutative convolution output on $\mathbb{S}^2$, we can express $g_{\pi-\varphi}(\vartheta,\varphi)$ as

$$g_{\pi-\varphi}(\vartheta,\varphi)=\sum_{t''=-L}^{L} e^{-it''\vartheta}J(t'',\varphi)K(t'',\varphi), \tag{3.32}$$

where

$$J(t'',\varphi)=\sum_{t=-s}^{s}\sum_{s=\max(|t|,|t''|)}^{L}(-i)^t\big(f\big)_s^{-t}\,d_s^{t''t}(\pi/2)e^{-it\varphi} \tag{3.33}$$

and

$$K(t'',\varphi)=\sum_{t'=-s}^{s}\sum_{s=\max(|t'|,|t''|)}^{L}(i)^{t'}\big(h\big)_s^{t'}\,d_s^{t''t'}(\pi/2)e^{it'\varphi}. \tag{3.34}$$

We note that the constraint $\omega=\pi-\phi$, which yields the commutativity, also allows the decoupling of Wigner-$D$ functions in (3.32), so that the summations over $t$ and $t'$, given in (3.33) and (3.34) respectively, can be computed independently. Since the computations of both $J(t'',\varphi)$ and $K(t'',\varphi)$ involve summation over complex exponentials, we can employ FFTs to compute the summations efficiently. For the convolution output on the grid $\mathfrak{S}(N)$ with $N\geq\max(L_f,L_h)$, both $J(t'',\varphi)$ and $K(t'',\varphi)$ for each $t''$ and for all $2N+1$ points along $\varphi$ can be computed in $O(LN\log_2 N)$ using FFT and the product of $J(t'',\varphi)$ and $K(t'',\varphi)$ can be computed in $O(N)$ computations for each $t''$. Thus the overall complexity to obtain the product of $J(t'',\varphi)$ and $K(t'',\varphi)$ for each $s$ and for each $t''$ is $O(LN\log_2 N)$ and for all $t''$ is $O(LN^2\log_2 N)$. Finally, the sum over $t''$ can be computed efficiently in $O(N^2\log_2 N)$ again using the FFT. Therefore, the overall complexity of proposed fast algorithm is $O(LN^2\log_2 N)$, which is better than the complexities of both the exact quadrature and semi-fast algorithms.

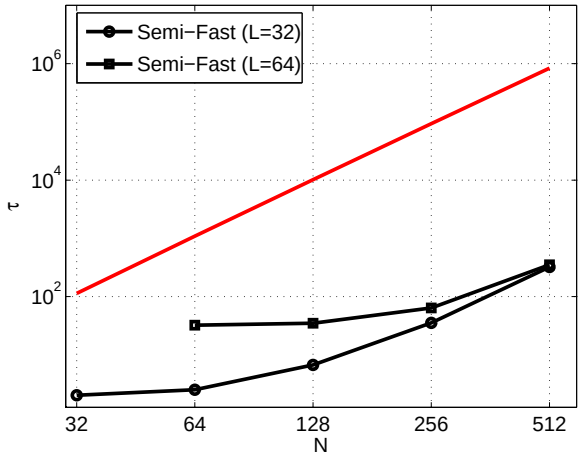


Figure 3.4: The computation time $\tau$ in seconds for the semi-fast algorithm to compute the convolution output $g_{\pi-\varphi}(\vartheta, \varphi)$ on grid $\mathfrak{S}(N)$ for $L = 32$ and 64. The computation time scales as $N^3 \log_2 N$ as indicated by red solid line (without markers).

### 3.4.5 Computation of Wigner-$d$ Function

We note that both the semi-fast and fast algorithms require Wigner-$d$ functions evaluated for argument $\pi/2$. By reviewing (3.31), (3.33) and (3.34), we note that we need to compute Wigner-$d$ function $d_s^{t'',t}(\pi/2)$ on the entire $(t'', t)$ plane. During implementation, the Wigner-$d$ function $d_s^{t'',t}(\pi/2)$ can be computed on the plane $(t'', t)$ for a given $s$ by using the recursion method proposed in [88] with complexity $O(L^2)$, which does not alter the overall complexity of the algorithms (either semi-fast or fast).

### 3.4.6 Computation Time Comparison

In this section, we demonstrate and compare the computation time of the semi-fast and fast algorithms to evaluate the commutative anisotropic convolution. We have implemented our algorithms using `MATLAB`, adopting the equiangular tessellations, defined in Section 3.4.1. We have recorded the computation time $\tau$ (in seconds) to evaluate convolution output $g_{\pi-\varphi}(\vartheta, \varphi)$ on the grid $\mathfrak{S}(N)$ for $L = 32$ and $L = 64$ and for different values of $N$. We generate the band-limited test signal on the sphere by using uniformly distributed spherical harmonic coefficients with real and imaginary parts in the range of $[-1, 1]$. The numerical experiments are conducted on a 2.4 GHz Intel Xeon processor with 64 GB of RAM and the computation times are averaged over twenty test signals.

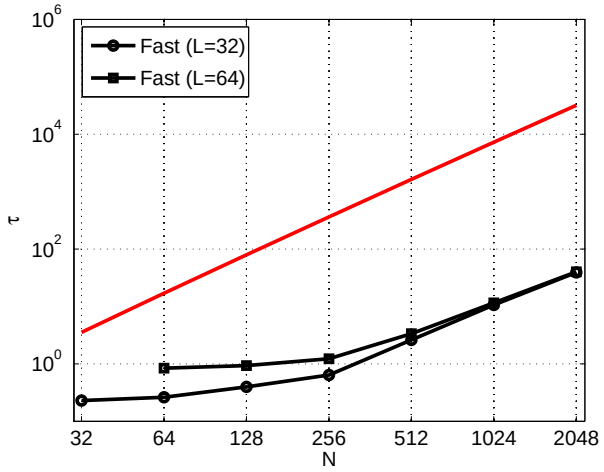


Figure 3.5: The computation time $\tau$ in seconds for proposed fast algorithm to compute the convolution output $g_{\pi-\varphi}(\vartheta, \varphi)$ on grid $\mathfrak{S}(N)$ for $L = 32$ and 64. The computation time scales as $N^2 \log_2$ N as indicated by red solid line(without markers).

The computation time $\tau$ taken by semi-fast algorithm to compute convolution output $g_{\pi-\varphi}(\vartheta, \varphi)$ is shown in Fig. 3.4 on log-log axes for different values of $N$, where the computation time grows as $N^3 \log_2 N$. For the proposed fast algorithm, the computation time $\tau$ scales as $N^2 \log_2 N$ as shown in Fig. 3.5. For comparison, we have also plotted the computation time for both semi-fast and fast algorithm on a linear scale along time axis as shown in Fig. 3.6. We note that the simulation results agree with the theoretically evaluated computational complexities of the algorithms and thus corroborate the mathematical developments.

## 3.5 Summary of Contributions

In this chapter, we have established a new type of convolution between two signals on the 2-sphere. Since, the proposed convolution admits anisotropic signals and filters and it is commutative with the output defined on the sphere, the proposed convolution serves as a close analog of the conventional Euclidean convolution. After presenting the new definition of convolution and discussing its properties, we have provided the spectral analysis of the convolution output. We have also developed fast algorithm to efficiently compute the proposed commutative convolution. The contributions made in this chapter are as follows.

Addressing Q1 posed in Section 1.2.1:

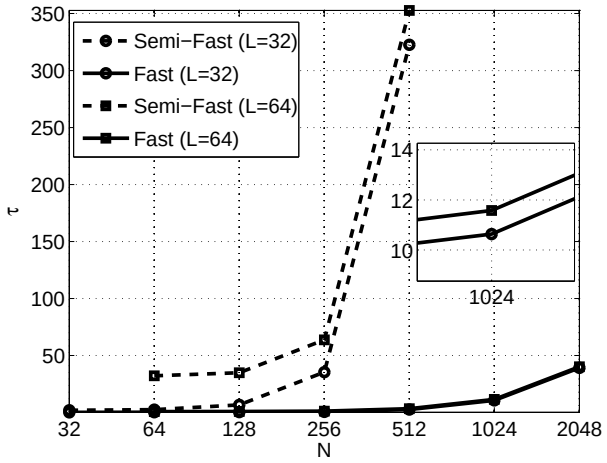


Figure 3.6: Comparison of the computation time $\tau$ (in seconds) for the semi-fast and fast algorithms to compute the convolution output $g_{\pi-\varphi}(\vartheta, \varphi)$ on grid $\mathfrak{S}(N)$ for $L = 32$ and 64.

- We have proposed the new definition of convolution on the sphere which well emulates its counterpart in Euclidean domain. The proposed convolution generates an output defined on $\mathbb{S}^2$ and is formulated as a double integral over $\mathbb{S}^2$. Furthermore, it is anisotropic and commutative in general, i.e., the directional features of both filter and signal contribute towards the output of convolution, and changing the roles of filter and signal does not change the outcome of convolution. We have also provided the geometrical interpretation and illustration of the proposed commutative convolution.

- We have provided the geometrical interpretation and illustration of the proposed commutative convolution. Moreover, the proposed convolution is also analyzed in spectral domain.

- We have proposed the fast algorithm which employs the factoring of rotation approach followed by the separation of variables technique. For the evaluation of the commutative convolution output on $O(N^2)$ samples on the 2-sphere, the proposed fast algorithm provides a saving of $O(N)$ in terms of the computational complexity over the semi-fast algorithm. Finally, simulation results have been presented to verify the theoretical improvement in the computational complexity.

# Chapter 4

# Spatially Localized Spherical Harmonic Transform for Spatio-spectral Analysis

In time-frequency analysis, the short-time Fourier transform (STFT) has been widely explored, investigated and used in many applications to analyze the localized spectral contents of the signal [64, 65, 72, 80, 89]. In this chapter, we develop a tool analogous to the STFT for signals defined on the unit sphere. The objective is to devise a distribution that represents how the signal spectrum varies in the spatial domain. We propose a transform, which we call the spatially localized spherical harmonic transform (SLSHT), as an analog of STFT to represent the signal jointly in spatial and spectral domains. For this purpose, we focus on the use of azimuthally symmetric window functions to achieve localization in the spatial domain and express the transform in terms of the rotation applied to the original window. We also give a succinct matrix representation of all possible SLSHT components, which we refer to as the SLSHT distribution. We also present a distribution transform operation inspired by the characteristic function in time-frequency analysis [64, 65], which transforms SLSHT distribution into a new spatio-spectral distribution which we call the complementary distribution.

We discuss the inherent trade-off between the spatial and spectral resolution of different window functions from the perspective of the uncertainty principle. This will help us in determining suitable choices for window functions for SLSHT. We propose and demonstrate the use of an eigenfunction window, obtained from

the Slepian concentration problem on the sphere [20], as a good choice for the window function in the SLSHT. As an illustration, we apply the SLSHT distribution with eigenfunction window to the example of the Mars topographic map and show that the localized contributions of spherical harmonics are apparent in the spatio-spectral domain.

The chapter is organized as follows. We summarize STFT in time-frequency analysis and its properties briefly in Section 4.1. The proposed spatially localized spherical harmonic transform, its matrix formulation and signal inversion are presented in Section 4.2. The complementary distribution and its properties are defined in Section 4.3. The window localization trade-off is discussed in Section 4.4 and an example to illustrate the usefulness of the proposed transform are presented in Section 4.5.

## 4.1 Time-Frequency Signal Analysis using Short Time Fourier Transform

A time domain signal can be equivalently represented in the frequency domain. While there is an equivalence between the signal representations in these two domains, the signal in one domain does not explicitly convey information about the localized contents in the other domain. Time-frequency signal processing deals with the analysis and processing of signals in a joint time-frequency domain.

### 4.1.1 Short-Time Fourier Transform (STFT)

The short-time Fourier transform (STFT) is a powerful tool which is widely used in time-frequency analysis to investigate time localized spectral characteristics of a signal [64, 65]. In order to study the time domain signal $f$ in the vicinity of time $t$ in frequency domain, a window function is used and Fourier analysis is performed. The STFT is given by

$$F(t,\omega) = \int f(\tau)\, h(t-\tau)\, e^{-i\omega\tau}\, d\tau, \tag{4.1}$$

where a time-shift of the window function, $h$, provides the localization in time. Hence, the time-frequency distribution using the STFT is the collection of Fourier transforms of the windowed signal about all points of translation $t$. For brevity,

the notation for the STFT, $F(t,\omega)$ in (4.1), suppresses the dependence on $h$.

The effectiveness of the STFT in (4.1) for various applications is sensitive to the selection of window function $h$ [64, 68, 89]. The basic problem in window selection is the trade-off between a greater window width for better frequency resolution and a lesser window width for capturing the localized temporal properties of the signal [89].

### 4.1.2 Signal Inversion from STFT Distribution

The STFT representation of the signal in (4.1) belongs to the class of linear representations which satisfy simple reconstruction properties [64, 65]. The signal $f(t)$ can be recovered from its STFT representation $F(t,\omega)$, up to a constant factor, through the weighted marginal

$$\int F(t,\omega)\, e^{i\omega t}\, d\omega = C_1\, f(t) \tag{4.2}$$

and the Fourier transform $F(\omega)$ of the signal $f(t)$ can be obtained from $F(t,\omega)$ as frequency marginal which is obtained by integrating out the time variable as

$$\int F(t,\omega)\, dt = C_2\, F(\omega), \tag{4.3}$$

where $C_1$ and $C_2$ are constants which depend upon the window function.

### 4.1.3 Characteristic Function for STFT Distribution

The characteristic function has been widely used to study the localized characteristics of time-frequency distributions [64, 65]. The characteristic function $M(\varsigma,\tau)$ for the STFT representation $F(t,\omega)$ is defined as [65]

$$M(\varsigma,\tau) = \iint \left|F(t,\omega)\right|^2 e^{i\varsigma t}\, e^{i\tau\omega}\, dt\, d\omega. \tag{4.4}$$

We can see that the characteristic function $M(\varsigma,\tau)$ is a transformed distribution which is equivalent to the two dimensional inverse Fourier transform of the squared magnitude of the STFT distribution $F(t,\omega)$ in (4.1). We make it clear here that the we are interested in the STFT based time-frequency representation of a signal, whereas the term "time-frequency distributions" in this thesis is used to represent

large class of time-frequency representations of a signal [64, 65].

## 4.2 Spatially Localized Spherical Harmonic Transform

### 4.2.1 Definition of SLSHT

We define the SLSHT in analogy to the STFT in time-frequency analysis. Judicious choices of rotations on the sphere serve as counterparts of translations in (4.1) in the time domain. We re-locate, through rotation, an azimuthally-symmetric window function (centered at the north pole) to achieve localization in the spatial domain. We first define the SLSHT and use it to define the SLSHT distribution as spatio-spectral representation of the signal.

**Definition 4.1 (Spatially Localized Spherical Harmonic Transform)** *For a signal $f \in L^2(\mathbb{S}^2)$, define the directional SLSHT $g(\hat{\boldsymbol{y}}; \ell, m) \in L^2(\mathbb{S}^2)$ of degree $\ell$ and order $m$ as the spherical harmonic transform of a localized signal where localization is provided by the rotation operator $\mathcal{D}(\varphi, \vartheta, 0)$ acting on azimuthally symmetric window function $h \in L^2(\mathbb{S}^2)$, i.e.,*

$$g(\hat{\boldsymbol{y}}; \ell, m) = g(\hat{\boldsymbol{y}}; n) \triangleq \int_{\mathbb{S}^2} \big(\mathcal{D}(\varphi, \vartheta, 0)h\big)(\hat{\boldsymbol{x}}) f(\hat{\boldsymbol{x}}) \overline{Y_\ell^m(\hat{\boldsymbol{x}})}\, ds(\hat{\boldsymbol{x}}),$$
$$\hat{\boldsymbol{y}} = \hat{\boldsymbol{y}}(\vartheta, \varphi),\ (\ell, m) \leftrightarrow n. \tag{4.5}$$

The SLSHT is dependent on the chosen window $h$, but for brevity, this dependence is not explicit in the notation. We emphasize that, unlike the spherical harmonic coefficient of the signal $f$, $\big(f\big)_\ell^m$, which is only a function of degree $\ell$ and order $m$, the SLSHT provides a spatially-varying spherical harmonic representation of the signal (i.e., $g(\hat{\boldsymbol{y}}; \ell, m)$ is a function of the spatial localization $\hat{\boldsymbol{y}}$ and degree and order). We call $g(\hat{\boldsymbol{y}}; \ell, m)$ the SLSHT of degree $\ell$ and order $m$.

### 4.2.2 SLSHT Harmonic Expansion

Here, we express the relation between the SLSHT $g(\hat{\boldsymbol{y}}; \ell, m)$ and the spherical harmonic coefficients of the signal $f$. First we determine the spherical harmonic coefficients corresponding to the rotated window. We are interested in the case

where both the signal $f(\hat{\boldsymbol{x}})$ and the window kernel $h(\hat{\boldsymbol{x}})$ are band-limited. Let us assume that $f(\hat{\boldsymbol{x}}) \in \mathcal{H}_{L_f}$ and $h(\hat{\boldsymbol{x}}) \in \mathcal{H}_{L_h}$ (since the kernel is assumed to be azimuthally symmetric, $h(\hat{\boldsymbol{x}}) \in \mathcal{H}^0_{L_h} \subset \mathcal{H}^0$ would be a more precise notation).

Specializing (2.31) for the SLSHT window kernel $h$ at point $\hat{\boldsymbol{x}} = \hat{\boldsymbol{x}}(\theta, \varphi)$, we define

$$\big(h\big)_r(\hat{\boldsymbol{y}}) \triangleq \big\langle \mathcal{D}(\varphi, \vartheta, 0)h, Y_r \big\rangle = \sqrt{\frac{4\pi}{2p+1}}\overline{Y_p^q(\hat{\boldsymbol{y}})}\big(h\big)_p^0, \quad \hat{\boldsymbol{y}} = \hat{\boldsymbol{y}}(\vartheta, \varphi), \quad (p,q) \leftrightarrow r. \tag{4.6}$$

Using (4.6), (2.12), (2.13) and the mapping $(s,t) \leftrightarrow u$, we can alternatively write $g(\hat{\boldsymbol{y}}; n)$ in (4.5) as

$$g(\hat{\boldsymbol{y}}; n) = \sum_{u=0}^{N_f} \big(f\big)_u \sum_{r=0}^{N_h} \big(h\big)_r(\hat{\boldsymbol{y}})\, T(u; r; n), \tag{4.7}$$

where $N_h = L_h^2 + 2L_h$ and

$$T(u; r; n) = T(r; u; n) \triangleq \int_{\mathbb{S}^2} Y_r(\hat{\boldsymbol{x}}) Y_u(\hat{\boldsymbol{x}}) \overline{Y_n(\hat{\boldsymbol{x}})}\, ds(\hat{\boldsymbol{x}}) \tag{4.8}$$

denotes the spherical harmonic triple product, the explicit expression of which is provided in (2.24).

**Remark 4.1** *It is implicit in the formulation of SLSHT that the signal of interest is band-limited to $L_f < \infty$. As a signal has finite energy, its spherical harmonic Fourier coefficients are square summable. Consequently, any signal can be arbitrarily closely approximated by a band-limited signal by making $L_f$ sufficiently large. The study of the involved approximation errors on the SLSHT is outside the scope of this thesis.*

**Remark 4.2** *It is important to note here that each SLSHT component of the form $g(\hat{\boldsymbol{y}}; n)$ is a band-limited function on the sphere with band-limit $L_h$, that is, $\big\langle g(\hat{\boldsymbol{y}}; n), Y_r^s \big\rangle = 0$ for all $r > L_h$.*

### 4.2.3 SLSHT Distribution and Matrix Formulation

**Definition 4.2 (SLSHT Distribution)** *The SLSHT distribution $\boldsymbol{g}(\hat{\boldsymbol{x}})$ of a signal $f \in L^2(\mathbb{S}^2)$ is an indexed vector of all SLSHT components of the form $g(\hat{\boldsymbol{y}}; n)$*

*as defined in (4.5) for* $n = 0, 1, \cdots, N_g$*, i.e.,*

$$\boldsymbol{g}(\hat{\boldsymbol{y}}) \triangleq \big(g(\hat{\boldsymbol{y}}; 0),\, g(\hat{\boldsymbol{y}}; 1),\, g(\hat{\boldsymbol{y}}; 2),\, \cdots,\, g(\hat{\boldsymbol{y}}; N_g)\big)', \tag{4.9}$$

*where* $N_g = L_g^2 + 2L_g$ *and* $L_g = L_f + L_h$*.*

**Remark 4.3** *The SLSHT distribution is a generalization of the transform in [4] and provides the representation of a signal in the joint spatio-spectral domain.*

Using the preceding formulation, the SLSHT distribution $\boldsymbol{g}(\hat{\boldsymbol{y}})$ in (4.9) can be written in matrix form as

$$\boldsymbol{g}(\hat{\boldsymbol{y}}) = \boldsymbol{\Psi}(\hat{\boldsymbol{y}})\boldsymbol{f}, \tag{4.10}$$

where $\boldsymbol{f} = \big(\mathcal{F}f\big)(\hat{\boldsymbol{x}})$ and $\boldsymbol{\Psi}$ is the transformation operator matrix of size $(N_g+1)\times(N_f+1)$, which transforms the given signal in spectral domain to the spatio-spectral domain and is given by

$$\boldsymbol{\Psi}(\hat{\boldsymbol{y}}) = \begin{bmatrix} \psi_{0,0}(\hat{\boldsymbol{y}}) & \psi_{0,1}(\hat{\boldsymbol{y}}) & \cdots & \psi_{0,N_f}(\hat{\boldsymbol{y}}) \\ \psi_{1,0}(\hat{\boldsymbol{y}}) & \psi_{1,1}(\hat{\boldsymbol{y}}) & \cdots & \psi_{1,N_f}(\hat{\boldsymbol{y}}) \\ \vdots & \vdots & & \vdots \\ \psi_{N_g,0}(\hat{\boldsymbol{y}}) & \psi_{N_g,1}(\hat{\boldsymbol{y}}) & \cdots & \psi_{N_g,N_f}(\hat{\boldsymbol{y}}) \end{bmatrix} \tag{4.11}$$

with entries

$$\psi_{n,u}(\hat{\boldsymbol{y}}) = \sum_{r=0}^{N_h} \big(h\big)_r(\hat{\boldsymbol{y}})\, T(u; r; n). \tag{4.12}$$

**Remark 4.4** *The matrix form in (4.10) transforms the spectral response of the signal* $\boldsymbol{f}$ *to the joint spatio-spectral domain. The size of the transformation matrix is dependent on the spectral bandwidth of the input signal* $f$ *and the window function* $h$*. The value of matrix elements is dependent on the applied rotation* $\hat{\boldsymbol{y}}$ *and the window function* $h$*, whose choice will be discussed in Section 4.4.*

### 4.2.4 Inversion of Signal from its SLSHT distribution

Recovery of the spectral components of the signal from its localized transform was first shown in [4]. For the sake of completeness, based on our matrix formulation, and explicit expression of the transform in terms of rotated window function, we provide an alternative formulation. We present the result in the following theorem.

**Theorem 4.1 (Inversion of Signal from SLSHT Distribution)** *If $\boldsymbol{g}(\hat{\boldsymbol{y}})$ represents the SLSHT distribution of the signal $f$ using an azimuthally symmetric window function $h$, where the distribution is of the form (4.9), then the spectral domain response $\boldsymbol{f}$ of $f$ can be recovered from $\boldsymbol{g}(\hat{\boldsymbol{y}})$ up to a multiplicative factor as the spherical harmonics marginal $\hat{\boldsymbol{f}}$, which is obtained by integrating the SLSHT distribution over the spatial domain as*

$$\hat{\boldsymbol{f}} = \int_{\mathbb{S}^2} \boldsymbol{g}(\hat{\boldsymbol{y}})\, ds(\hat{\boldsymbol{y}}) = \sqrt{4\pi}\,\big(h\big)_0^0 \times \big(\,\big(f\big)_0,\, \big(f\big)_1,\, \cdots,\, \big(f\big)_{N_f},\, 0,\, \cdots,\, 0\,\big)', \quad (4.13)$$

*where $\hat{\boldsymbol{f}}$ denotes the spherical harmonics marginal and is a vector of length $N_g + 1$ where only the first $N_f + 1$ elements are non-zero.*

**Proof**

Integrating (4.10) over the spatial domain gives

$$\int_{\mathbb{S}^2} \boldsymbol{g}(\hat{\boldsymbol{y}})\, ds(\hat{\boldsymbol{y}}) = \big(\int_{\mathbb{S}^2} \boldsymbol{\Psi}(\hat{\boldsymbol{y}})\, ds(\hat{\boldsymbol{y}})\big)\, \boldsymbol{f}. \quad (4.14)$$

The integral of kernel matrix $\boldsymbol{\Psi}$ is obtained by integrating each matrix element $\psi_{n,u}(\hat{\boldsymbol{y}})$ in (4.12), that is,

$$\psi_{n,u}(\hat{\boldsymbol{y}})\, ds(\hat{\boldsymbol{y}}) = \sum_{r=0}^{N_h} T(u;r;n) \int_{\mathbb{S}^2} \big(h\big)_r(\hat{\boldsymbol{y}})\, ds(\hat{\boldsymbol{y}}) \quad (4.15)$$

Now, using the definition of $\big(h\big)_r(\hat{\boldsymbol{y}})$ in (4.6) with mapping $(p,q) \leftrightarrow r$, we obtain

$$\begin{aligned} \big(h\big)_r(\hat{\boldsymbol{y}}) &= \sqrt{\frac{4\pi}{2p+1}}\big(h\big)_p^0 \int_{\mathbb{S}^2} \overline{Y_p^q(\hat{\boldsymbol{y}})} ds(\hat{\boldsymbol{y}}) \\ &= \frac{4\pi}{\sqrt{2}p+1}\big(h\big)_p^0 \delta_{p,0}\delta_{q,0} \\ &= 4\pi\,\big(h\big)_0^0 \delta_{r,0}. \end{aligned} \quad (4.16)$$

Using (4.16), all the summation terms in (4.15) become zero except for $r = 0$. From the orthonormal property of spherical harmonics, $T(0;r;n) = \delta_{r,n}/\sqrt{4\pi}$. Incorporating these results in (4.15), we get

$$\int_{\mathbb{S}^2} \psi_{n,u}(\hat{\boldsymbol{y}})\, ds(\hat{\boldsymbol{y}}) = \sqrt{4\pi}\big(h\big)_0^0\, \delta_{n,u}. \quad (4.17)$$

Substituting (4.17) in integrating the elements of $\boldsymbol{\Psi}(\hat{\boldsymbol{x}})$ in (4.14), we obtain (4.13).□

**Remark 4.5** *From Theorem 4.1, we can see that we only need to know the DC-component of the window function in order to recover the signal exactly from its SLSHT distribution.*

## 4.3 Complementary Distribution

In this section, we present the distribution transform operation that metamorphoses the proposed SLSHT distribution in (4.9) into a new type of distribution which we call its complementary distribution. We present a method to transform the SLSHT distribution into the complementary distribution using the definition inspired by the characteristic function in (4.4) in time-frequency analysis. As our proposed SLSHT distribution in (4.9) is not quadratic in nature, we use the proposed SLSHT distribution itself instead of its squared magnitude. We will show that the complementary distribution exhibits some desired properties as it reveals information about both the signal and window function. Here, we present the mathematical definition of complementary distribution and formulate a relation to express the complementary distribution in terms of the signal and the window function. We also develop a matrix formulation for the complementary distribution.

### 4.3.1 Complementary Distribution Transformation

In analogy with (4.4), the sought distribution transform transforms the spatial domain component to a corresponding spectral domain component and the spectral domain component to a spatial domain component.

**Definition 4.3 (Spatio-spectral Complementary Distribution)** *We define the spatio-spectral complementary distribution* $\boldsymbol{\kappa}(\hat{\boldsymbol{x}})$ *as:*

$$\boldsymbol{\kappa}(\hat{\boldsymbol{x}}) = \big(\, \kappa(0, \hat{\boldsymbol{x}}),\, \kappa(1, \hat{\boldsymbol{x}}),\, \kappa(2, \hat{\boldsymbol{x}}),\, \cdots,\, \kappa(N_h, \hat{\boldsymbol{x}}) \,\big)', \tag{4.18}$$

*where each element* $\kappa(c, \hat{\boldsymbol{x}})$ *of the complementary distribution is related to the components of SLSHT distribution* $\boldsymbol{g}(\hat{\boldsymbol{x}})$ *in* (4.9) *by*

$$\kappa(c, \hat{\boldsymbol{x}}) \triangleq \sum_{n=0}^{N_g} Y_n(\hat{\boldsymbol{x}}) \int_{\mathbb{S}^2} g(\hat{\boldsymbol{y}}, n) \overline{Y_c(\hat{\boldsymbol{y}})}\, ds(\hat{\boldsymbol{y}}). \tag{4.19}$$

**Remark 4.6** *By comparing* (4.19) *with* (2.12)*, we note that* $\kappa(c, \hat{\boldsymbol{x}})$ *is a band-limited function on the sphere with band-limit* $L_g = L_f + L_h$*.*

Using the expansion of $g(\hat{\boldsymbol{y}}, n)$ in (4.7) and matrix formulation in (4.10), the complementary distribution can be expressed in matrix form as

$$\kappa(\hat{\boldsymbol{x}}) = \boldsymbol{\Upsilon}(\hat{\boldsymbol{x}})\boldsymbol{f}, \tag{4.20}$$

where $\boldsymbol{\Upsilon}(\hat{\boldsymbol{x}})$ is a matrix of size $(N_h + 1) \times (N_f + 1)$ that transforms the signal into its complementary distribution and the entries of the matrix $\boldsymbol{\Upsilon}(\hat{\boldsymbol{x}})$ are given by

$$\Upsilon_{u,c}(\hat{\boldsymbol{x}}) = (-1)^b \sqrt{\frac{4\pi}{2a+1}} \big(h\big)_a^0 \sum_{n=0}^{N_g} Y_n(\hat{\boldsymbol{x}})\, T(s, t; a, -b; \ell, m) \tag{4.21}$$

with mappings $(r, s) \leftrightarrow u$, $(a, b) \leftrightarrow c$ and $(\ell, m) \leftrightarrow n$. The matrix formulation in (4.20) transforms the signal directly into its complementary distribution and $\boldsymbol{\Upsilon}(\hat{\boldsymbol{x}})$ acts as the transformation matrix for this distribution transform operation.

### 4.3.2 Spherical Harmonics Marginal of Complementary Distribution

We present the spherical harmonics marginal of complementary distribution in the form of the following Theorem.

**Theorem 4.2 (Spherical Harmonics Marginal of Complementary Distribution)** *If* $\kappa$ *represents the complementary distribution of the signal* $f$ *as defined in* (4.18) *using azimuthally symmetric window function* $h$*, then the spherical harmonics marginal of* $\kappa$ *is obtained by integrating the distribution over the spatial domain and is given by*

$$\int_{\mathbb{S}^2} \kappa(\hat{\boldsymbol{x}})\, ds(\hat{\boldsymbol{x}}) = \big( [hf]_0,\, [hf]_1,\, \cdots,\, [hf]_{N_h} \big)', \tag{4.22}$$

*where*

$$[hf]_c = \frac{1}{\sqrt{4\pi(2a+1)}} \big(h\big)_a^0 \big(f\big)_a^b \tag{4.23}$$

*with* $(a, b) \leftrightarrow c$*.*

**Proof**

We obtain the spherical harmonics marginal of the distribution $\kappa$ by integrating (4.20) over the spatial domain

$$\int_{\mathbb{S}^2} \kappa(\hat{\boldsymbol{x}})\, d\hat{\boldsymbol{x}} = \Big( \int_{\mathbb{S}^2} \boldsymbol{\Upsilon}(\hat{\boldsymbol{x}})\, ds(\hat{\boldsymbol{x}}) \Big) \boldsymbol{f}. \tag{4.24}$$

The integral of kernel matrix $\boldsymbol{\Upsilon}(\hat{\boldsymbol{x}})$ is obtained by integrating each matrix element. Using the definition of $\Upsilon_{u,c}(\hat{\boldsymbol{x}})$ in (4.21), we can write

$$\int_{\mathbb{S}^2} \Upsilon_{u,c}(\hat{\boldsymbol{x}})\, ds(\hat{\boldsymbol{x}}) = (-1)^b \sqrt{\frac{4\pi}{2a+1}} \big(h\big)_a^0 \sum_{n=0}^{N_g} T(s,t;a,-b;\ell,m) \int_{\mathbb{S}^2} Y_n(\hat{\boldsymbol{x}}) ds(\hat{\boldsymbol{x}}). \tag{4.25}$$

As a consequence of the integration over the whole sphere, all the summation terms in (4.25) become zero except for $n = 0$, which implies $\ell = 0$ and $m = 0$. In addition, using the orthonormal property of spherical harmonics and the definition of the spherical harmonics triple product in (4.8), we have

$$T(s,t;a,-b;0,0) = \frac{(-1)^b \delta_{s,a} \delta_{t,b}}{\sqrt{4\pi}}, \tag{4.26}$$

with $(a,b) \leftrightarrow c$ and $(r,s) \leftrightarrow t$. Incorporating these results in (4.25), we get

$$\int_{\mathbb{S}^2} \Upsilon_{u,c}(\hat{\boldsymbol{x}})\, ds(\hat{\boldsymbol{x}}) = \frac{\big(h\big)_a^0}{\sqrt{4\pi(2a+1)}} \delta_{s,a} \delta_{t,b}. \tag{4.27}$$

Upon substituting (4.27) for matrix elements of $\boldsymbol{\Upsilon}$ in (4.24), we obtain the result (4.22) stated in Theorem 4.2. □

**Remark 4.7** *The result in Theorem 4.2 states that the spherical harmonics marginal of complementary distribution gives the element-wise product of spherical harmonic coefficients of the signal $f$ and window function $h$ with a scaling factor that depends upon the degree of the spherical harmonic coefficients. Using this property of complementary distribution* (4.22)*, we can recover the window function completely from its distribution assuming we obtain the signal first from its SLSHT distribution $\boldsymbol{g}(\hat{\boldsymbol{x}})$. In conclusion, all we need is the DC-component of the window function $\big(h\big)_0^0$ to recover both the signal and window function from its proposed SLSHT distribution or complementary distribution. Note that the window function cannot be*

*directly recovered from the SLSHT distribution.*

## 4.4 Optimal Spatio-spectral Concentration of Window Function

The SLSHT distribution does not depend solely on the signal because the distribution entangles the signal and the window. The effectiveness of SLSHT distribution to reveal the information about the localized spectral contents of a signal in the spatio-spectral domain depends on the chosen window function. If we require higher resolution in one domain, the window should be narrower in that domain. From the uncertainty principle on the unit sphere, a signal cannot be locally concentrated in both the spatial and spectral domains [78]. If a window is chosen to obtain the desired resolution in one domain, it is said to be an optimal window if it is also optimally localized in the other domain [65].

We study the window functions jointly in both spatial and spectral domains using the definition of uncertainty principle on the unit sphere. The following inequality, referred as the uncertainty principle, holds for unit energy azimuthally symmetric functions defined on the unit sphere [78, 90]

$$\frac{\sigma_{\mathrm{S}}}{\sqrt{1-\sigma_{\mathrm{S}}^2}} \cdot \sigma_{\mathrm{L}} \geq 1, \tag{4.28}$$

where $\sigma_{\mathrm{S}}$ and $\sigma_{\mathrm{L}}$ denote the variance of the window function in the spatial domain and spectral domain respectively and are defined as [1, 78]

$$\sigma_{\mathrm{S}}^2 = 1 - \Big(\pi \int_0^{\pi} \sin(2\theta) \left|h(\theta)\right|^2 d\theta \Big)^2, \quad \sigma_{\mathrm{L}}^2 = \sum_{\ell=0}^{\infty} \ell(\ell+1) |\big(h\big)_{\ell}^{0}|^2. \tag{4.29}$$

Note that a unit energy window function is assumed in (4.29), which ensures that $0 \leq \sigma_{\mathrm{S}} \leq 1$.

In this work, we consider and compare the following unit energy normalized azimuthally symmetric window functions: rectangular window, triangular window, cosine window, Hamming window, Hanning window, the window of Simons *et al.* [4], Gaussian window and the *eigenfunction window*, all of which are parameterized by $\theta_c$ denoting the window truncation width. The first five windows are defined in [91]. The window in [4] is obtained by truncating the rectangular win-

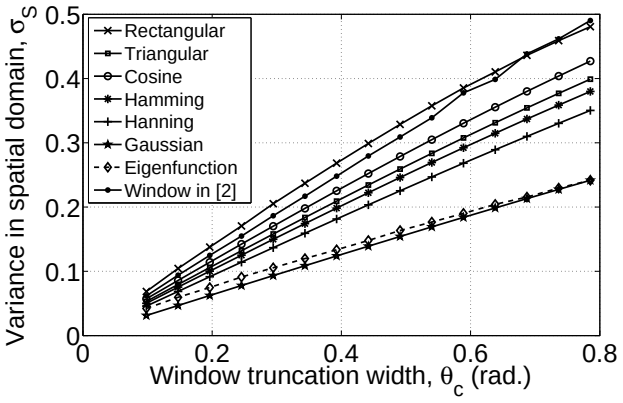


(a)

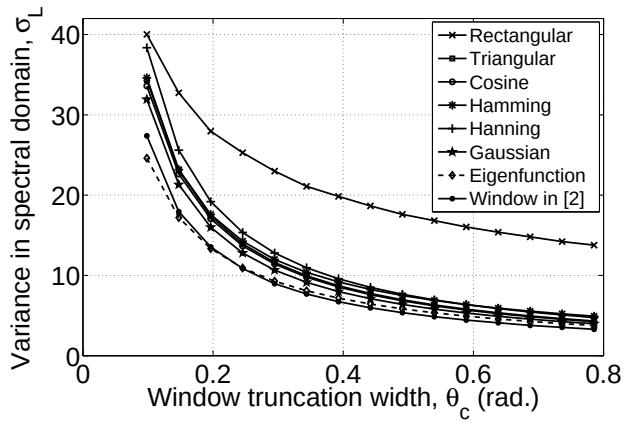


(b)

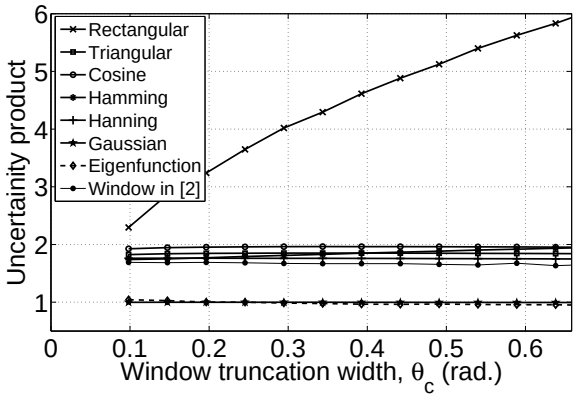


(c)

Figure 4.1: (a) Variance $\sigma_{\mathrm{S}}$ in spatial domain, (b) variance $\sigma_{\mathrm{L}}$ in spectral domain and (c) uncertainty product in (4.28) for different types of azimuthally symmetric window functions.

dow in the spectral domain within the main spectral lobe. The Gaussian window is a unit energy normalized function that decays exponentially with the square of

the colatitude and its variance is chosen such that 99% of the energy lies within the truncation width. The eigenfunction window $h(\hat{\boldsymbol{x}})$ arises as a solution of a Slepian concentration problem on the sphere [27]. To maximize the spatial concentration of a band-limited signal $h(\hat{\boldsymbol{x}})$ with maximum spherical harmonic degree $L_h$, equivalently represented by the column vector $\boldsymbol{h}^0$ containing the entries $\big(h\big)_\ell^0$ for $0 \leq \ell \leq L_h$, within a polar cap region $R$ characterized by truncation width $\theta_c$, one needs to maximize the spatial concentration ratio [1, 27]

$$\lambda = \frac{\int_R |h(\hat{\boldsymbol{x}})|^2 \, d\hat{\boldsymbol{x}}}{\int_{\mathbb{S}^2} |h(\hat{\boldsymbol{x}})|^2 \, d\hat{\boldsymbol{x}}}. \tag{4.30}$$

The solution that maximizes (4.30) gives rise to the standard eigenvalue problem $\mathbf{D}\boldsymbol{h}^0 = \lambda \boldsymbol{h}^0$, which can be solved numerically. As we are considering an azimuthally symmetric region $R$, $\boldsymbol{h}^0 = [\big(h\big)_0^0, \, \big(h\big)_1^0, \, \ldots, \, \big(h\big)_{L_h}^0]$ denotes the spectral response of $h(\hat{\boldsymbol{y}})$ and $\mathbf{D}$ is the $(L_h + 1) \times (L_h + 1)$ real and symmetric matrix where the entries are given by $D_{\ell\ell'} = \int_R Y_\ell^0(\hat{\boldsymbol{x}}) Y_{\ell'}^0(\hat{\boldsymbol{x}}) \, d\hat{\boldsymbol{x}}$. We use the band-limited eigenfunction as window function, the one corresponding to the largest eigenvalue and having minimum possible bandwidth $L_h$ is related to truncation width $\theta_c$ as $L_h = (2\pi/\theta_c) - 1$ [27].

Fig. 4.1 plots the (a) variance $\sigma_{\mathrm{S}}$ in spatial domain, (b) variance $\sigma_{\mathrm{L}}$ in spectral domain and (c) uncertainty product in (4.28) for different types of azimuthally symmetric window functions and different values of truncation width $\pi/32 \leq \theta_c \leq \pi/4$. Fig. 4.1(a) and Fig. 4.1(b) show that generally the variance in spatial domain increases with truncation width and the variance in spectral domain decreases with the truncation width. The rectangular window has the poorest localization because the discontinuity at truncation points increases its variance in the spectral domain. As expected, the window in [4] performs very well in the spectral domain, but poorly in the spatial domain. The figure also shows that the Gaussian window and the eigenfunction window exhibit better localization behavior. Comparatively, these two windows have the lowest variances in both domains. Note that the smaller value for variance indicates better localization. Fig. 4.1(c) confirms that both the eigenfunction window and the Gaussian window nearly attain the lower bound of 1 for the uncertainty product of (4.28). The rectangular window has the largest uncertainty product as expected. The product for other windows, including the window in [4], lie between these two extremes.

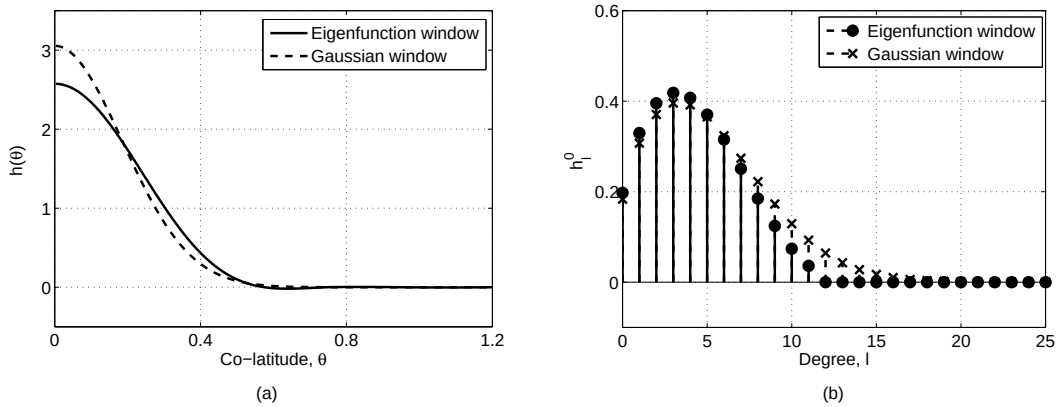


Figure 4.2: Gaussian window and eigenfunction window for truncation width, $\theta_c = \pi/6$ in (a) spatial domain, $h(\hat{\boldsymbol{x}}) = h(\theta)$ and (b) spectral domain, $\left(h\right)_\ell^0$. The eigenfunction window has less spectral bandwidth relative to the Gaussian window.

The optimal truncation width depends on the required resolution in both the spatial and spectral domains. As indicated in the variance plot in Fig. 4.1, the spatial variance $\sigma_{\mathrm{S}}$ of the eigenfunction window is very close to that of the Gaussian window. But the spectral variance $\sigma_{\mathrm{L}}$ of the eigenfunction window is lower than that of the Gaussian window, especially at lower truncation widths. The Gaussian window and eigenfunction window are plotted for truncation width $\theta_c = \pi/6$ in both spatial and spectral domains in Fig. 4.2. Both windows are normalized to unit energy and chosen such that 99% of energy lies within the truncation width. It is observed that the eigenfunction window has smaller bandwidth and its energy is more uniformly distributed relative to Gaussian window in the spatial domain. Thus, the eigenfunction window can be a good choice for window function in the SLSHT distribution.

It must be noted that compared to space-scale techniques, the spectral-space resolution of the SLSHT is fixed for all spectral components and spatial positions. Incorporating multi-resolution capability in SLSHT is possible, but would require using different bandwidth window functions for different SLSHT distribution components, consideration of which is beyond the scope of this correspondence. Finally, we remark that with appropriate modifications it is possible to incorporate non-azimuthally symmetric windows into our formulation.

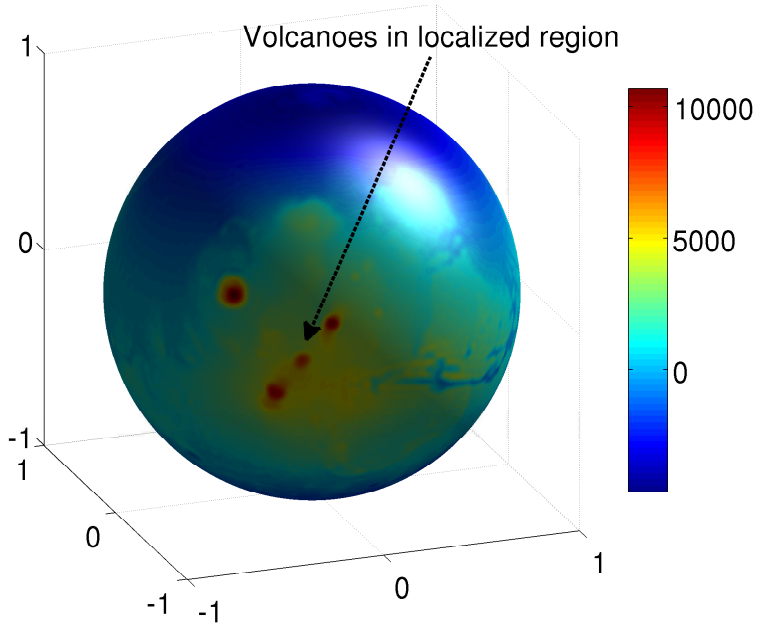


Figure 4.3: Mars topographic map $f(\hat{\boldsymbol{x}})$, obtained using band-limited spectral model of Mars with maximum spectral degree 128.

## 4.5 Simulation Results

In this section, we demonstrate the spatially localized spherical harmonics transform and our proposed window to study the signals in joint spatio-spectral domain. We consider a Mars topographic map (height above geoid) as a signal on the sphere that has higher degree harmonic components in a localized mountainous spatial region. We study the high resolution Mars topographic map (size $= 512 \times 512$) using SLSHT and illustrate that the SLSHT distribution reveals localized spectral contributions of spherical harmonics in the spatial domain. In the simulation results, we have implemented the method outlined in [31] to calculate the spherical harmonic components and triple product in `MATLAB`. We use equiangular sampling with $N \times N$ samples on the sphere as $\theta_n = \pi n/N$, $\phi_n = 2\pi n/N$ for $n = 0, 1, \ldots, N-1$. Note that exact quadrature can be performed using this tessellation with errors on the order of numerical precision. We use the azimuthally symmetric band-limited Slepian eigenfunction window to obtain localization in spatial domain. For SLSHT distribution computation using a window with bandwidth $L_h$, we use a very high resolution $N = 256 \gg 2L_h$ to obtain smooth plots. Finally, for inverse spherical harmonic transform of a function with maximum spherical harmonics degree $L_f$, we use minimum resolution $N = 2L_f$ [31] for exact quadrature.

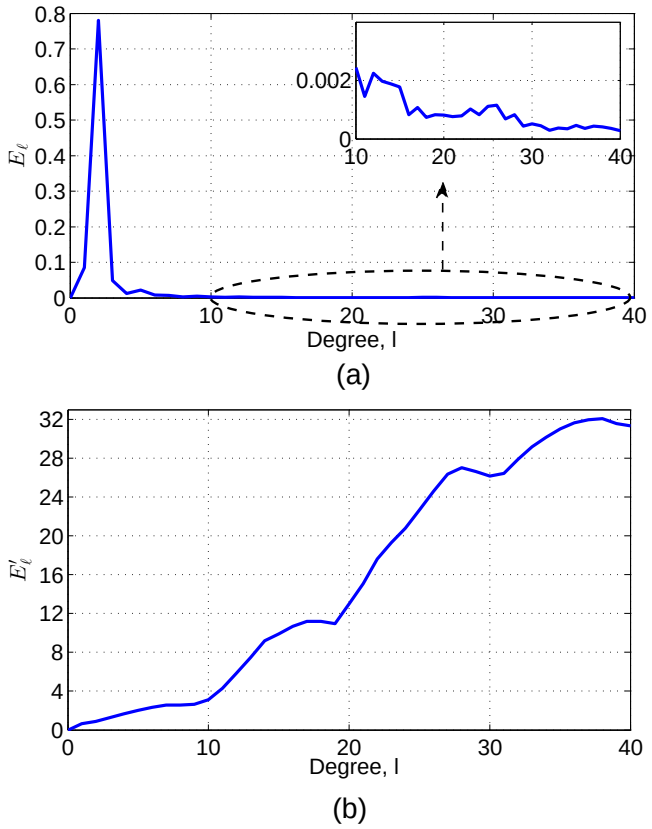


Figure 4.4: (a) Energy per spherical harmonic degree $E_\ell$ ((4.31)) and (b) Energy ratio per degree $E'_\ell$ in (4.32) for components of the SLSHT distribution $\mathbf{g}$ in (4.9) of the Mars topographic map for degree $0 \leq \ell \leq 40$.

Fig. 4.3 shows the Mars topographic map $f(\hat{\boldsymbol{x}})$ in the spatial domain. The Mars topographic map $f(\hat{\boldsymbol{x}})$ is obtained in the spatial domain using its spherical harmonics topographic model up to degree of 128. There are volcanoes leading to high frequency content in the signal which are localized in the vicinity of $\theta = \pi/2$ and $\phi = -\pi/3$. We use the unit energy normalized Mars signal with DC-component eliminated. If $\big(f\big)_\ell^m$ denotes the spherical harmonic coefficients for the Mars signal $f(\hat{\boldsymbol{x}})$, we define the energy per degree $E_\ell$ as

$$E_\ell = \sum_{m=-\ell}^{\ell} |\big(f\big)_\ell^m|^2. \tag{4.31}$$

Fig. 4.4(a) shows the energy per degree $E_\ell$ in the spectrum of Mars, which indicates that 90% of the energy is contributed by the spherical harmonics with degree less than 10. The higher degree spherical harmonics contribute towards high frequency regions in a signal and contain very little energy. The higher degree

spherical harmonic coefficients do not clearly provide information about the region of their contributions in the signal $f(\hat{\boldsymbol{x}})$. We determine all SLSHT components of the form $g(\hat{\boldsymbol{x}}, c)$ for $1 \leq c \leq 960$ or $g(\hat{\boldsymbol{x}}, \ell, m)$ for $1 \leq \ell \leq 30$ and all orders $|m| \leq \ell$ using an eigenfunction window with truncation width $\theta_c = \pi/8$. We calculate the energy contribution by spherical harmonics in a region around volcanoes. We expect that higher spherical harmonics would have significant energy concentrated around the volcanoes. We define the energy ratio per degree $E'_\ell$ as a measure of energy contribution by all order spherical harmonics for a particular degree in the localized region as

$$E'_\ell = \sum_{m=-\ell}^{\ell} \frac{\int_R |g(\hat{\boldsymbol{x}}, \ell, m)|^2 \, d\hat{\boldsymbol{x}}}{\int_{\mathbb{S}^2} |g(\hat{\boldsymbol{x}}, \ell, m)|^2 \, d\hat{\boldsymbol{x}}}, \tag{4.32}$$

where $R$ denotes the spherical cap region of width $\pi/8$ centered at $\theta = \pi/2$ and $\phi = -\pi/3$. The region $R$ only covers 3.81% area of the whole sphere and captures the magnitude of the SLSHT distribution component around the volcanoes. Fig. 4.4(b) shows the energy ratio per degree $E'_\ell$, which indicates that the higher degree spherical harmonics, despite their low energy content in overall spectrum, have their energy localized in a region $R$.

Fig. 4.5 shows the magnitude of zero order distribution components of the form $g(\hat{\boldsymbol{x}}, \ell, 0)$ for $11 \leq \ell \leq 30$, which indicate the spatial contribution of zero order spherical harmonics. These distribution components indicate that the contribution of higher order spherical harmonics is mainly around the region where volcanoes are located. Note that it is also possible to resolve topographic features such as volcanoes using wavelets, as demonstrated in [5]. However, the SLSHT distribution provides interpretation about the spectral contributions of a particular spherical harmonic in a localized region in the spatial domain, which is not explicitly available using wavelets.

## 4.6 Concentration Uncertainty Principle

In the previous section, we analyzed different window functions from the perspective of the classic uncertainty principle that relates the variances of the signal in the spatial and spectral domains [1, 78, 90]. A more general notion of uncertainty, herein referred to as a concentration uncertainty principle, was provided by Donoho

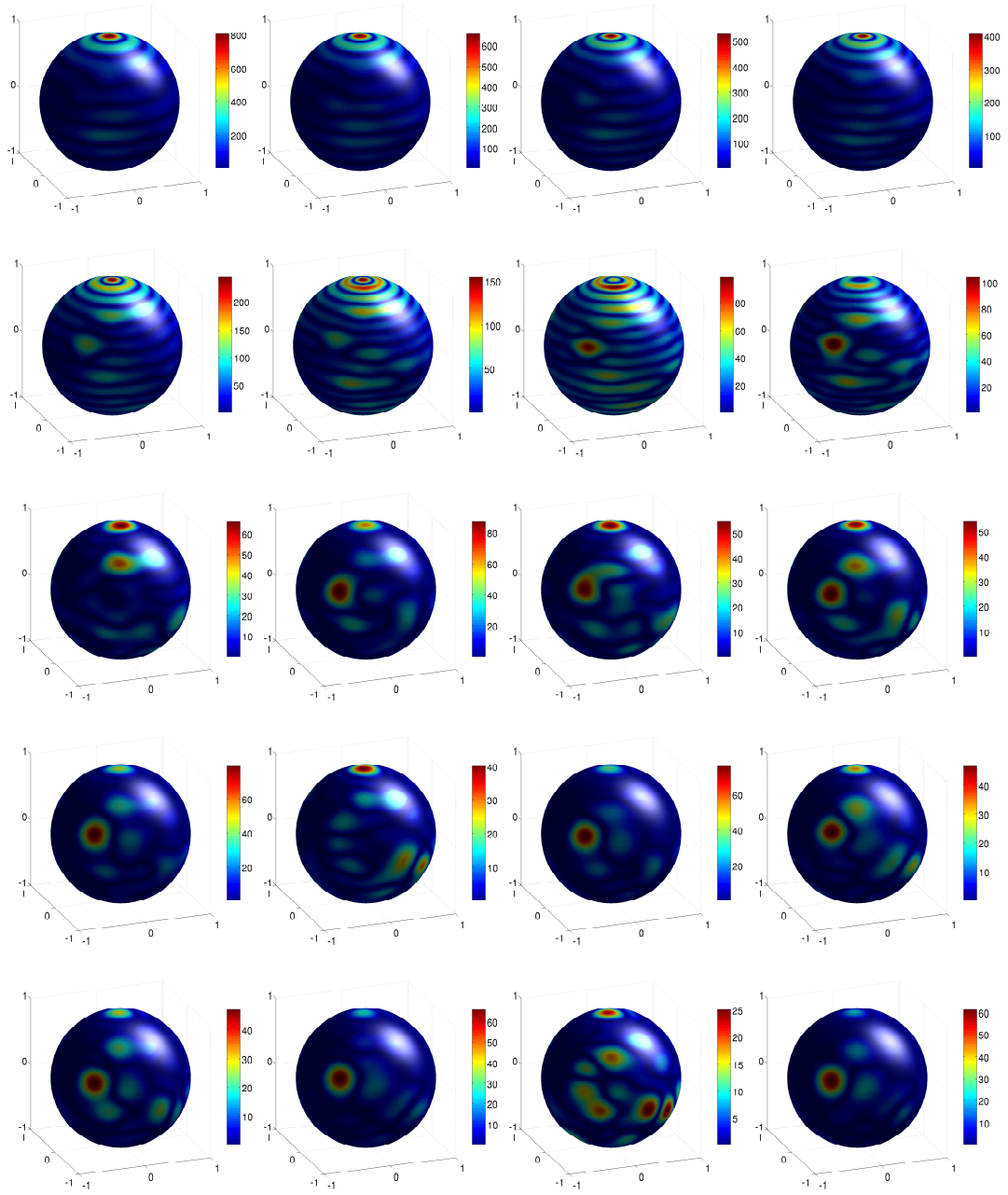

Figure 4.5: Magnitude of components of SLSHT distribution $\mathbf{g}$ in (4.9) of Mars topographic map $f(\hat{\boldsymbol{x}})$. The distribution components $g(\hat{\boldsymbol{x}}, \ell, m)$ are shown for $m = 0$ and $11 \leq \ell \leq 30$ in a sorted manner; that the degree $\ell$ increments from left to right, with the lowest degree $\ell = 11$ is plotted on the top left and the highest degree $\ell = 30$ on the lower right.

and Stark. It holds that a function and its Fourier transform cannot be simultaneously concentrated on any set of small measure [92]. The authors in [92] defined two criteria for measuring concentrations as the integral of an absolute value of the signal ($L_1$-norm) and as the signal energy ($L_2$-norm). We note that concentration uncertainty principles have also been extensively applied in problems of

signal reconstruction and recovery [92], signal extrapolation [93] and compressive sampling [94].

In this section, we formulate concentration uncertainty principles for signals on the sphere where the concentration is measured using the $L_1$-norm and $L_2$-norm of a signal respectively. More precisely, if the signal $f(\hat{\boldsymbol{x}})$ on the sphere is concentrated on some spatial region $R \subset \mathbb{S}^2$ and also concentrated on some spectral region $N = [N_1, N_2]$ which denotes the spherical harmonic coefficients $\big(f\big)_\ell^m$ with $N_1 \leq \ell \leq N_2$ and $-\ell \leq m \leq \ell$, we develop the principles which relate the concentration measures and concentration regions in both spatial and spectral domains. Note that the region $R$ does not need to be connected, whereas for the sake of simplicity, we consider the connected interval $N$ in spectral domain but this can also be generalized for non-connected intervals. Here connected interval means that $N = [N_1, N_2]$ contains all degrees between $N_1$ and $N_2$. We first define the selection operators in both spatial and spectral domains which select the part of a signal in a selected spatial or spectral region [95]. Then we state and prove the uncertainty principles. We first define $L_p$ norm of a signal defined on the sphere and the $L_p$ norm of an operator on $L^2(\mathbb{S}^2)$. Later, we formulate selection operators in the spatial and spectral domain and then we provide the concentration uncertainty principles.

### 4.6.1 $L_p$ norm of Signal and Operator

For a signal $f \in L^2(\mathbb{S}^2)$, its $L_p$-norm is defined as [96]

$$\|f\|_p = \Big( \int_{\mathbb{S}^2} |f(\hat{\boldsymbol{x}})|^p \, ds(\hat{\boldsymbol{x}}) \Big)^{1/p}. \tag{4.33}$$

Define an operator $\mathcal{K}$ for signals on the sphere using general Fredholm integral equation [85]

$$(\mathcal{K}f)(\hat{\boldsymbol{x}}) \; = \; \int_{\mathbb{S}^2} K(\hat{\boldsymbol{x}}, \hat{\boldsymbol{y}}) \, f(\hat{\boldsymbol{y}}) ds(\hat{\boldsymbol{y}}), \tag{4.34}$$

where $K(\hat{\boldsymbol{x}}, \hat{\boldsymbol{y}})$ is the kernel for an operator $\mathcal{K}$. Since it is important in the sequel, we define the $L_p$-norm of an operator $\mathcal{K}$ as

$$\|\mathcal{K}\|_p = \sup_{f \in \mathbb{S}^2} \frac{\|\mathcal{K}f\|_p}{\|f\|_p}. \tag{4.35}$$

Also, the Hilbert-Schmidt norm of an operator $\mathcal{K}$ with kernel $K(\hat{\boldsymbol{x}}, \hat{\boldsymbol{y}})$ is given by [92]

$$\|\mathcal{K}\|_H = \left( \int_{\mathbb{S}^2} \int_{\mathbb{S}^2} |K(\hat{\boldsymbol{x}}, \hat{\boldsymbol{y}})|^2 ds(\hat{\boldsymbol{x}})\, ds(\hat{\boldsymbol{y}}) \right)^{1/2}, \tag{4.36}$$

which is a bound on $\|\mathcal{K}\|_2$. We note that the kernel $K(\hat{\boldsymbol{x}}, \hat{\boldsymbol{y}})$ will always be taken as Hilbert-Schmidt, meaning $\|\mathcal{K}\|_H < \infty$, which is a sufficient condition to make the integral operator compact.

### 4.6.2 Selection Operators on the Sphere

**Definition 4.4 (Spatial Selection Operator)** Define the spatial selection operator $\mathcal{K}_R$ which selects the function in a region $R$ with kernel $K_R(\hat{\boldsymbol{x}}, \hat{\boldsymbol{y}})$ as

$$K_R(\hat{\boldsymbol{x}}, \hat{\boldsymbol{y}}) \triangleq I_R(\hat{\boldsymbol{x}}) \delta(\hat{\boldsymbol{x}}, \hat{\boldsymbol{y}}), \tag{4.37}$$

where $I_R(\hat{\boldsymbol{x}}) = 1$ for $\hat{\boldsymbol{x}} \in R \subset \mathbb{S}^2$ and $I_R(\hat{\boldsymbol{x}}) = 0$ for $\hat{\boldsymbol{x}} \in \mathbb{S}^2 \backslash R$ is an indicator function of the region $R$ and $\delta(\hat{\boldsymbol{x}}, \hat{\boldsymbol{y}})$ denotes the Dirac delta function on the sphere given in (2.21) .

**Definition 4.5 (Spectral Selection Operator)** Define the spectral selection operator $\mathcal{K}_N$ with $N = [N_1, N_2]$, which selects the contribution of spherical harmonics in spectral region $N$ in a signal and has the kernel $K_N$ as

$$K_N(\hat{\boldsymbol{x}}, \hat{\boldsymbol{y}}) \triangleq \sum_{\ell=N_1}^{N_2} \sum_{m=-\ell}^{\ell} Y_\ell^m(\hat{\boldsymbol{x}})\, \overline{Y_\ell^m(\hat{\boldsymbol{y}})}. \tag{4.38}$$

We note that both the spatial and spectral selection operators are idempotent and self-adjoint. That is, they are projection operators.

### 4.6.3 The $L_1$-norm Uncertainty Principle

We first present the $L_1$-norm uncertainty principle which relates the concentration of signal in spatial and spectral domains to the measure of spatial and spectral regions, where the concentration is determined using the $L_1$-norm of a signal. We say that $f$ is $\epsilon_R$ concentrated in the spatial domain and $\epsilon_N$ concentrated in the spectral domain if $\|f - \mathcal{K}_R f\|_1 \leq \epsilon_R$ and $\|f - \mathcal{K}_N f\|_1 \leq \epsilon_N$ respectively.

**Theorem 4.3 ($L_1$-norm Uncertainty Principle)** If the unit $L_1$-norm signal $f$ is $\epsilon_R$ concentrated in the region $R \subset \mathbb{S}^2$ and $\epsilon_N$ concentrated in the spectral region $N = [N_1, N_2]$, then

$$\frac{A}{4\pi}\left((N_2+1)^2 - N_1^2\right) \geq \frac{1-\epsilon_R-\epsilon_N}{1+\epsilon_N}, \tag{4.39}$$

where $A = \int_{\mathbb{S}^2} I_R(\hat{\boldsymbol{x}}) ds(\hat{\boldsymbol{x}})$ denotes the area of the region $R$.

**Proof**

Since, the signal $f$ is unit-norm, we have

$$\|f\|_1 = \int_{\mathbb{S}^2} |f(\hat{\boldsymbol{x}})| ds(\hat{\boldsymbol{x}}) = 1 \tag{4.40}$$

and using the given $\|f - \mathcal{K}_R f\|_1 \leq \epsilon_R$ and $\|f - \mathcal{K}_N f\|_1 \leq \epsilon_N$ and the fact that $\|f - \mathcal{K}_R f\|_1 \geq \|f\|_1 - \|\mathcal{K}_R f\|_1$, we obtain

$$\|\mathcal{K}_R f\|_1 + \epsilon_R \geq 1\,, \quad \|\mathcal{K}_N f\| + \epsilon_N \geq 1. \tag{4.41}$$

Define a composite operator $\mathcal{K}_{RN} = \mathcal{K}_R \mathcal{K}_N$. From (4.40) and (4.41), we obtain the $L_1$-norm of this composite operator as

$$\|\mathcal{K}_{RN}\|_1 \geq \|\mathcal{K}_{RN} f\|_1 \geq 1 - \epsilon_R - \epsilon_N. \tag{4.42}$$

Since, the operator $\mathcal{K}_N$ is idempotent, using the spherical harmonic expansion of $f$, we can write

$$(\mathcal{K}_N f)(\hat{\boldsymbol{x}}) = \sum_{\ell=N_1}^{N_2} \sum_{m=-\ell}^{\ell} \int_{\mathbb{S}^2} Y_\ell^m(\hat{\boldsymbol{x}})\, \overline{Y_\ell^m(\hat{\boldsymbol{y}})} (\mathcal{K}_N f)(\hat{\boldsymbol{y}})\, ds(\hat{\boldsymbol{y}}). \tag{4.43}$$

Using the spherical harmonics addition theorem in (2.9), we can obtain from (4.43) that

$$|(\mathcal{K}_N f)(\hat{\boldsymbol{x}})| = \sum_{\ell=N_1}^{N_2} \frac{2\ell+1}{4\pi} \int_{\mathbb{S}^2} |P_\ell^0(\hat{\boldsymbol{x}} \cdot \hat{\boldsymbol{y}})| ds(\hat{\boldsymbol{y}}) \tag{4.44}$$

and we have $\sup \|P_\ell^0(\hat{\boldsymbol{x}} \cdot \hat{\boldsymbol{y}})\|_1 = 1$ and $\|(\mathcal{K}_N f)\|_\infty = \max |(\mathcal{K}_N f)(\hat{\boldsymbol{x}})|$ for $\hat{\boldsymbol{x}} \in \mathbb{S}^2$,

which implies

$$\|(\mathcal{K}_N f)\|_\infty \leq \frac{1}{4\pi}\Big((N_2+1)^2 - N_1^2\Big)\|(\mathcal{K}_N f)\|_1. \tag{4.45}$$

For the composite operator $\mathcal{K}_{RN}$, we have

$$\|\mathcal{K}_{RN} f\|_1 = \int_R |(\mathcal{K}_N f)(\hat{\boldsymbol{x}})| ds(\hat{\boldsymbol{x}}) \leq \|\mathcal{K}_N f\|_\infty A, \tag{4.46}$$

where $A$ is the area of the region $R$. Using (4.46) and (4.45), we obtain

$$\|\mathcal{K}_{RN} f\|_1 \leq \frac{A}{4\pi}\Big((N_2+1)^2 - N_1^2\Big)\|(\mathcal{K}_N f)\|_1. \tag{4.47}$$

Combining (4.40), (4.41) and (4.42) with (4.47) gives the stated result. □

**Remark 4.8** The factor $\frac{A}{4\pi}\Big((N_2+1)^2 - N_1^2\Big)$ on the left hand side of (4.39) can be defined as a generalized space-bandwidth product, with the term $A/4\pi$ being a measure of the spatial region $R$ and the term $(N_2+1)^2 - N_1^2$ being a measure of the spectral region $N = [N_1, N_2]$. For $N_1 = 0$, this space-bandwidth product is referred to as an equivalent of the Shannon number in [27] for signals defined on the sphere.

### 4.6.4 The $L_2$-norm Uncertainty Principle

Next, we present the uncertainty principle for the case in which the concentration is measured using $L_2$-norm, which is a measure of energy of the signal and makes this principle more appealing and practical.

**Theorem 4.4 ($L_2$-norm Uncertainty Principle)** If the unit $L_2$-norm signal $f$ is $\epsilon_R$ concentrated in the region $R \subset \mathbb{S}^2$ such that $\|f - \mathcal{K}_R f\|_2 \leq \epsilon_R$ and $\epsilon_N$ concentrated in the spectral region $N = [N_1, N_2]$ such that $\|f - \mathcal{K}_N f\|_2 \leq \epsilon_N$, then

$$\frac{A}{4\pi}\Big((N_2+1)^2 - N_1^2\Big) \geq (1 - \epsilon_R - \epsilon_N)^2, \tag{4.48}$$

where $A = \int_{\mathbb{S}^2} I_R(\hat{\boldsymbol{x}}) d\hat{\boldsymbol{x}}$ denotes the area of the region $R$.

**Proof**

By definition, $\|f\|_2 = 1$, $\|f - \mathcal{K}_R f\|_2 \leq \epsilon_R$ and $\|f - \mathcal{K}_N f\|_2 \leq \epsilon_N$, which implies

$$\|\mathcal{K}_R f\|_2 \geq 1 - \epsilon_R\,, \quad \|\mathcal{K}_N f\|_2 \geq 1 - \epsilon_N. \tag{4.49}$$

Define a composite operator $\mathcal{K}_{NR} = \mathcal{K}_N \mathcal{K}_R$ composed of spatial selection operation $\mathcal{R}$ followed by spectral selection $\mathcal{K}_N$. By substituting (4.37) and (4.38) in (4.34) and using the representation of Dirac delta in (2.21), we obtain the kernel $K_{NR}(\hat{\boldsymbol{x}}, \hat{\boldsymbol{y}})$ as

$$K_{NR}(\hat{\boldsymbol{x}}, \hat{\boldsymbol{y}}) = \sum_{\ell=N_1}^{N_2} \sum_{m=-\ell}^{\ell} Y_\ell^m(\hat{\boldsymbol{x}}) \, \overline{Y_\ell^m(\hat{\boldsymbol{y}})} I_R(\hat{\boldsymbol{y}}). \tag{4.50}$$

The Hilbert-Schmidt norm of the composite operator $\mathcal{K}_{NR}$ can be obtained using (4.36) along with the spherical harmonics addition theorem in (2.9) and the fact that $P_\ell^0(1) = 1$ as

$$\begin{aligned} \|\mathcal{K}_{NR}\|_H &= \left( \sum_{\ell=N_1}^{N_2} \frac{2\ell+1}{4\pi} \int_R ds(\hat{\boldsymbol{x}}) \right)^{1/2} \\ &= \left( \frac{A}{4\pi} \left( (N_2+1)^2 - N_1^2 \right) \right)^{1/2}. \end{aligned} \tag{4.51}$$

Now, the effect of the composite operator on the concentration can be readily obtained from (4.49) as

$$\|\mathcal{K}_{NR} f\|_2 \geq 1 - \epsilon_R - \epsilon_N. \tag{4.52}$$

Using definition of the norm of operator in (4.35), $\|\mathcal{K}_{NR}\|_2 \geq \|\mathcal{K}_{NR} f\|_2$ and the fact that $\|\mathcal{K}_{NR}\|_H \geq \|\mathcal{K}_{NR}\|_2$ and combined with (4.51) and (4.52) gives the result in (4.48). □

**Remark 4.9** We can infer from the proof of Theorem 4.4 that the composite operator $\mathcal{K}_{RN} = \mathcal{K}_R \mathcal{K}_N$ is an adjoint of the operator $\mathcal{K}_{NR}$ which implies that the Hilbert-Schmidt norm of these two composite operators is equal and given by (4.51).

### 4.6.5 Sharpness of the Uncertainty Principle Bound

We provide an analysis of the bound imposed by the $L_2$-norm uncertainty principle on simultaneous spatial and spectral signal concentration. We compare this bound with the largest eigenvalue obtained from the Slepian concentration problem for azimuthally symmetric signals on the sphere proposed in [1, 27, 39]. First, we

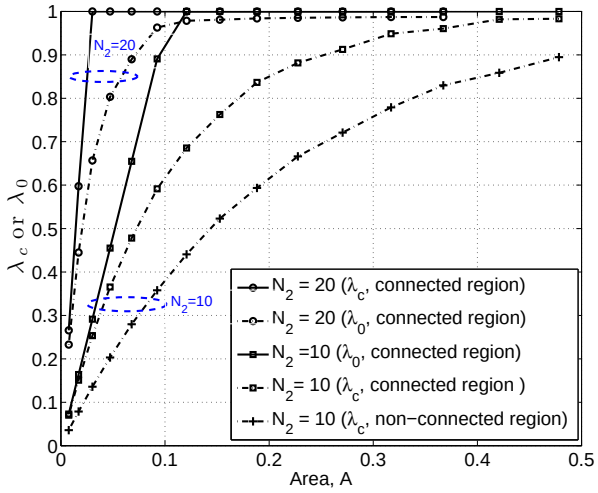


Figure 4.6: Comparison of the uncertainty bound $\lambda_0 = (N_2+1)^2(1-\cos\Theta)/2$ obtained from (4.48) and the largest eigenvalue $\lambda_c$ associated with the most concentrated band-limited eigenfunction obtained from Slepian's concentration problem on the sphere [1]. Results are shown as a function of the area $A$ of the spatial polar cap regions with consideration of spectral regions $N = [0, N_2]$ for $N_2 = 10$ and $N_2 = 20$.

consider the spatial polar cap regions $R$ characterized by central angle $\Theta$ with area $A = \int_o^{\pi}\int_0^{\Theta} \sin\theta d\theta d\phi = 2\pi(1-\cos\Theta)$ and the spectral regions $N = [0, N_2]$. We use $\lambda_c(\Theta, N_2)$ to denote the largest eigenvalue obtained numerically by solving the concentration problem on the sphere [1], which finds the band-limited signal of maximum spectral degree $N_2$ with maximum energy concentration in the polar cap region of angle $\Theta$. We obtain a simplified form of the product on the left hand side in (4.48) for spatial and spectral regions under consideration as $\lambda_0(\Theta, N_2) = (N_2+1)^2(1-\cos\Theta)/2$, which serves as an uncertainty bound. Fig 4.6 shows the comparison of $\lambda_c(\Theta, N_2)$ and $\lambda_0(\Theta, N_2)$ against $\Theta$ for $N_2 = 10$ and $N_2 = 20$, which suggests that $\lambda_0$ serves as a sharp bound for the spatial polar cap region $R$ and it gets tighter for smaller values of $\lambda_0$.

In the preceding analysis, we considered the connected polar cap region of central angle $\Theta$. Next, we consider a non-connected region of two polar caps centered at opposite poles ($\theta = 0$ and $\theta = \pi$) with the central angle of each polar cap being $\cos^{-1}(1+\cos\Theta)/2$. It can be easily shown that the region of two polar caps have the same area $A = 2\pi(1-\cos\Theta)$, thus the same uncertainty bound holds. But the tightness of the bound is comparatively reduced as illustrated by the 'non-connected region' curve in Fig 4.6. For an example considered here, we note that

the bound or the limit imposed by concentration uncertainty principle is more sharper and tighter for connected regions and smaller values of space-bandwidth product respectively.

## 4.7 Summary of Contributions

In this chapter, we have proposed a transform which we have called the spatially localized spherical harmonics transform (SLSHT) for signals defined on the unit sphere. The proposed technique transforms signals on the sphere into joint spatio-spectral SLSHT distribution that represents how the signal spectrum is changing in the spatial domain. We also presented the complementary distribution, analogous to characteristic function in the time-frequency analysis. We formulated the matrix representation of the proposed transforms and proved that the signal and window can be recovered from the SLSHT distribution. We used an azimuthally symmetric window to achieve spatial localization and analyzed the localization trade-off for a window function in both spatial and spectral domains from the perspective of the uncertainty principle. In this work, we have also investigated concentration uncertainty principles for the signals on the sphere that relate the localization of concentration of a signal in spatial and spectral domains. The contributions made in this chapter are as follows.

Addressing Q2 posed in Section 1.2.1:

- We have employed a localized spherical harmonic transform, herein referred as SLSHT, to represent the signal in spatio-spectral domain. In spirit, the proposed transform is analogous to STFT in time-frequency analysis.
- We have provided the matrix representation of the transform, resulting in spatio-spectral representation which we call SLSHT distribution. To support our formulation of spatio-spectral distribution, we have presented the inversion relation to obtain signal from its SLSHT distribution.
- Later, we have illustrated with the help of an example that the SLSHT distribution of a signal reveals the spatially localized contributions of spherical harmonics, which are not clearly visible in the global spectrum of the signal.

Addressing Q3 posed in Section 1.2.1:

- From the perspective of uncertainty principle, we have studied the localization trade-off for different window functions in both spatial and spectral domains and proposed to use the eigenfunction window, obtained from the Slpeian concentration problem on the sphere [1, 39], for spatial localization in obtaining the SLSHT distribution of a signal.

Addressing Q4 posed in Section 1.2.1:

- We have derived new uncertainty principles for the signals on the sphere that relate the localization of concentration of a signal in spatial and spectral domains. Considering the concentration as an integral of the absolute value of a signal over the sphere, the $L_1$-norm uncertainty principle has been derived. We also derived the more practical $L_2$-norm uncertainty principle using the Hilbert-Schmidt norm of the composite selection operator on the sphere.

# Chapter 5

# Spatially Varying Spectral Filtering

## 5.1 Introduction

In this chapter, we extend the signal transformation based on the concept of STFT in the time-frequency domain to the joint spatio-spectral domain on the sphere. Joint spatio-spectral filtering is of significant importance when we wish to filter and modify *spatially-varying* spectral contents of signals. For this purpose, the spherical harmonic transform is not adequate because it cannot directly reveal " spatially localized" contributions of spectral contents of a signal in the spectral domain.

We use the SLSHT distribution presented in Chapter 4 as the representation of the signal in joint spatio-spectral domain. The concept of SLSHT has been used for localized spectral analysis [1] and spectral estimation [20] on the sphere. However, the application of SLSHT for signal filtering has not been considered before. In this context, we consider filtering and modification of signals in the joint spatio-spectral domain. As illustrated in Fig. 5.1, the SLSHT distribution of the input signal is first obtained, then the SLSHT distribution is processed in the joint spatio-spectral domain to yield the modified distribution, which is ultimately transformed back to the spatial domain using a suitably devised inverse operation. Since the SLSHT distribution is modified in the spatio-spectral domain, there is a possibility that there exists no physical signal which corresponds to the modified distribution—an analogous problem is well known in time-frequency

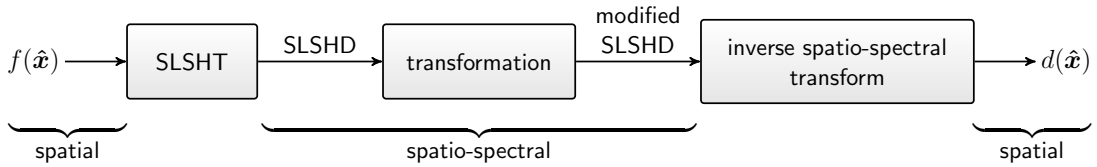


Figure 5.1: General schematic for signal transformation via the spatio-spectral domain. The spatial signal, $f(\hat{\boldsymbol{x}})$, on the unit sphere, is first mapped to the spatio-spectral domain using the spatially localized spherical harmonic transform (SLSHT). Then its SLSHT distribution (denoted by SLSHD in the figure) is transformed in spatio-spectral domain. Finally the result is mapped back to the spatial domain using an inverse spatio-spectral transform.

analysis [73, 74, 79–81]. Therefore, there is a need to find the signal that best approximates the modified distribution.

The rest of this Chapter is organized as follows. In Section 5.2, we present a general integral operator that transforms the SLSHT distribution of a signal to a modified spatio-spectral distribution. For the case when the modified spatio-spectral distribution is not a valid SLSHT distribution, we devise a suitable inverse spatio-spectral transform in Section 5.2.2, which finds a signal whose distribution best approximates the modified distribution in the least squares sense. Then, we formulate this spatio-spectral modification as a linear transformation of the signal in the spectral domain. Later, we investigate two types of filtering operations in spatio-spectral domain. First in Section 5.3.1, we consider filtering as multiplication of the filter function defined in spatio-spectral domain and the given SLSHT distribution. Later in Section 5.3.2, we perform filtering as a convolution of the filter function and the SLSHT distribution of a signal. Finally, some specific numerical examples are given in Section 5.4.

## 5.2 Signal Transformation in Spatio-spectral Domain

In Chapter 4, we saw that the SLSHT distribution represents the spatially-varying spectral representation of a signal as a function of both spatial location $\hat{\boldsymbol{y}}$ and degree and order $\ell, m$. As a result, it offers the opportunity to transform, modify and filter the signal in the joint spatio-spectral domain, which can be very useful for the processing of signals that contain spatially-varying spectral contents. Here, we use a general integral operator approach to transform the SLSHT distribution.

Later in Sections 5.3 and 5.4, we specify two types of transformations and analyze their properties and usefulness.

For this purpose, we use a set of $N_g + 1$ kernels defined on the domain $\mathbb{S}^2 \times \mathbb{S}^2$ and denoted by $\boldsymbol{\zeta}(\hat{\boldsymbol{x}}, \hat{\boldsymbol{y}}; n)$. Each kernel operates on its corresponding SLSHT component $g(\hat{\boldsymbol{y}}; n)$ as follows

$$v(\hat{\boldsymbol{x}}; n) = \int_{\mathbb{S}^2} \zeta(\hat{\boldsymbol{x}}, \hat{\boldsymbol{y}}; n)\, g(\hat{\boldsymbol{y}}; n)\, ds(\hat{\boldsymbol{y}}), \quad 0 \leq n \leq N_g \tag{5.1}$$

to generate a modified component $v(\hat{\boldsymbol{x}}; n)$ in the spatio-spectral domain. For a given $\hat{\boldsymbol{x}}$ and $\hat{\boldsymbol{y}}$ and by arranging all the kernels in vector form as

$$\boldsymbol{\zeta}(\hat{\boldsymbol{x}}, \hat{\boldsymbol{y}}) \triangleq \big(\zeta(\hat{\boldsymbol{x}}, \hat{\boldsymbol{y}}; 0),\, \zeta(\hat{\boldsymbol{x}}, \hat{\boldsymbol{y}}; 1),\, \zeta(\hat{\boldsymbol{x}}, \hat{\boldsymbol{y}}; 2),\, \cdots,\, \zeta(\hat{\boldsymbol{x}}, \hat{\boldsymbol{y}}; N_g)\big)',$$

we can write the overall operation on the SLSHT distribution in the concise form

$$\boldsymbol{v}(\hat{\boldsymbol{x}}) = \big(\mathcal{K}\boldsymbol{g}\big)(\hat{\boldsymbol{x}}) \triangleq \int_{\mathbb{S}^2} \boldsymbol{\zeta}(\hat{\boldsymbol{x}}, \hat{\boldsymbol{y}}) \odot \boldsymbol{g}(\hat{\boldsymbol{y}})\, ds(\hat{\boldsymbol{y}}), \tag{5.2}$$

where $\odot$ denotes component-wise operation of the kernel elements in $\boldsymbol{\zeta}(\hat{\boldsymbol{x}}, \hat{\boldsymbol{y}})$ on corresponding SLSHT components in $\boldsymbol{g}(\hat{\boldsymbol{y}})$. Note that the kernels $\zeta(\hat{\boldsymbol{x}}, \hat{\boldsymbol{y}}; n)$ for $N_v < n \leq N_g$ can be zero and hence, in general the "effective" length of the modified distribution $\boldsymbol{v}(\hat{\boldsymbol{x}})$ satisfies $N_v + 1 \leq N_g + 1$. Nevertheless for consistency with the transformation operator matrix $\boldsymbol{\Psi}$, we will deal with a full-length modified distribution $\boldsymbol{v}(\hat{\boldsymbol{x}})$ of length $N_g+1$, even though some of its last components may be zero. We also note that while $\boldsymbol{v}(\hat{\boldsymbol{x}})$ is a form of modified spatio-spectral distribution, it is not necessarily a valid SLSHT distribution. This will be further elaborated shortly.

Using the formulation of SLSHT distribution in (4.10), we can relate the modified distribution (5.2) to the vector spectral representation of the signal, $\boldsymbol{f}$, and the SLSHT distribution transformation operator matrix $\boldsymbol{\Psi}(\hat{\boldsymbol{y}})$ as

$$\boldsymbol{v}(\hat{\boldsymbol{x}}) = \big(\mathcal{K}\boldsymbol{\Psi}\big)(\hat{\boldsymbol{x}})\boldsymbol{f} = \Big(\int_{\mathbb{S}^2} \mathrm{diag}\big(\boldsymbol{\zeta}(\hat{\boldsymbol{x}}, \hat{\boldsymbol{y}})\big)\boldsymbol{\Psi}(\hat{\boldsymbol{y}})\, ds(\hat{\boldsymbol{y}})\Big)\boldsymbol{f}, \tag{5.3}$$

where $\mathrm{diag}\big(\boldsymbol{\zeta}(\hat{\boldsymbol{x}}, \hat{\boldsymbol{y}})\big)$ returns the diagonal matrix with diagonal entries specified by the vector $\boldsymbol{\zeta}(\hat{\boldsymbol{x}}, \hat{\boldsymbol{y}})$.

**Remark 5.1** *In the formulation of the spatio-spectral transformation of signal in*

(5.2), *we note that* $\boldsymbol{g}(\hat{\boldsymbol{y}})$ *can be any representation of signals in spatio-spectral domain. However, here, we are specifically considering SLSHT distribution as the signal representation in spatio-spectral domain.*

### 5.2.1 Exact Inverse Spatio-Spectral Transform

We note that not every spatio-spectral distribution, $\boldsymbol{v}(\hat{\boldsymbol{x}})$, is a valid SLSHT distribution. In other words, it is possible that there exists no signal belonging to $L^2(\mathbb{S}^2)$ for which $\boldsymbol{v}(\hat{\boldsymbol{x}})$ is its corresponding SLSHT distribution. An obvious example would be a spatio-spectral distribution truncated both in spatial and spectral domains. From the uncertainty principle, one can expect that there exists no signal which corresponds to this type of modified distribution.

But first, let us assume that the modified distribution vector $\boldsymbol{v}(\hat{\boldsymbol{x}})$ is indeed a valid SLSHT distribution. Then there exists a signal $d(\hat{\boldsymbol{x}}) \in L^2(\mathbb{S}^2)$ with spectral response $\boldsymbol{d}$ corresponding to $\boldsymbol{v}(\hat{\boldsymbol{x}})$, which can be recovered through the "inversion formula" presented in Theorem 4.1

$$\big(d\big)_u = \frac{1}{K} \int_{\mathbb{S}^2} v(\hat{\boldsymbol{y}}; u)\, ds(\hat{\boldsymbol{y}}), \tag{5.4}$$

where $K = \sqrt{4\pi}\big(h\big)_0^0$. Applying this back into (4.7) results in the following admissibility condition

$$\begin{aligned} v(\hat{\boldsymbol{x}}; n) &= \frac{1}{K} \sum_{u=0}^{N_f} \big(d\big)_u \sum_{r=0}^{N_h} \big(h\big)_r(\hat{\boldsymbol{x}})\, T(u; r; n) \\ &= \frac{1}{K} \sum_{u=0}^{N_f} \sum_{r=0}^{N_h} \big(h\big)_r(\hat{\boldsymbol{x}})\, T(u; r; n) \int_{\mathbb{S}^2} v(\hat{\boldsymbol{y}}; u)\, ds(\hat{\boldsymbol{y}}). \end{aligned} \tag{5.5}$$

The admissibility condition in (5.5) is expressed on the modified distribution $v(\hat{\boldsymbol{x}}; n)$. By using the definition of SLSHT distribution in (4.10), the formulation of modified distribution $\boldsymbol{v}(\hat{\boldsymbol{x}})$ in (5.3) and the inversion relation in Theorem 4.1, we can also express the admissibility condition on the set of kernels $\boldsymbol{\zeta}(\hat{\boldsymbol{x}}, \hat{\boldsymbol{y}})$ as

$$K \int_{\mathbb{S}^2} \operatorname{diag}\big(\boldsymbol{\zeta}(\hat{\boldsymbol{x}}, \hat{\boldsymbol{y}})\big)\, \boldsymbol{\Psi}(\hat{\boldsymbol{y}})\, ds(\hat{\boldsymbol{y}}) = \boldsymbol{\Psi}(\hat{\boldsymbol{x}}) \Big( \int_{\mathbb{S}^2} \int_{\mathbb{S}^2} \operatorname{diag}\big(\boldsymbol{\zeta}(\hat{\boldsymbol{x}}, \hat{\boldsymbol{y}})\big)\, \boldsymbol{\Psi}(\hat{\boldsymbol{y}})\, ds(\hat{\boldsymbol{x}}) ds(\hat{\boldsymbol{y}}) \Big). \tag{5.6}$$

If the modified distribution satisfies the condition in (5.5) or the set of kernels

$\boldsymbol{\zeta}(\hat{\boldsymbol{x}}, \hat{\boldsymbol{y}})$ are chosen to satisfy the condition in (5.6), we can find a signal $d(\hat{\boldsymbol{x}}) = \mathcal{F}^{-1}\boldsymbol{d}$, such that $\boldsymbol{v}(\hat{\boldsymbol{x}}) = \boldsymbol{\Psi}(\hat{\boldsymbol{x}})\boldsymbol{d}$. We remind ourselves that according to the discussion following (5.2), the effective length of $\boldsymbol{d}$, $N_d+1$, can be smaller than $N_f+1$. For example, if we choose each kernel $\zeta(\hat{\boldsymbol{x}}, \hat{\boldsymbol{y}}; n)$ as a band-limited Dirac-delta function given by

$$\zeta(\hat{\boldsymbol{x}}, \hat{\boldsymbol{y}}; n) = K_n \sum_{u=0}^{N_{\zeta n}} Y_u(\hat{\boldsymbol{x}}) Y_u(\hat{\boldsymbol{y}}), \tag{5.7}$$

where $N_h \leq N_{\zeta_n} < \infty$ and $K_n$ denotes any complex number, the set of kernels $\boldsymbol{\zeta}(\hat{\boldsymbol{x}}, \hat{\boldsymbol{y}})$ satisfies the condition in (5.6) and the modified distribution distribution $\boldsymbol{v}(\hat{\boldsymbol{x}})$ is a valid SLSHT distribution of the signal $d$ such that $\big(d\big)_u = K_u\big(f\big)_u$. The choice of kernel in (5.7) is the simplest case and we note that any set of kernels which satisfies the admissibility condition results in a valid SLSHT distribution $\boldsymbol{v}(\hat{\boldsymbol{x}})$.

### 5.2.2 Least Squares Solution

For the case that the modified distribution $\boldsymbol{v}(\hat{\boldsymbol{x}})$ is not a valid SLSHT distribution, we seek to solve an optimization problem to find a signal $d(\hat{\boldsymbol{x}}) \in L^2(\mathbb{S}^2)$ having the spectral response $\boldsymbol{d} = \big(\mathcal{F}\, d\big)(\hat{\boldsymbol{x}})$ and the SLSHT distribution $\boldsymbol{\Psi}(\hat{\boldsymbol{x}})\boldsymbol{d}$, which approximates $\boldsymbol{v}(\hat{\boldsymbol{x}})$ in the least squares sense. For this purpose, we define the error term

$$e(\hat{\boldsymbol{x}}; n) \triangleq v(\hat{\boldsymbol{x}}; n) - \Psi_{n,:}(\hat{\boldsymbol{x}})\boldsymbol{d},$$

where $\Psi_{n,:}(\hat{\boldsymbol{x}})$ is the $n$-th row of $\boldsymbol{\Psi}(\hat{\boldsymbol{x}})$. The total error is then

$$E = \big\|\boldsymbol{v} - \boldsymbol{\Psi}\boldsymbol{d}\big\|^2 \triangleq \int_{\mathbb{S}^2} \sum_{n=0}^{N_g} \big|e(\hat{\boldsymbol{x}}; n)\big|^2 \, ds(\hat{\boldsymbol{x}}), \tag{5.8}$$

where the norm is, in fact, the norm of vectors in the spatio-spectral domain. Setting the gradient of $E$ with respect to $\boldsymbol{d}$ to zero will result in the least squares approximate solution and we summarize this in the following theorem, which is also shown in Fig. 5.2.

**Theorem 5.1 (Least Squares Solution)** *Let the SLSHT distribution $\boldsymbol{g}(\hat{\boldsymbol{y}}) = \boldsymbol{\Psi}(\hat{\boldsymbol{y}})\,\boldsymbol{f}$, as defined in* (4.9)-(4.12)*, be modified into $\boldsymbol{v}(\hat{\boldsymbol{x}})$ according to* (5.1)-(5.2)*. The signal $\boldsymbol{d}(\hat{\boldsymbol{x}}) \in L^2(\mathbb{S}^2)$ that best describes $\boldsymbol{v}(\hat{\boldsymbol{x}})$ in the least squares sense has its*

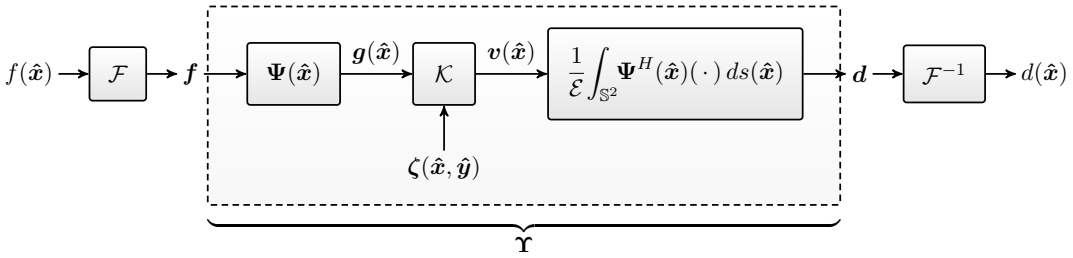


Figure 5.2: The spatio-spectral processing: $\boldsymbol{f} = \big(\mathcal{F}f\big)(\hat{\boldsymbol{x}})$ is the spectral response of the signal $f(\hat{\boldsymbol{x}})$ on the unit sphere, $\boldsymbol{g}(\hat{\boldsymbol{x}})$ is corresponding SLSHT distribution in the spatio-spectral domain, $\boldsymbol{v}(\hat{\boldsymbol{x}})$ is the modified SLSHT distribution under the operator $\mathcal{K}$ with kernel $\boldsymbol{\zeta}(\hat{\boldsymbol{x}},\hat{\boldsymbol{y}})$ in the spatio-spectral domain, and $\boldsymbol{d}$ is the spectral response of the output signal $d(\hat{\boldsymbol{x}})$ on the unit sphere. The transformation between the spectral responses is linear and given by the spatio-spectral transformation matrix $\boldsymbol{\Upsilon}$.

*spectral response defined through*

$$\boldsymbol{d} \triangleq \arg\min_{\widetilde{\boldsymbol{d}}} \big\|\boldsymbol{v} - \boldsymbol{\Psi}\widetilde{\boldsymbol{d}}\big\|^2, \tag{5.9}$$

*and is found to be*

$$\boldsymbol{d} = \frac{1}{\mathcal{E}}\int_{\mathbb{S}^2} \boldsymbol{\Psi}^H(\hat{\boldsymbol{x}})\,\boldsymbol{v}(\hat{\boldsymbol{x}})\,ds(\hat{\boldsymbol{x}}), \tag{5.10}$$

*where $(\cdot)^H$ denotes Hermitian transpose and $\mathcal{E}$ is defined as the energy of the window kernel $h$ given by*

$$\mathcal{E} \triangleq \big\langle h, h\big\rangle = \sum_{p=0}^{L_h} \big|\big(h\big)_p^0\big|^2. \tag{5.11}$$

**Proof**

See Appendix A.1. □

**Corollary 5.1** *If the modified distribution is a valid SLSHT distribution, by plugging $\boldsymbol{v}(\hat{\boldsymbol{x}}) = \boldsymbol{\Psi}(\hat{\boldsymbol{x}})\boldsymbol{d}$ into* (5.10) *and following the mathematical details provided Appendix A.1, it is easy to verify that the result stated in Theorem 5.1 (see* (5.10)*) becomes the exact solution.*

### 5.2.3 Spatio-spectral Transformation as Linear Transformation

From Fig. 5.2, it becomes clear that we can express the overall process of transforming the band-limited signal with spectral response $\boldsymbol{f}$, with the maximum spectral

degree $L_f$, to another band-limited signal $\boldsymbol{d}$ according to the following linear transformation

$$\boldsymbol{d} = \boldsymbol{\Upsilon}\, \boldsymbol{f}, \tag{5.12}$$

where $\boldsymbol{\Upsilon}$ is a matrix of size $(N_f + 1) \times (N_f + 1)$ and is referred to as the spatio-spectral transformation matrix as shown in Fig. 5.2. This transformation matrix is useful because in a single step it encapsulates 1) transformation of $\boldsymbol{f}$ into the spatio-spectral domain to obtain $\boldsymbol{g}(\hat{\boldsymbol{x}})$, 2) processing in the spatio-spectral domain which yields $\boldsymbol{v}(\hat{\boldsymbol{x}})$, and 3) transformation from the spatio-spectral domain back to spectral domain to obtain $\boldsymbol{d}$. Therefore, knowing $\boldsymbol{\Upsilon}$ is enough for spatio-spectral transformation of $\boldsymbol{f}$. Using the result in Theorem 5.1, the formulation of the modified distribution in (5.3) and the SLSHT distribution expression in (4.10), we can express $\boldsymbol{\Upsilon}$ as

$$\boldsymbol{\Upsilon} = \frac{1}{\mathcal{E}} \int_{\mathbb{S}^2}\int_{\mathbb{S}^2} \boldsymbol{\Psi}^H(\hat{\boldsymbol{x}}) \big(\mathrm{diag}\big(\boldsymbol{\zeta}(\hat{\boldsymbol{x}}, \hat{\boldsymbol{y}})\big) \boldsymbol{\Psi}(\hat{\boldsymbol{y}})\big)\, ds(\hat{\boldsymbol{y}})\, ds(\hat{\boldsymbol{x}}), \tag{5.13}$$

which depends on the kernel vector $\boldsymbol{\zeta}(\hat{\boldsymbol{x}}, \hat{\boldsymbol{y}})$ and the SLSHT distribution operator matrix $\boldsymbol{\Psi}(\hat{\boldsymbol{x}})$. Since $\boldsymbol{\Psi}(\hat{\boldsymbol{x}})$ depends on the chosen window function used for spatial localization, the kernel and the window function completely characterize the spatio-spectral transformation and processing of signals in the proposed framework.

## 5.3 Filtering in Spatio-Spectral Domain

In the previous section, we provided a general framework for modification of the SLSHT distribution using integral operators and discussed how the modified distribution can be transformed back to a valid signal on the sphere. We aim to study specific, but useful types of signal filtering in joint spatio-spectral domain. The filtering can be either taken as multiplication or convolution of the filter function and the SLSHT distribution in the spatio-spectral domain, which will be discussed in the following two subsections. But first, we define the filter function in the spatio-spectral domain that modifies the given SLSHT distribution of a signal.

**Definition 5.1 (Filter Function in Spatio-spectral Domain)** *Define $\boldsymbol{z}(\hat{\boldsymbol{x}})$ to be the filter function in the spatio-spectral domain as*

$$\boldsymbol{z}(\hat{\boldsymbol{x}}) \triangleq \big(z(\hat{\boldsymbol{x}}; 0), z(\hat{\boldsymbol{x}}; 1), z(\hat{\boldsymbol{x}}; 2), \cdots, z(\hat{\boldsymbol{x}}; N_g)\big)', \tag{5.14}$$

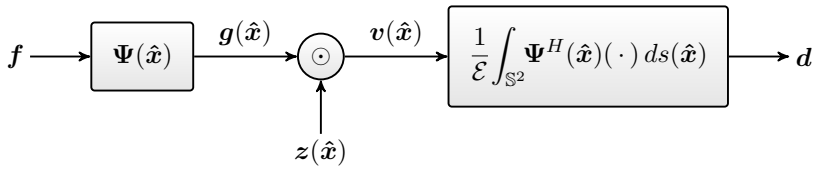


(a)

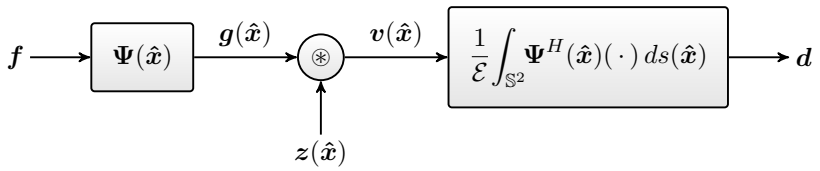


(b)

Figure 5.3: The block diagram that represents the concept of filtering in spatio-spectral domain as (a) multiplicative modification of the SLSHT distribution and (b) convolutive modification of the SLSHT distribution.

*where each element* $z(\hat{\boldsymbol{x}}; n)$ *for* $0 \leq n \leq N_g$ *can be a finite-norm, square integrable function on the unit sphere with the maximum spectral degree* $L_{z_n}$ *and spherical harmonic expansion* $z(\hat{\boldsymbol{x}}; n) = \sum_{c=0}^{N_{z_n}} \big(z_n\big)_c Y_c(\hat{\boldsymbol{x}})$*, where* $N_{z_n} = L_{z_n}^2 + 2L_{z_n}$*. The spectral response of each component of the filter function is defined as* $\boldsymbol{z}_n \triangleq \big(\big(z_n\big)_0, \big(z_n\big)_1, \cdots, \big(z_n\big)_{N_{z_n}}\big) \triangleq \big(\mathcal{F}z\big)(\hat{\boldsymbol{x}}; n)$*.*

We use the definition of signal transformation in the joint spatio-spectral domain using the operator $\mathcal{K}$ as defined in (5.2) and relate the kernel $\boldsymbol{\zeta}(\hat{\boldsymbol{x}}, \hat{\boldsymbol{y}})$ to the filter function $\boldsymbol{z}(\hat{\boldsymbol{x}})$ to define filtering operations in joint spatio-spectral domain. The modified distribution $\boldsymbol{v}(\hat{\boldsymbol{x}})$, which is obtained as either multiplication or convolution of the filter function and the SLSHT distribution of the signal, may not be a valid SLSHT distribution and it may not be possible to find the signal $d(\hat{\boldsymbol{x}})$, which exactly describes the distribution $\boldsymbol{v}(\hat{\boldsymbol{x}})$. Thus, the approximate approach as described in Theorem 5.1 can be employed to determine the signal $d(\hat{\boldsymbol{x}})$, whose SLSHT distribution is closest to the modified distribution in the least squares sense.

In the following two subsections, we define multiplicative and convolutive filtering operations in the spatio-spectral domain, respectively, and formulate expressions to determine the signal $d(\hat{\boldsymbol{x}})$ from the modified distribution $\boldsymbol{v}(\hat{\boldsymbol{x}})$. We also present the proposed filtering operations as linear transformations of the signal as given in (5.12) and provide specific expressions for the spatio-spectral transformation matrix $\boldsymbol{\Upsilon}$ in (5.13) for these two types of filtering operations.

### 5.3.1 Multiplicative Modification of SLSHT Distribution

In time-frequency analysis, a time-domain signal can be filtered in the joint time-frequency domain through multiplication of its time-frequency representation and the filter function as described in [64, 65, 72–74, 80, 81]. Using SLSHT distribution as a spatio-spectral representation of a signal on the sphere, we define analogous multiplicative filtering in joint spatio-spectral domain.

**Definition 5.2 (Multiplicative SLSHT Modification)** *Relating the kernel* $\boldsymbol{\zeta}(\hat{\boldsymbol{x}}, \hat{\boldsymbol{y}})$ *in* (5.2) *to the filter function* $\boldsymbol{z}(\hat{\boldsymbol{x}})$ *as*

$$\boldsymbol{\zeta}(\hat{\boldsymbol{x}}, \hat{\boldsymbol{y}}) \triangleq \boldsymbol{z}(\hat{\boldsymbol{x}})\, \delta(\hat{\boldsymbol{x}}, \hat{\boldsymbol{y}}), \tag{5.15}$$

*where* $\delta(\hat{\boldsymbol{x}}, \hat{\boldsymbol{y}})$ *is the Dirac delta function on the sphere, we define component-wise multiplication of the SLSHT distribution* $\boldsymbol{g}(\hat{\boldsymbol{x}})$ *and the filter function* $\boldsymbol{z}(\hat{\boldsymbol{x}})$ *to obtain the multiplicative modified distribution (MMD),* $\boldsymbol{v}(\hat{\boldsymbol{x}})$ *through*

$$v(\hat{\boldsymbol{x}}; n) \triangleq z(\hat{\boldsymbol{x}}; n)\, g(\hat{\boldsymbol{x}}; n), \tag{5.16}$$

*for* $0 \leq n \leq N_g$*, which results in*

$$\boldsymbol{v}(\hat{\boldsymbol{x}}) \triangleq \boldsymbol{z}(\hat{\boldsymbol{x}}) \odot \boldsymbol{g}(\hat{\boldsymbol{x}}). \tag{5.17}$$

*Multiplicative modification of the SLSHT distribution in spatio-spectral domain is depicted in the first two blocks of Fig. 5.3(a).*

**Remark 5.2** *Since each component of the SLSHT distribution describes the spatially varying contribution of a spherical harmonic in the spatial domain, the multiplication of the filter function* $\boldsymbol{z}(\hat{\boldsymbol{x}})$ *and the SLSHT distribution* $\boldsymbol{g}(\hat{\boldsymbol{x}})$ *can be thought of as a type of spatially-varying spectral filtering.*

**Remark 5.3** *If the filter function* $\boldsymbol{z}(\hat{\boldsymbol{x}})$ *is real, then the kernel* $\boldsymbol{\zeta}(\hat{\boldsymbol{x}}, \hat{\boldsymbol{y}})$ *in* (5.15) *is real and satisfies* $\boldsymbol{\zeta}(\hat{\boldsymbol{x}}, \hat{\boldsymbol{y}}) = \boldsymbol{\zeta}(\hat{\boldsymbol{y}}, \hat{\boldsymbol{x}})$*, which implies that the corresponding operator is self adjoint.*

The general least squares approximation method of $\boldsymbol{v}(\hat{\boldsymbol{x}})$ is shown in the third block of Fig. 5.3(a) according to (5.10). For the special case of exact recovery, we can explicitly provide the expression for obtaining the signal exactly from the modified distribution $\boldsymbol{v}(\hat{\boldsymbol{x}})$.

**Lemma 5.1** *If the MMD, $\boldsymbol{v}(\hat{\boldsymbol{x}})$ given in* (5.17)*, is a valid SLSHT distribution, then the n-th spherical harmonic coefficient of the transformed signal $d(\hat{\boldsymbol{x}})$, denoted by $\big(d\big)_n$, is related to the signal $f(\hat{\boldsymbol{x}})$ by*

$$\big(d\big)_n = \frac{1}{K}\int_{\mathbb{S}^2} f(\hat{\boldsymbol{x}}) w_n(\hat{\boldsymbol{x}}) \overline{Y_n(\hat{\boldsymbol{x}})}\, ds(\hat{\boldsymbol{x}}), \tag{5.18}$$

*where $w_n(\hat{\boldsymbol{x}})$ is the result of isotropic convolution of the n-th filter component $z(\hat{\boldsymbol{x}}; n)$ and the azimuthally symmetric window function $h(\hat{\boldsymbol{x}})$. That is,*

$$w_n(\hat{\boldsymbol{x}}) = \int_{\mathbb{S}^2} \big(\mathcal{D}(\phi,\theta,0)h\big)(\hat{\boldsymbol{y}})\, z(\hat{\boldsymbol{y}}; n)\, ds(\hat{\boldsymbol{y}}), \quad \hat{\boldsymbol{x}} = \hat{\boldsymbol{x}}(\theta,\phi). \tag{5.19}$$

**Proof**

See Appendix A.2. □

In what follows, we first explicitly discuss the case where the MMD, $\boldsymbol{v}(\hat{\boldsymbol{x}})$, is a valid SLSHT distribution and provide the elements of the transformation matrix $\boldsymbol{\Upsilon}$ for this special case. We then discuss the elements of the transformation matrix $\boldsymbol{\Upsilon}$ in the general approximation approach.

**Lemma 5.2** *Assume that the MMD, $\boldsymbol{v}(\hat{\boldsymbol{x}})$, is a valid SLSHT distribution. Then the spatio-spectral transformation matrix $\boldsymbol{\Upsilon}$ in* (5.12)*, which relates $\boldsymbol{d}$ to $\boldsymbol{f}$, is given by*

$$\boldsymbol{\Upsilon} = \frac{1}{K}\int_{\mathbb{S}^2} \Big\{ \mathrm{diag}\big(\boldsymbol{z}(\hat{\boldsymbol{x}})\big)\, \boldsymbol{\Psi}(\hat{\boldsymbol{x}}) \Big\}_{N_f} ds(\hat{\boldsymbol{x}}), \tag{5.20}$$

*where $\mathrm{diag}\big(\boldsymbol{z}(\hat{\boldsymbol{x}})\big)$ is the diagonal matrix with diagonal entries specified by $\boldsymbol{z}(\hat{\boldsymbol{x}})$ and $\{\cdot\}_{N_f}$ selects the first sub-matrix of size $(N_f+1)\times(N_f+1)$. The entries of $\boldsymbol{\Upsilon}$ are*

$$\begin{aligned}\Upsilon_{u,u'} &= \frac{1}{K}\int_{\mathbb{S}^2} z(\hat{\boldsymbol{x}}; u)\, \psi_{u,u'}(\hat{\boldsymbol{x}})\, ds(\hat{\boldsymbol{x}}) \\ &= \sum_{r=0}^{\min(N_h,\, N_{z_u})} \frac{1}{\big(h\big)_0^0 \sqrt{2p+1}}\, T(u'; r; u)\, \big(h\big)_p^0 \big(z_u\big)_r, \quad (p,q) \leftrightarrow r. \end{aligned} \tag{5.21}$$

**Proof**

See Appendix A.2. □

**Lemma 5.3** *For the multiplicative modification of the SLSHT distribution, the general spatio-spectral transformation matrix $\boldsymbol{\Upsilon}$ in* (5.13) *is simplified to*

$$\boldsymbol{\Upsilon} = \frac{1}{\mathcal{E}}\Big( \int_{\mathbb{S}^2} \boldsymbol{\Psi}^H(\hat{\boldsymbol{x}}) \big(\mathrm{diag}\big(\boldsymbol{z}(\hat{\boldsymbol{x}})\big)\, \boldsymbol{\Psi}(\hat{\boldsymbol{x}})\big)\, ds(\hat{\boldsymbol{x}}) \Big), \tag{5.22}$$

*with entries given by*

$$\Upsilon_{u,u'} = \frac{1}{\mathcal{E}} \sum_{n=0}^{N_g} \sum_{r=0}^{N_h} \sum_{r'=0}^{N_h} \sum_{c=0}^{N_{z_n}} \frac{4\pi}{\sqrt{(2p+1)(2p'+1)}} \overline{(h)_p^0}(h)_{p'}^0(z_n)_c \times T(u;r;n)\, T(u';r';n)\, T(r;c;r'), \tag{5.23}$$

*where the mappings* $(\ell, m) \leftrightarrow n$, $(p, q) \leftrightarrow r$, $(p', q') \leftrightarrow r'$ *and* $(s, t) \leftrightarrow u$ *are used.*

**Proof**

See Appendix A.2. □

We note that this approximate solution cannot be further simplified because of the coupling of Wigner-3$j$ symbols.

### 5.3.2 Convolutive Modification of the SLSHT Distribution

We now consider a signal transformation in the spatio-spectral domain as the convolutive modification of the SLSHT distribution, which can be achieved through convolution of the filter function $\boldsymbol{z}(\hat{\boldsymbol{x}})$ and the SLSHT distribution $\boldsymbol{g}(\hat{\boldsymbol{x}})$. The convolutive modification can also be thought of as spatially-varying spectral filtering of the signal, which is accomplished by filtering the spatially-varying spectral components of the signal in the spatial domain. The analog of convolutive modification in time-frequency analysis is smoothing of the time-frequency distribution to remove artifacts in the time-frequency domain [65, 97]. We first specify the kernel $\boldsymbol{\zeta}(\hat{\boldsymbol{x}}, \hat{\boldsymbol{y}})$ in terms of the convolutive filter function and then express this operation as a linear transformation of the signal. Later, we discuss the special case in which each component of the filter function is azimuthally symmetric.

**Definition 5.3 (Convolutive SLSHT Modification)** *Let* $\hat{\boldsymbol{x}} = \hat{\boldsymbol{x}}(\theta, \phi)$ *and a spatio-spectral filter function* $\boldsymbol{z}(\hat{\boldsymbol{y}})$ *be given according to Definition 5.1. The kernel* $\boldsymbol{\zeta}(\hat{\boldsymbol{x}}, \hat{\boldsymbol{y}})$ *in* (5.2) *is obtained by rotating each component of* $\boldsymbol{z}(\hat{\boldsymbol{y}})$*, such as* $z(\hat{\boldsymbol{y}}; n)$*, as follows*

$$\begin{aligned}\boldsymbol{\zeta}(\hat{\boldsymbol{x}}, \hat{\boldsymbol{y}}) &\triangleq \big(\mathcal{D}(\phi, \theta, 0)\boldsymbol{z}\big)(\hat{\boldsymbol{y}}) \\ &= \Big(\big(\mathcal{D}(\phi, \theta, 0)z\big)(\hat{\boldsymbol{y}}; 0),\ \big(\mathcal{D}(\phi, \theta, 0)z\big)(\hat{\boldsymbol{y}}; 1),\ \cdots,\ \big(\mathcal{D}(\phi, \theta, 0)z\big)(\hat{\boldsymbol{y}}; N_g)\Big)'.\end{aligned} \tag{5.24}$$

*As a result, the convolutive modified distribution (CMD)* $\boldsymbol{v}(\hat{\boldsymbol{x}})$ *will have elements given by*

$$v(\hat{\boldsymbol{x}};n) = \int_{\mathbb{S}^2} \big(\mathcal{D}(\phi,\theta,0)z\big)(\hat{\boldsymbol{y}};n)\, g(\hat{\boldsymbol{y}};n)\, ds(\hat{\boldsymbol{y}}), \quad \hat{\boldsymbol{x}} = \hat{\boldsymbol{x}}(\theta,\phi), \tag{5.25}$$

*for* $0 \leq n \leq N_g$*. More concisely, we can write*

$$\boldsymbol{v}(\hat{\boldsymbol{x}}) \triangleq \big(\boldsymbol{z} \circledast \boldsymbol{g}\big)(\hat{\boldsymbol{x}}), \tag{5.26}$$

*where '*$\circledast$*' denotes spherical convolution. This type of filtering in spatio-spectral domain as convolutive modification of the SLSHT distribution is depicted in the first two blocks of Fig. 5.3(b).*

We note here that the convolution definition here, given by the operand symbol '$\circledast$' is different from the definition of convolutions presented in Chapter 3. Here, we consider the special case of SO(3) convolution presented in (3.2) in Chapter 3, with the consideration that the initial rotation around $z$-axis is zero.

Using the definition of the SLSHT distribution $\boldsymbol{g}(\hat{\boldsymbol{x}})$ for signal $f(\hat{\boldsymbol{x}})$, we now formulate an expression that relates the CMD $\boldsymbol{v}(\hat{\boldsymbol{x}})$ to $\boldsymbol{f} = \big(\mathcal{F}f\big)(\hat{\boldsymbol{x}})$. Such a relation will be useful in finding the signal $d(\hat{\boldsymbol{x}})$ with spectral response $\boldsymbol{d}$ that corresponds to the CMD $\boldsymbol{v}(\hat{\boldsymbol{x}})$, and in expressing $\boldsymbol{d}$ as a linear transformation of $\boldsymbol{f}$. This is accomplished by defining the matrix $\boldsymbol{\Gamma}(\hat{\boldsymbol{x}}) \triangleq \boldsymbol{z}(\hat{\boldsymbol{x}}) \circledast \boldsymbol{\Psi}(\hat{\boldsymbol{x}})$ of size $(N_g+1)\times(N_f+1)$ with entries

$$\begin{aligned}\Gamma_{n,u}(\hat{\boldsymbol{x}}) &= \int_{\mathbb{S}^2} \big(\mathcal{D}(\phi,\theta,0)z\big)(\hat{\boldsymbol{y}};n)\, \psi_{n,u}(\hat{\boldsymbol{y}})\, ds(\hat{\boldsymbol{y}}) \\ &= \sum_{r=0}^{\min(N_h,N_{z_n})} \sum_{q'=-p}^{p} \sqrt{\frac{4\pi}{2p+1}} \big(h\big)_p^0 \big(z_n\big)_p^{q'}\, T(u;r;n)\, D_p^{q,q'}(\phi,\theta,0),\end{aligned} \tag{5.27}$$

with $\hat{\boldsymbol{x}} = \hat{\boldsymbol{x}}(\theta,\phi)$ and $r \leftrightarrow (p,q)$, which is obtained using (4.6) and (4.12). Therefore, referring to (4.10) we express the CMD $\boldsymbol{v}(\hat{\boldsymbol{x}})$ in (5.26) as

$$\boldsymbol{v}(\hat{\boldsymbol{x}}) = \boldsymbol{\Gamma}(\hat{\boldsymbol{x}})\boldsymbol{f}. \tag{5.28}$$

Now, we derive the expressions for the spatio-spectral transform matrix $\boldsymbol{\Upsilon}$ in (5.12) for both exact and approximate cases.

**Lemma 5.4** *If the CMD* $\boldsymbol{v}(\hat{\boldsymbol{x}})$ *defined in* (5.26) *is a valid SLSHT distribution, the spatio-spectral transform matrix* $\boldsymbol{\Upsilon}$ *is obtained by using the inversion operation defined in Theorem 4.1 as*

$$\boldsymbol{\Upsilon} = \frac{1}{K} \int_{\mathbb{S}^2} \Big\{ \boldsymbol{\Gamma}(\hat{\boldsymbol{x}}) \Big\}_{N_f} ds(\hat{\boldsymbol{x}}), \tag{5.29}$$

*where the entries are obtained by integrating the elements of* $\boldsymbol{\Gamma}(\hat{\boldsymbol{x}})$ *in* (5.27) *as*

$$\Upsilon_{u,u'} = \sum_{r=0}^{\min(N_h, N_{z_u})} \sum_{q'=-p}^{p} \frac{1}{(h)_0^0 \sqrt{2p+1}} (h)_p^0 \, (z_u)_p^{q'} \, T(u'; r, u) \int_{\mathbb{S}^2} D_p^{q,q'}(\phi, \theta, 0) \, ds(\hat{\boldsymbol{x}}). \tag{5.30}$$

*The integral above can be evaluated using the relation between spherical harmonic function and Wigner-D function in* (2.30) *and the expression for the integral of associated Legendre function [98] as*

$$\int_{\mathbb{S}^2} D_p^{q,q'}(\phi, \theta, 0) \, ds(\hat{\boldsymbol{x}}) = 2\pi \, \delta_{q,0} \int_0^{\pi} d_p^{0,q'}(\theta) \sin\theta \, d\theta \tag{5.31}$$

$$= 2\pi \begin{cases} -\dfrac{2q' \, (p/2)! \, (p/2)! \, \sqrt{(p-q')!(p+q')!}}{p \, \big((p+q')/2\big)! \, \big((p-q')/2\big)! \, (p+1)!} \\ \qquad \textit{if } p \textit{ is even, } q' \textit{ is even, and } q = 0, \\ -\dfrac{q'\pi \, (p+1)! \, \sqrt{(p-q')!(p+q')!}}{p \, 2^{2p+1} \, \big((p+q')/2\big)! \, \big((p-q')/2\big)! \, \big((p+1)/2\big)!} \\ \qquad \textit{if } p \textit{ is odd, } q' \textit{ is odd, and } q = 0, \\ 0 \quad \textit{otherwise.} \end{cases} \tag{5.32}$$

**Proof**

The proof follows directly from (5.27) and is omitted for brevity. □

**Lemma 5.5** *For the case that the CMD* $\boldsymbol{v}(\hat{\boldsymbol{x}})$ *in* (5.26) *is not a valid SLSHT distribution, the approximate solution presented in Theorem 5.1 specializes to*

$$\boldsymbol{\Upsilon} = \frac{1}{\mathcal{E}} \int_{\mathbb{S}^2} \boldsymbol{\Psi}^H(\hat{\boldsymbol{x}}) \, \boldsymbol{\Gamma}(\hat{\boldsymbol{x}}) \, ds(\hat{\boldsymbol{x}}), \tag{5.33}$$

*with entries*

$$\Upsilon_{u,u'} = \frac{1}{\mathcal{E}} \sum_{n=0}^{N_g} \int_{\mathbb{S}^2} \overline{\psi_{n,u}(\hat{\boldsymbol{x}})} \Gamma_{n,u'}(\hat{\boldsymbol{x}}) \, ds(\hat{\boldsymbol{x}})$$

$$= \frac{1}{\mathcal{E}} \sum_{n=0}^{N_g} \sum_{r=0}^{N_h} \sum_{r'=0}^{\min(N_h, N_{z_n})} \sum_{q''=-p'}^{p'} \frac{4\pi}{\sqrt{(2p+1)}} \overline{(h)_p^0} \frac{1}{\sqrt{(2p'+1)}} (h)_{p'}^0 \times \left(z_n\right)_{p'}^{q''} T(u;r;n)\, T(u';r';n) \int_{\mathbb{S}^2} D_{p'}^{q',q''}(\phi,\theta,0) Y_r(\hat{\boldsymbol{x}})\, ds(\hat{\boldsymbol{x}}), \quad (5.34)$$

*where the mappings* $(p,q) \leftrightarrow r$ *and* $(p',q') \leftrightarrow r'$ *are used. The integral in* (5.34) *is the projection of Wigner-D function* $D_{p'}^{q',q''}(\phi,\theta,0)$ *onto spherical harmonics and can be evaluated by employing the expansion of the product of Wigner-D functions using Wigner* $3j$ *symbols. Following the relation between Wigner-D functions and spherical harmonics in* (2.30)*, the integral in* (5.34) *can be expressed as*

$$\int_{\mathbb{S}^2} D_{p'}^{q',q''}(\phi,\theta,0) Y_p^q(\hat{\boldsymbol{x}})\, ds(\hat{\boldsymbol{x}}) = \sqrt{\frac{4\pi}{2p+1}} \int_0^{\pi} d_{p'}^{q',q''}(\theta) d_p^{q,0}(\theta) \sin\theta d\theta \int_0^{2\pi} e^{-i(q-q')\phi} d\phi$$
$$= 2\pi \sqrt{\frac{4\pi}{2p+1}} \int_0^{\pi} d_{p'}^{q',q''}(\theta) d_p^{q',0}(\theta) \sin\theta d\theta, \quad (5.35)$$

*where the integral over* $\theta$ *can be evaluated by employing the following expansion of product of Wigner-d functions in terms of Wigner-*$3j$ *symbols and then using the computation of integral given in* (5.31)

$$d_{p'}^{q',q''}(\theta) d_p^{q',0}(\theta) = (-1)^{q''} \sum_{c=|p'-p|}^{p'+p} (2c+1)\, d_c^{0,q''}(\theta) \begin{pmatrix} p' & p & c \\ q' & q' & -2q' \end{pmatrix} \begin{pmatrix} p' & p & c \\ q'' & 0 & -q'' \end{pmatrix}. \quad (5.36)$$

**Proof**

We use (5.10), (5.12), and (5.28) to infer (5.33). Equation (5.34) follows from (5.27) and (A.10), where the latter is defined in Appendix A.2. □

Again, further simplification of this approximate solution is not possible because of coupling of Wigner-$3j$ symbols and irreducible Wigner-D functions. However, for the special case where each component of the filter function is azimuthally symmetric, we obtain further simplifications as follows.

#### 5.3.2.1 Special Case – Azimuthally Symmetric Filter Function

If each component of the filter function is azimuthally symmetric, then $\left(z_n\right)_{p'}^{q''} = 0$ for $q'' \neq 0$ in (5.34) for all $n \in [0, N_g]$. Using the relation between Wigner-$D$ functions and spherical harmonics in (2.30) and the orthonormal property of

spherical harmonics, the expression for the entries $\Upsilon_{u,u'}$ in (5.34) simplifies to

$$\Upsilon_{u,u'} = \frac{1}{\mathcal{E}} \sum_{n=0}^{N_g} \sum_{r=0}^{\min(N_h, N_{z_n})} \left(\frac{4\pi}{2p+1}\right)^{3/2} \left|(h)_p^0\right|^2 (z_n)_p^0 \times T(u;r;n)\, T(u';r;n), \qquad (p,q) \leftrightarrow r. \tag{5.37}$$

Let us assume that in addition to being azimuthally symmetric, the components of the filter function also satisfy $z(\hat{\boldsymbol{x}};n) = z(\hat{\boldsymbol{x}};\ell)$ with the mapping $(\ell,m) \leftrightarrow n$ for all $n \in [0, N_g]$, which indicates that there is the same filter function component of degree $\ell$ for all the spherical harmonic orders $-\ell \leq m \leq \ell$. With this assumption and employing the orthogonality relations of Wigner-3$j$ symbols [40], $\Upsilon_{u,u'}$ in (5.37) simplifies to

$$\Upsilon_{u,u'} = \frac{1}{\mathcal{E}} \sum_{\ell=0}^{L_g} \sum_{p=0}^{\min(L_h, L_{z_n})} (2\ell+1) \sqrt{\frac{4\pi}{2p+1}}\, (z_\ell)_p^0 \left|(h)_p^0\right|^2 \begin{pmatrix} s & p & \ell \\ 0 & 0 & 0 \end{pmatrix}^2 \delta_{u,u'} \tag{5.38}$$

and the spatio-spectral transformation matrix $\boldsymbol{\Upsilon}$ becomes a diagonal matrix.

## 5.4 Examples

In this section, we provide an illustration of the filtering operation in the spatio-spectral domain. In our experiments, we have implemented the method outlined in [31] to calculate the spherical harmonic coefficients and the triple product (2.23) in `MATLAB`. We use equiangular sampling with $M \times M$ samples on the sphere as $\theta_m = \pi m/M$, $\phi_m = 2\pi m/M$ for $m = 0, 1, \ldots, M-1$. Note that the exact quadrature rule can be evaluated using this tessellation. We use the most optimally concentrated azimuthally symmetric band-limited Slepian eigenfunction as the window function to obtain the SLSHT distribution of a signal [1,27]. For inverse spherical harmonic transform of a function with the maximum spherical harmonic degree $L$, we use the minimum resolution $M = 2(L+1)$ for the exact quadrature rule [31]. Furthermore, we consider unit energy normalized functions in our experiments.

### 5.4.1 First Example

In our first example, we consider the band-limited azimuthally symmetric signal $f(\hat{\boldsymbol{x}}) = f(\theta)$ on the sphere with maximum spherical harmonic degree $L_f = 60$.

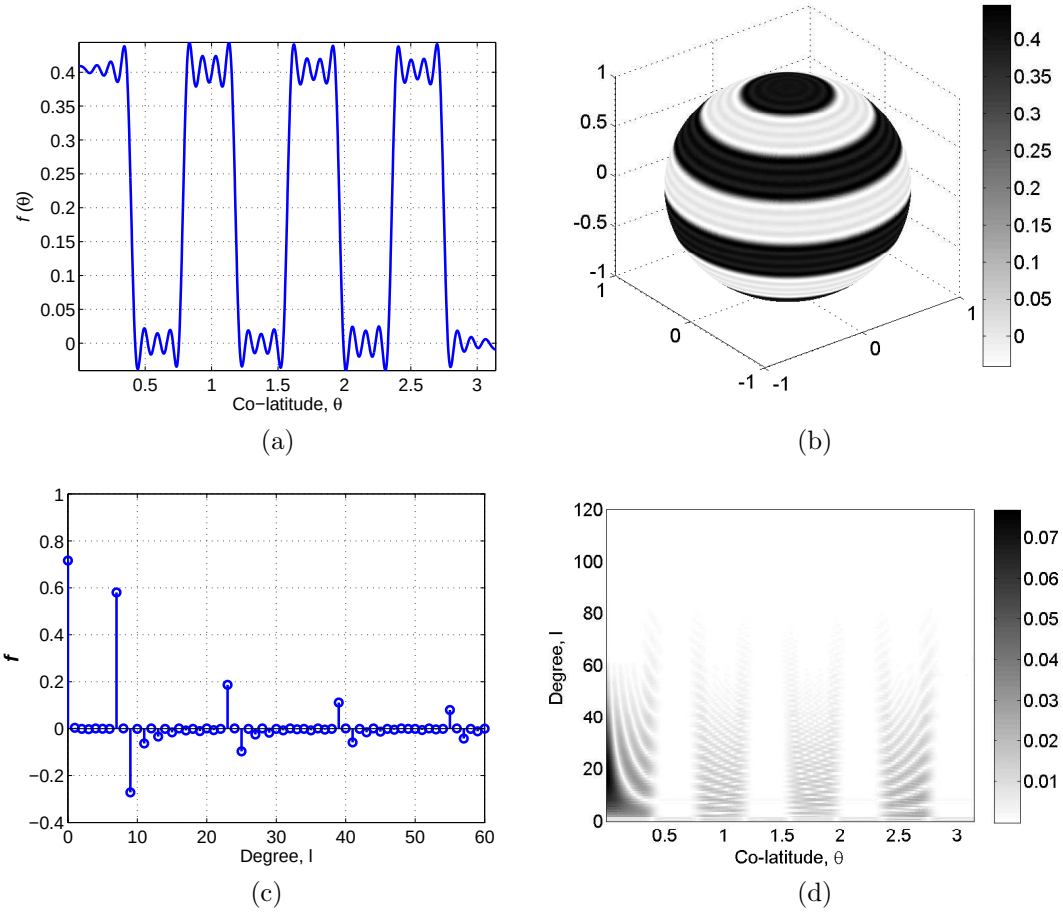


Figure 5.4: Signal $f(\hat{\boldsymbol{x}}) = f(\theta)$: (a) as a function of co-latitude $\theta$ and (b) on the sphere. (c) Spectrum of the signal $\boldsymbol{f}$ vs degree $\ell$ for order $m = 0$, $\left(f\right)_\ell^0$. (d) SLSHT distribution $\boldsymbol{g}(\hat{\boldsymbol{x}})$ of the signal as a function of degree $\ell$ and co-latitude $\theta$.

The signal under consideration is shown in Fig. 5.4(a) and (b) and is obtained by spectrally truncating the following signal $f_1(\hat{\boldsymbol{x}})$ defined as

$$f_1(\hat{\boldsymbol{x}}) = f_1(\theta) \triangleq \begin{cases} 1, & \theta \in [0, \pi/8] \cup [\pi/4, 3\pi/8] \cup [\pi/2, 5\pi/8] \cup [3\pi/4, 7\pi/8]; \\ 0, & \text{otherwise}; \end{cases} \tag{5.39}$$

to a maximum spherical harmonic degree $L_f$. Since the signal is azimuthally symmetric, only zero-order spherical harmonic coefficients $\left(f\right)_\ell^0$ can be non-zero, which are shown in Fig. 5.4(c). Since we are seeking the contribution of zero-order spherical harmonics, the SLSHT distribution $\boldsymbol{g}(\hat{\boldsymbol{x}})$ is shown in Fig. 5.4(d) as a function of co-latitude $\theta$ and degree $\ell$. The SLSHT distribution is obtained using an azimuthally symmetric eigenfunction window of maximum degree $L_h = 60$, which is

spatially concentrated in the region $0 \leq \theta \leq \pi/30$. We are interested to obtain the MMD $\boldsymbol{v}(\hat{\boldsymbol{x}})$, defined in (5.17), using the following filter function $\boldsymbol{z}(\hat{\boldsymbol{x}})$

$$z(\hat{\boldsymbol{x}}; \ell, 0) = \begin{cases} 1, & 30 \leq \ell \leq 50,\ \pi/4 \leq \theta \leq \pi/2,\ 0 \leq \phi < 2\pi; \\ 0, & \text{otherwise;} \end{cases} \tag{5.40}$$

where the maximum spectral degree is considered to be $L_{z_n} = 60$ for each non-zero filter component $z(\hat{\boldsymbol{x}}; \ell, 0)$ for $30 \leq \ell \leq 50$. The filter function $\boldsymbol{z}(\hat{\boldsymbol{x}})$ is shown in the spatio-spectral domain in Fig. 5.5(a) as a function of degree $\ell$ and co-latitude $\theta$. The negligible ringing, which can be observed outside the spatio-spectral region defined in (5.40) along the spatial domain, is due to the consideration that each component of filter function is band-limited with $L_{z_n} = 60$. Since the filter function truncates $\boldsymbol{g}(\hat{\boldsymbol{x}})$ in both the spatial and spectral domains, the resulting MMD $\boldsymbol{v}(\hat{\boldsymbol{x}})$ is not a valid SLSHT distribution. Therefore, we employ the approximate solution to determine the signal $d(\hat{\boldsymbol{x}}) = d(\theta)$, the SLSHT distribution of which best approximates the MMD $\boldsymbol{v}(\hat{\boldsymbol{x}})$ in the least squares sense. The approximated distribution $\hat{\boldsymbol{v}}(\hat{\boldsymbol{x}})$ is shown in Fig. 5.5(b) which is the SLSHT distribution of signal $d(\hat{\boldsymbol{x}})$. The signal $d(\hat{\boldsymbol{x}})$ is shown in Fig. 5.5(c) and Fig. 5.5(d) in the spatial and spectral domains, respectively. The approximated distribution $\hat{\boldsymbol{v}}(\hat{\boldsymbol{x}})$ shows that the signal is concentrated around the desired spatio-spectral region. There are some artifacts near the poles at $\theta = 0$ and $\theta = \pi$, which is due to the fact that zero-order spherical harmonics have relatively higher values near the poles.

### 5.4.2 Second Example

The type of filtering shown in Section 5.4.1 which truncates the signal in the spatio-spectral domain can also be considered as spatial truncation followed by spectral truncation. However, this will not ensure concentration of the filtered signal in the spatio-spectral domain. In order to further illustrate the capability of the proposed framework, we consider another example of multiplicative modification of the SLSHT distribution, in which we carry out spatially-varying spectral filtering in the spatio-spectral domain.

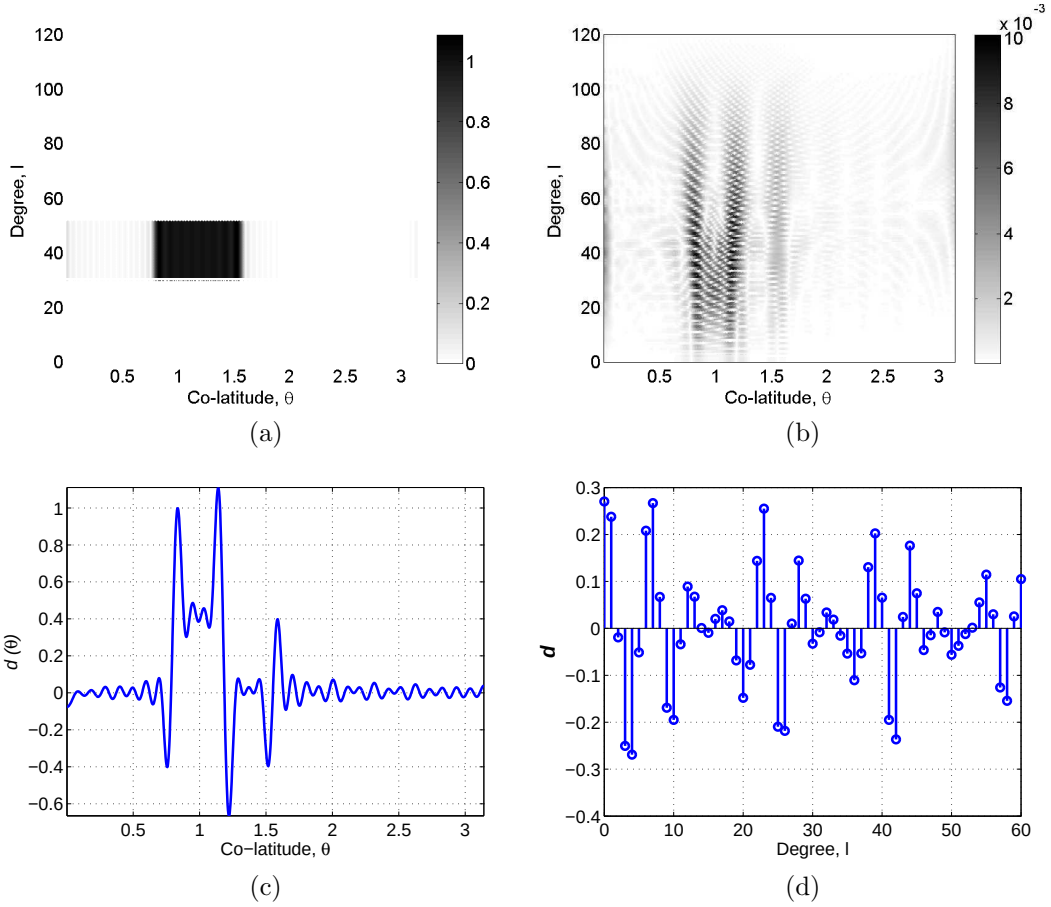


Figure 5.5: (a) Spatially-varying filter $\boldsymbol{z}(\hat{\boldsymbol{x}})$ as defined in (5.40). (b) The approximated distribution $\hat{\boldsymbol{v}}(\hat{\boldsymbol{x}})$ as the SLSHT distribution of the signal $d(\hat{\boldsymbol{x}})$. (c) Signal $d(\hat{\boldsymbol{x}}) = d(\theta)$ in the spatial domain as a function of co-latitude $\theta$ and (d) in the spectral domain as $\boldsymbol{d}$ vs degree $\ell$ for order $m = 0$.

We consider the following filter function $\boldsymbol{z}(\hat{\boldsymbol{x}})$ in the spatio-spectral domain

$$z(\hat{\boldsymbol{x}};\ell,0) = \begin{cases} 1, & 0 \leq \ell \leq 10,\ 0 \leq \theta \leq \pi,\ 0 \leq \phi < 2\pi; \\ 1, & 11 \leq \ell \leq 70,\ (\ell+20)\pi/120 \leq \theta \leq \pi; 0 \leq \phi < 2\pi \\ 1, & 71 \leq \ell \leq 120,\ 3\pi/4 \leq \theta \leq \pi,\ 0 \leq \phi < 2\pi; \\ 0, & \text{otherwise;}, \end{cases} \tag{5.41}$$

which is shown in Fig. 5.6(a), where we have again assumed that each filter function component is band-limited with the maximum spherical harmonic degree equal to $L_{z_n} = 60$. It is evident from Fig. 5.6(a) that the filter function is spatially-varying in the spatio-spectral domain and thus filters out different spectral contents in different spatial regions. For example, it filters the contribution of all spherical

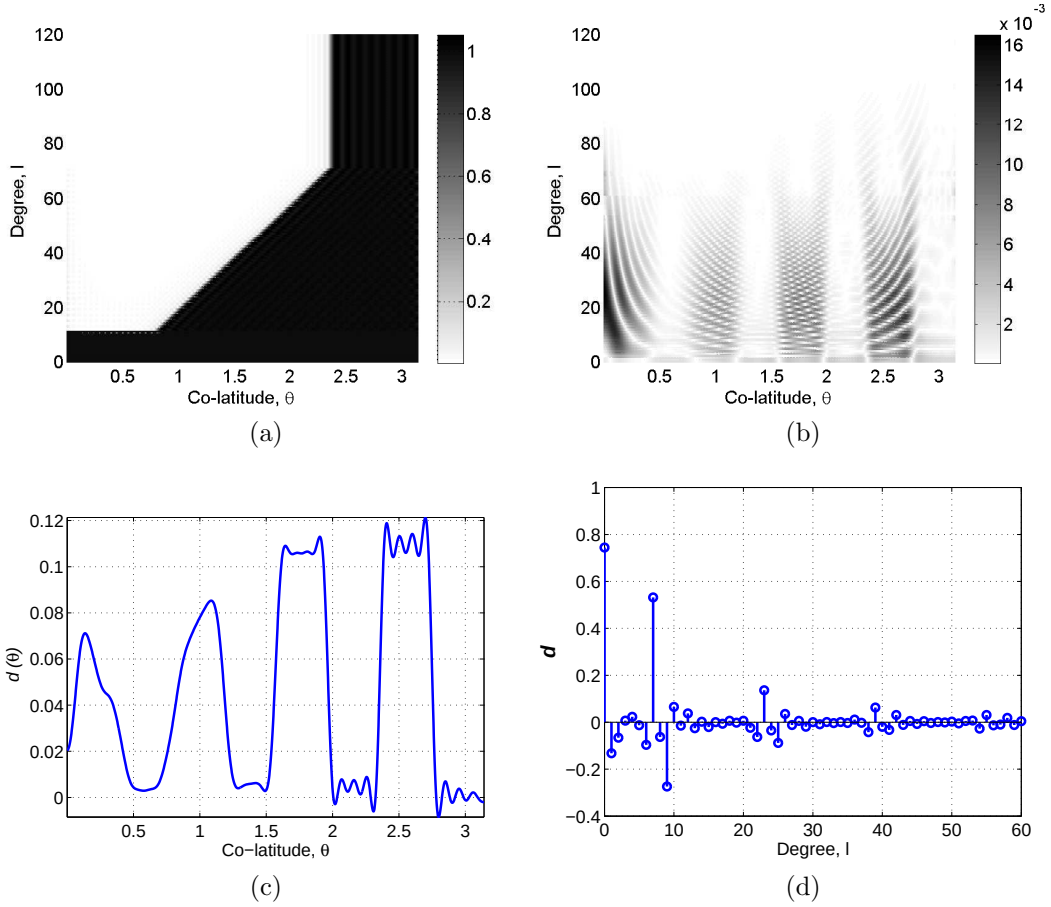


Figure 5.6: (a) Spatially-varying filter $\boldsymbol{z}(\hat{\boldsymbol{x}})$ as defined in (5.41). (b) The approximated distribution $\hat{\boldsymbol{v}}(\hat{\boldsymbol{x}})$ as the SLSHT distribution of the signal $d(\hat{\boldsymbol{x}})$. (c) Signal $d(\hat{\boldsymbol{x}}) = d(\theta)$ in the spatial domain as a function of co-latitude $\theta$ and (d) in the spectral domain as $\boldsymbol{d}$ vs degree $\ell$ for order $m = 0$.

harmonics of degree greater than 10 around $\theta = \pi/4$, whereas it filters spherical harmonics of degree greater than 70 around $\theta = 3\pi/4$. Thus such type of filtering can be regarded as spatially-varying low pass filtering, where the bandwidth of the filter function is changing with the co-latitude. Using the proposed least squares solution, we determine the signal $d(\hat{\boldsymbol{x}})$ whose SLSHT distribution best approximates the MMD $\boldsymbol{v}(\hat{\boldsymbol{x}})$ in the least squares sense. The approximated distribution $\hat{\boldsymbol{v}}(\hat{\boldsymbol{x}})$ in the spatio-spectral domain and the signal $d(\hat{\boldsymbol{x}})$ in spatial and spectral domains are shown in Fig. 5.6(b), (c) and (d), where the effect of spatially-varying low-pass filtering is apparent.

## 5.5 Summary of Contributions

In this chapter, we have presented a framework to transform a signal in the spatio-spectral domain using SLSHT distribution of a signal presented in Chapter 4. Due to transformation of SLSHT distribution of a signal in spatio-spectral domain, there is a possibility that there exists no signal which corresponds to the modified distribution. To address this problem, we have presented solution to find a signal, the SLSHT distribution of which optimally approximates the modified distribution in the least square sense. The proposed framework has also been formulated as a linear transformation of a signal.

Later, we investigated multiplicative and convolutive modification of SLSHT distribution in the spatio-spectral domain. The power of the technique was illustrated in two examples of spatially-varying spectral filtering that allows processing of signals in joint spatio-spectral domain, in a way that cannot be accomplished separately in either spatial or spectral domain. The contributions made in this chapter are as follows.

Addressing Q5 posed in Section 1.2.1:

- Using the SLSHT distribution as a spatio-spectral representation of a signal, we have presented a mechanism to transform, modify and filter the signal in the joint spatio-spectral domain to realize spatially varying spectral filtering.
- The signal transformation or modification has been formulated using an integral operator acting on SLSHT distribution in spatio-spectral domain. We have also presented the action of integral operator as linear transformation of the signal, where the linear transformation matrix is expressed in terms of the kernel of an integral operator.

Addressing Q6 posed in Section 1.2.1:

- As in the time-frequency analogy, the transformation in the spatio-spectral domain can lead to a modified distribution that is not a SLSHT distribution of physically valid spatial signal. We have presented an admissibility condition on the kernel of an integral operator, which if satisfied, ensures that the modified distribution is a SLSHT distribution of a valid signal.
- For the case when the admissibility condition is not satisfied, we have formulated and solved an optimization problem to find the closest physically valid

signal to the modified SLHT distribution by deriving an expression for an appropriate inverse spatio-spectral transform.

Addressing Q7 posed in Section 1.2.1:

- We illustrated two types of transformation to the SLSHT distribution, both being instances of a general linear integral operator. However, the technique we developed to recover a spectral response of a valid signal on the unit sphere from a modified SLSHT distribution is not limited to linear transformations in the spatio-spectral domain.
- Multiplicative modification and convolutive modification of the SLSHT distribution have been considered. Both can be regarded as representing spatially varying spectral filtering. For both multiplicative modification and convolutive modification, we haveformulated these modifications as linear transformation on the signal.

# Chapter 6

# Directional Spatially Localized Spherical Harmonic Transform

## 6.1 Introduction

In obtaining the SLSHT distribution presented in Chapter 4 for spatio-spectral representation of a signal, we used an azimuthally symmetric window function for spatial localization. The use of azimuthally symmetric window provides simplification in the sense that each component of the SLSHT distribution is defined on $\mathbb{S}^2$. However, the use of an azimuthally symmetric window function cannot discriminate localized directional features in the spatio-spectral domain. Here, we extend the definition of SLSHT distribution presented in Chapter 4 and propose a transform for signals defined on the sphere that reveals their localized directional content in the spatio-spectral domain when used in conjunction with an asymmetric window function. We call this transform the directional spatially localized spherical harmonic transform (directional SLSHT). We present an inversion relation to synthesize the original signal from its directional-SLSHT distribution for an arbitrary window function. As an example of an asymmetric window, we propose to use the most concentrated band-limited eigenfunction in an elliptical region for spatial localization. As an illustration, we apply the proposed directional SLSHT on the Mars topographic data-set and show its capability to reveal directional features in spatio-spectral domain. Finally, since such typical data-sets on the sphere are of considerable size and the directional SLSHT is intrinsically computationally demanding depending on the band-limits of the signal and window, we develop a

fast algorithm for efficient computation of the transform. The floating point precision numerical accuracy of the fast algorithm is demonstrated and a full numerical complexity analysis is presented.

This chapter is organized as follows. We present the formulation of the directional SLSHT, its harmonic analysis and signal reconstruction from the SLSHT distribution in Section 6.2. Different algorithms for evaluation of the SLSHT distribution are provided in Section 6.3 and detailed analysis of the asymmetric window function is presented in Section 6.4. In Section 6.5, we show timing and accuracy results of our algorithms and an illustration of the transform.

## 6.2 Directional SLSHT

We describe in this section the directional SLSHT, which is capable of revealing directional features of signals in the spatio-spectral[1] domain. For spatial localization, we consider the band-limited azimuthally asymmetric window function which is spatially concentrated in some asymmetric region around the north pole. Since the rotation around the $z$-axis does not have any effect on an azimuthally symmetric function, the localized spherical harmonic transform using an azimuthally symmetric window function can be parameterized on the sphere. However, if an azimuthally asymmetric window is used to obtain localization in the spatial domain, the rotation of the window function is fully parameterized with the consideration of all three Euler angles $(\varphi, \vartheta, \omega) \in \mathrm{SO}(3)$. We refer to the spatially localized transform using an asymmetric window as the directional SLSHT. Here, we first define the directional SLSHT distribution which presents the signal in the spatio-spectral domain. Later in this section, we present the harmonic analysis of SLSHT distribution and provide an inversion relation to obtain the signal from its given directional SLSHT distribution.

### 6.2.1 Forward Directional SLSHT

**Definition 6.1 (Directional SLSHT)** *For a signal $f \in L^2(\mathbb{S}^2)$, define the directional SLSHT distribution component $g(\rho; \ell, m) \in L^2(\mathrm{SO}(3))$ of degree $\ell$ and order $m$ as the spherical harmonic transform of a localized signal where localization is*

[1] In this chapter, when we refer to spatio-spectral, we consider the SO(3) spatial domain, instead of $\mathbb{S}^2$. This is because that we are considering all possible rotations, parameterized using Euler angles which form the SO(3) domain.

*provided by the rotation operator $\mathcal{D}_\rho$ acting on the window function $h \in L^2(\mathbb{S}^2)$, i.e.,*

$$g(\rho;\ell,m) \triangleq \int_{\mathbb{S}^2} f(\hat{\boldsymbol{x}}) \big(\mathcal{D}_\rho h\big)(\hat{\boldsymbol{x}}) \, \overline{Y_\ell^m(\hat{\boldsymbol{x}})} \, ds(\hat{\boldsymbol{x}}) \tag{6.1}$$

*for $0 \leq \ell \leq L_g$, $|m| \leq \ell$, where $L_g = L_f + L_h$ denotes the maximum spherical harmonic degree for which the distribution components $g(\rho;\ell,m)$ are non-zero, and $L_f$ and $L_h$ denote the band-limits of the signal $f$ and the window function $h$, respectively. Also, each distribution component $g(\rho;\ell,m)$ is band-limited in $\rho = (\varphi,\vartheta,\omega) \in \mathrm{SO}(3)$ with maximum degree $L_h$, i.e., when expressed in terms of Wigner-D functions. We elaborate on this later in this chapter. Furthermore, we consider unit energy normalized window functions such that $\langle h, h\rangle = 1$.*

**Remark 6.1** *The directional SLSHT distribution component in* (6.1) *can be interpreted as the spherical harmonic transform of the localized signal where the window function $h$ provides asymmetric localization at spatial position $\hat{\boldsymbol{x}} = \hat{\boldsymbol{x}}(\vartheta,\varphi) \in \mathbb{S}^2$ and the first rotation, through $\omega$, determines the orientation of the window function at $\hat{\boldsymbol{x}}$. If the window function is azimuthally symmetric, this orientation of the window function by $\omega$ becomes invariant and the SLSHT distribution components are defined on $L^2(\mathbb{S}^2)$ as presented in Chapter 4.*

Since the maximum spectral degree for which the SLSHT distribution is defined is $L_g = L_f + L_h$, we consider the band-limited window function such that $L_h \leq L_f$ to avoid extending $L_g$ significantly above $L_f$. We discuss the localization of the window function in the spatial and spectral domains later in the chapter.

In order to represent functions on $\mathbb{S}^2$ and SO(3), it is necessary to adopt appropriate tessellation schemes to discretize both the unit sphere domain and the Euler angle domain of SO(3). We first describe our chosen tessellation schemes and then we provide harmonic analysis of directional SLSHT and the inversion of signal from direction SLSHT.

### 6.2.2 Discretization of $\mathbb{S}^2$ and SO(3)

We consider tessellation (sampling) schemes that support a sampling theorem for band-limited functions, which is equivalent to supporting an exact quadrature.

For the unit sphere domain, we adopt the equiangular tessellation scheme [41] defined as $\mathfrak{S}_L = \{\theta_{n_\theta} = \pi(2n_\theta+1)/(2L+1),\, \phi_{n_\phi} = 2\pi n_\phi/(2L+1) : 0 \leq n_\theta \leq$

$L, 0 \leq n_\phi \leq 2L\}$, which is a grid of $(L+1) \times (2L+1)$ sample points on the sphere (including repeated samples of the south pole) that keeps the sampling in $\theta$ and $\phi$ independent. For a band-limited function on the sphere $f \in L^2(\mathbb{S}^2)$ with maximum spherical harmonic degree $L_f$, sampling on the grid $\mathfrak{S}_{L_f}$ ensures that all information of the function is captured in the finite set of samples and, moreover, that exact quadrature can be performed [41]. Note that this sampling theorem was developed only recently [41] and requires approximately half as many samples on the sphere as required by alternative equiangular sampling theorems on the sphere [31].

For the Euler angle representation of the rotation group SO(3), we consider the equiangular tessellation scheme $\mathfrak{E}_L = \{\varphi_{n_\varphi} = 2\pi n_\varphi/(2L+1), \vartheta_{n_\vartheta} = 2\pi n_\vartheta/(2L+1), \omega_{n_\omega} = 2\pi n_\omega/(2L+1) : 0 \leq n_\varphi, n_\omega \leq 2L, 0 \leq n_\vartheta \leq L\}$. Again for a function $f \in L^2(\mathrm{SO}(3))$ with maximum spectral degree $L_f$, the sampling of a function $f$ on $\mathfrak{E}_{L_f}$ ensures that all information of the function is captured and also permits exact quadrature (which follows from the results developed on the sphere [41]).

### 6.2.3 Harmonic Analysis

We now present the formulation of the directional SLSHT distribution if the signal $f$ and the window function $h$ are represented in the spectral domain. Using the expression for the spherical harmonics of a rotated function in (2.27), we can write the SLSHT distribution component $g(\rho; \ell, m)$ in (6.1) as

$$g(\rho;\ell,m) = \sum_{\ell'=0}^{L_f} \sum_{m'=-\ell'}^{\ell'} (f)_{\ell'}^{m'} \sum_{p=0}^{L_h} \sum_{q=-p}^{p} \sum_{q'=-p}^{p} (h)_p^{q'} D_p^{q,q'}(\rho)\, T(\ell',m';p,q;\ell,m), \quad (6.2)$$

where

$$T(\ell',m';p,q;\ell,m) = \int_{\mathbb{S}^2} Y_{\ell'}^{m'}(\hat{\boldsymbol{x}})\, Y_p^q(\hat{\boldsymbol{x}})\, \overline{Y_\ell^m(\hat{\boldsymbol{x}})}\, ds(\hat{\boldsymbol{x}})$$

denotes the spherical harmonic triple product and is given in (2.23) and (2.24).

**Remark 6.2** *By comparing $g(\rho; \ell, m)$ in (6.2) with (2.33), we note that the band-limit of $g(\rho; \ell, m)$ in $\rho$ is given by $L_h$. Since $\ell' \leq L_f$ and $p \leq L_h$ in (6.2), our statement that the distribution component $g(\rho; \ell, m)$ is non-zero for $\ell \leq L_g = L_f + L_h$ follows since the triple product $T(\ell', m'; p, q; \ell, m)$ is non-zero for $\ell \leq L_f + L_h$ only.*

### 6.2.4 Inverse Directional SLSHT

Here, we define the inverse directional SLSHT to reconstruct a signal from its SLSHT distribution. The original signal can be reconstructed from its directional SLSHT distribution through the spectral domain marginal, that is, by integrating the SLSHT distribution components over the spatial domain SO(3) [4]. Using our harmonic formulation in (6.2), define $\big(\hat{f}\big)_\ell^m$ as the integral of the SLSHT distribution component $g(\rho;\ell,m)$ over SO(3) giving

$$\begin{aligned}
\big(\hat{f}\big)_\ell^m &= \int_0^{2\pi}\int_0^{\pi}\int_0^{2\pi} g(\rho;\ell,m)d\rho, \quad 0\le \ell \le L_f \\
&= \sum_{\ell'=0}^{L_h}\sum_{m'=-\ell'}^{\ell'} \big(f\big)_{\ell'}^{m'} \sum_{p=0}^{L_h}\sum_{q=-p}^{p}\sum_{q'=-p}^{p} \big(h\big)_p^{q'}\, T(\ell',m';p,q;\ell,m) \int_0^{2\pi}\int_0^{\pi}\int_0^{2\pi} D_p^{q,q'}(\rho)\, d\rho \\
&= 8\pi^2 \sum_{\ell'=0}^{L_h}\sum_{m'=-\ell'}^{\ell'} \big(f\big)_{\ell'}^{m'} \big(h\big)_0^0\, T(\ell',m';0,0;\ell,m) \\
&= \sqrt{16\pi^3}\, \big(h\big)_0^0\, \big(f\big)_\ell^m,
\end{aligned} \tag{6.3}$$

where we have used the orthogonality relation of Wigner-$D$ functions (see (2.32)). Using the expression in (6.3), we can find the spherical harmonic coefficient $\big(f\big)_\ell^m$ of the signal $f$ as

$$\big(f\big)_\ell^m = \frac{\big(\hat{f}\big)_\ell^m}{\sqrt{16\pi^3}\,\big(h\big)_0^0}, \tag{6.4}$$

which indicates that we only need to know the DC-component of the window function $\big(h\big)_0^0$ in order to obtain the signal from its directional SLSHT distribution. It further imposes the condition that the DC-component of the window function must be non-zero. Although the distribution components in (6.2) are defined up to degree $L_g = L_f + L_h$, we only require the components up to $L_f$ for signal reconstruction.

**Remark 6.3** *The signal can also be reconstructed from its SLSHT distribution by evaluating*

$$\int_0^{2\pi}\int_0^{\pi}\int_0^{2\pi} g(\rho;\ell,m)\overline{D_{q,q'}^p(\rho)}d\rho = 8\pi^2 \sum_{\ell'=0}^{L_h}\sum_{m'=-\ell'}^{\ell'} \big(f\big)_{\ell'}^{m'} \sum_{p=0}^{L_h}\sum_{q=-p}^{p}$$

$$\times \sum_{q'=-p}^{p} \frac{(h)_p^{q'}}{2p+1} T(\ell', m'; p, q; \ell, m) \qquad (6.5)$$

*for all* $p \leq L_h$, $|q|$, $q'| \leq p$ *and for all* $\ell \leq L_g$, $|m| \leq \ell$ *and then employing the orthogonality relations of Wigner-*$3j$ *symbols to decouple the spherical harmonic coefficients of the window function* $h$ *and the signal* $f$*. We used this approach in Chapter 5 (see Theorem 5.1) to invert the signal from its modified SLSHT distribution, where the SLSHT distribution is obtained using azimuthally symmetric window function. This approach does not impose restriction on the DC-component of the window function to be non-zero, instead, it requires the knowledge of the energy of the window function. In this work, we consider the inversion of a signal presented in* (6.3) *and* (6.4)*, as this is the most efficient formulation in terms of computational complexity.*

Computing the forward and inverse directional SLSHT is computationally demanding. Since the directional SLSHT distribution components $g(\rho; \ell, m)$ in (6.1) are defined for $\ell \leq L_g$, the number of distribution components are of the order $L_g^2$, while the sampling of $\rho$ is of the order $L_h^3$; thus, direct evaluation of the directional SLSHT distribution is prohibitively computationally expensive for large values of $L_g$. Therefore efficient algorithms need to be developed which reduce the computational complexity. We address this problem in the next section.

## 6.3 Efficient Computation of Directional SLSHT Distribution

Here, we present efficient algorithms for the computation of the directional SLSHT distribution of a signal and reconstruction of a signal from its directional SLSHT distribution. First, we discuss the computational complexities if the SLSHT distribution components are computed using direct quadrature as given in (6.1) or using the harmonic formulation in (6.2). Later, we develop an alternative harmonic formulation which reduces the computational burden. Finally, we present an efficient algorithm that incorporates a factoring of rotations [84] and exploits the FFT.

First we need to parameterize the required tessellation schemes for $\mathbb{S}^2$ for the representation of the signal $f$ and the window $h$ and for SO(3) which forms the spatial domain of the directional SLSHT distribution. Since the maximum spectral

degree of the signal $f$ is $L_f$, we therefore consider the equiangular tessellation $\mathfrak{S}_{L_f}$ to represent $f$. Since the maximum degree for all SLSHT distribution components $g(\rho; \ell, m)$ in $\rho$ is $L_h$, we therefore consider the tessellation $\mathfrak{E}_{L_h}$ to represent the SLSHT distribution components on $L^2(\mathrm{SO}(3))$.

### 6.3.1 Direct Quadrature and Harmonic Formulation

We define the forward spatio-spectral transform as evaluation of each SLSHT distribution component $g(\rho; \ell, m)$. Evaluation of the forward spatio-spectral transform using exact quadrature in (6.1) requires the computation of a two dimensional summation over the tessellation of $\mathbb{S}^2$ for each 3-tuple $(\varphi, \vartheta, \omega)$. Since there are $O(L_h^3)$ such 3-tuples in the tessellation scheme $\mathfrak{E}_{L_h}$ and the SLSHT distribution components are of the order $O(L_f^2)$, the computational complexity to compute all distribution components using direct quadrature is $O(L_f^4 L_h^3)$. Using the harmonic formulation in (6.2), the complexity to compute each SLSHT distribution component is $O(L_f^2 L_h^6)$ and to compute all SLSHT distribution components is $O(L_f^4 L_h^6)$. Although the harmonic formulation in (6.2) is useful to establish that the signal can be reconstructed from the directional SLSHT distribution, it is much more computationally demanding than direct quadrature. We develop efficient algorithms in the next subsection which improve the computational complexity of the harmonic formulation and make it more efficient than direct quadrature.

For the inverse directional SLSHT distribution, we only need to integrate over SO(3) to obtain the signal in the spherical harmonic domain as proposed in (6.3). Since the integral can be evaluated by a summation over all Euler angles using quadrature weights, an efficient way to recover the signal from its SLSHT distribution is through direct quadrature, with complexity of $O(L_h^3)$ for each distribution component and $O(L_f^2 L_h^3)$ for all components.

In order to evaluate the integral in (6.3) exactly, we need to define quadrature weights along Euler angle $\vartheta$ in the tessellation $\mathfrak{E}_{L_h}$. We evaluate the integral in

(6.3) by the following summation[2]

$$\big(\hat{f}\big)_\ell^m \;=\; \frac{1}{(2L_h+1)^3}\sum_{n_\varphi=0}^{2L_h}\sum_{n_\vartheta=0}^{L_h}\sum_{n_\omega=0}^{2L_h} g(\varphi_{n_\varphi},\vartheta_{n_\vartheta},\omega_{n_\omega};\ell,m)\,q(\vartheta_{n_\vartheta}), \tag{6.6}$$

where the quadrature weights $q(\vartheta_{n_\vartheta})$ follow from [41], with

$$q(\vartheta_{n_\vartheta}) = \begin{cases} 4\pi^2\big(\lfloor\frac{L_h}{2}\rfloor+\frac{1}{2}\big)^{-1}, & \vartheta_{n_\vartheta}=0; \\ 8\pi^2\sum\limits_{m=-L_h}^{L_h} w(-m)\,\cos m\vartheta_{n_\vartheta}, & \text{otherwise;} \end{cases} \tag{6.7}$$

where $w(m)$ is defined as [41]

$$w(m) = \begin{cases} \frac{\pm i\pi}{2}, & m=\pm 1; \\ 0, & m \text{ odd},\ m\neq 1; \\ \frac{2}{1-m^2}, & m \text{ even}. \end{cases} \tag{6.8}$$

### 6.3.2 Fast Algorithm for Forward Directional SLSHT

Here, we develop a fast algorithm to reduce the computational complexity of the forward SLSHT. We first consider an alternative harmonic formulation of the forward SLSHT and then employ the factoring of rotations approach which was first proposed in [84] and has been used in the implementations of the fast spherical convolution [45] and the directional spherical wavelet transform [24].

We may write the directional SLSHT distribution component $g(\rho;\ell,m)$ in (6.1) as a spherical convolution [24] of $h$ and the spherical harmonic modulated signal $\overline{f}\,Y_\ell^m$, giving

$$g(\rho;\ell,m) \;=\; \sum_{p=0}^{L_h}\sum_{q=-p}^{p}\sum_{q'=-p}^{p} \overline{\big(\overline{f}Y_\ell^m\big)_p^q}\big(h\big)_p^{q'}\,D_p^{q,q'}(\varphi,\vartheta,\omega), \tag{6.9}$$

[2]In the evaluation of (6.6) we have computed the summation over $2L_h+1$ sample points in both $\varphi$ and $\omega$. This is due to the tessellation $\mathfrak{E}_{L_h}$ required to capture the entire information content of $g(\varphi,\vartheta,\omega;\ell,m)$. However, if one were interested in recovering $f$ only, then given the quadrature rule in [41] $\big(\hat{f}\big)_\ell^m$ in (6.6) could be computed exactly with only $L_h+1$ sample points in $\varphi$ and $\omega$.

which can be expressed, using the definition of the Wigner-$D$ function in (2.28), as

$$g(\rho;\ell,m) \;=\; \sum_{p=0}^{L_h}\Bigg(\sum_{q=-p}^{p}\Big(\sum_{q'=-p}^{p}\overline{(\overline{f}Y_\ell^m)_p^q}(h)_p^{q'}\,d_p^{q,q'}(\vartheta)e^{-iq'\omega}\Big)e^{-iq\varphi}\Bigg). \tag{6.10}$$

The band-limit of the spherical harmonic modulated signal $\overline{f}\,Y_\ell^m$ is $L_f+\ell$. Since the maximum $\ell$ for which $g$ is non-zero is $L_f+L_h$, we must compute up to $\overline{f}\,Y_{L_f+L_h}^m$, which is band-limited to $2L_f+L_h$. However, we *only* need to compute the spherical harmonic coefficients $\big(\overline{f}Y_\ell^m\big)_p^q$ of the modulated signal up to degree $p\le L_h$, for all $\ell$ and $m$. Therefore, the computation of the spherical harmonic transform of $\overline{f}\,Y_\ell^m$ is an interesting sub-problem. In order to serve the purpose, we use a separation of variable technique given by

$$\big(\overline{f}\,Y_\ell^m\big)_p^q \;=N_\ell^m N_p^q\int_0^\pi P_\ell^m(\cos\theta)P_p^q(\cos\theta)\underbrace{\int_0^{2\pi}\overline{f(\theta,\phi)}e^{i(m-q)\phi}d\phi}_{I(\theta,m-q)}\sin\theta d\theta. \tag{6.11}$$

Since $0\le\ell\le L_f+L_h$ and $0\le p\le L_h$, we need to consider the signal $\overline{f}\,Y_\ell^m$ sampled on the grid $\mathfrak{S}_{2L_f+2L_h}$ for the explicit evaluation of exact quadrature (note that sampling in $\phi$ could be optimized given $|m-q|\le L_f+2L_h$ but this would require a different tessellation of the sphere and will not alter the overall complexity of the computation). Using (6.11), the integral over $\phi$, giving $I(\theta,m-q)$, can be computed first in $O(L_f^2\log_2 L_f)$ for all $m-q$. Once $I(\theta,m-q)$ is computed, the exact quadrature weights that follow from [41] can be used to evaluate the integral over $\theta$ in $O(L_f)$ for each $p$, $q$, $\ell$, $m$ and in $O(L_f^3L_h^2)$ for all $p$, $q$, $\ell$, $m$. Thus the overall complexity to compute the spherical harmonic transform of the modulated signal $\overline{f}\,Y_\ell^m$ up to degree $L_h$ is $O(L_f^3L_h^2)$.

By factoring the single rotation by $(\varphi,\vartheta,\omega)$ into two rotations [24, 45, 84]

$$\mathcal{D}_\rho=\mathcal{D}_{\rho_1}\mathcal{D}_{\rho_2},\quad \rho=(\varphi,\vartheta,\omega),\ \rho_1=(\varphi-\pi/2,-\pi/2,\vartheta),\ \rho_2=(0,\pi/2,\omega+\pi/2), \tag{6.12}$$

and noting the effect of rotation on spherical harmonic coefficients in (2.27), we can write the Wigner-$D$ function in (2.28) as

$$D_p^{q,q'}(\varphi,\vartheta,\omega)=\;i^{q-q'}\sum_{q''=-p}^{p}\Delta_p^{q''q}\,\Delta_p^{q''q'}\,e^{-iq\varphi-iq''\vartheta-iq'\omega}, \tag{6.13}$$

where $\Delta_p^{qq'} = d_p^{q,q'}(\pi/2)$ and we have used the following symmetry properties of Wigner-$d$ functions [87]

$$d_p^{q,q'}(\vartheta) = (-1)^{q-q'} d_p^{q,q'}(-\vartheta) = (-1)^{q-q'} d_p^{-q,-q'}(\vartheta) = (-1)^{q-q'} d_p^{q',q}(\vartheta) = d_p^{-q',-q}(\vartheta) \tag{6.14}$$

Using the Wigner-$D$ expansion given in (6.13), we can write the alternative harmonic formulation of the SLSHT distribution component $g(\rho;\ell,m)$ in (6.9) as

$$g(\rho;\ell,m) \;=\; \sum_{p=0}^{L_h} \sum_{q=-p}^{p} \sum_{q'=-p}^{p} \overline{\big(\overline{f} Y_\ell^m\big)_p^q}\big(h\big)_p^{q'}\, i^{q-q'} \sum_{q''=-p}^{p} \Delta_p^{q''q}\, \Delta_p^{q''q'}\, e^{-iq\varphi - iq''\vartheta - q'\omega}, \tag{6.15}$$

where $\rho = (\varphi,\vartheta,\omega)$. By reordering the summations we can write

$$g(\rho;\ell,m) \;=\; \sum_{q=-L_h}^{L_h} \sum_{q'=-L_h}^{L_h} \sum_{q''=-L_h}^{L_h} C_{q,q',q''}(\ell,m)\, e^{-iq\varphi - iq''\vartheta - q'\omega}, \quad \rho = (\varphi,\vartheta,\omega), \tag{6.16}$$

where

$$C_{q,q',q''}(\ell,m) = i^{q-q'} \sum_{p=\max(|q|,|q'|,|q''|)}^{L_h} \Delta_p^{q''q}\, \Delta_p^{q''q'} \overline{\big(\overline{f} Y_\ell^m\big)_p^q}\big(h\big)_p^{q'}. \tag{6.17}$$

Comparatively, computation of the SLSHT distribution components using the expression given by (6.16) is not more efficient than the initial expression (6.10). However, the presence of complex exponentials can be exploited by employing FFTs to evaluate the involved summations.

The objective of factoring the rotations is to carry out the $\vartheta$ rotation along the $y$-axis as a rotation along the $z$-axis. The rotations along the $z$-axis are expressed using complex exponentials and thus these rotations can be applied with much less computational burden, by exploiting the power of an FFT, relative to a rotation about the $y$-axis. All three rotations which characterize the spatial domain of the SLSHT distribution components appear in complex exponentials in (6.16) and thus we can use FFTs to evaluate the summation of $C_{q,q',q''}(\ell,m)$ over $q$, $q'$ and $q''$. First we need to compute $C_{q,q',q''}(\ell,m)$ for each $\ell$ and for each $m$ which requires a one-dimensional summation over three dimensional grid formed by $q$, $q'$ and $q''$ and thus

can be computed in $O(L_h^4)$. Using $C_{q,q',q''}(\ell, m)$, the summation over the complex exponentials in (6.16) can be carried out in $O(L_h^3 \log_2 L_h)$ using FFTs. The overall complexity of this approach is dominated by the computation of $C_{q,q',q''}(\ell, m)$, that is, $O(L_h^4)$ for each SLSHT distribution component and $O(L_f^2 L_h^4)$ for the complete SLSHT distribution. We note that the evaluation of $C_{q,q',q''}(\ell, m)$ requires the computation of $\Delta^p_{qq'}$ which can be evaluated over the $(q, q')$ plane for each $p$ using the recursion formula of [88] with a complexity of $O(L_h^2)$. Since $p$ is of order $L_h$, the $\Delta$ matrices can be evaluated in $O(L_h^3)$, which does not change the overall complexity of our proposed algorithm. The overall asymptotic complexity of our fast algorithm is thus $O(L_f^3 L_h^2 + L_f^2 L_h^4)$.

**Remark 6.4** *Since the complexity to compute the spherical harmonic transform of the modulated signal $\overline{f}\, Y_\ell^m$ up to degree $L_h$ is $O(L_f^2 \log_2 L_f + L_f L_h^2)$ for each $\ell$, $m$, the complexity of our fast algorithm to compute one SLSHT distribution component is $O(L_f^2 \log_2 L_f + L_f L_h^2 + L_h^4)$. The factor $L_f^2 \log_2 L_f$ in the complexity does not change if we compute spherical harmonic transform of $\overline{f}\, Y_\ell^m$ up to degree $L_h$ for all $\ell$, $m$ instead of each $\ell$, $m$.*

**Remark 6.5** *In order to evaluate* (6.10)*, we note that the separation of variables approach [28] can be used as an alternative to the factoring of rotation approach to develop a fast algorithm. This is due to the factorized form of Wigner-D function and consideration of the equiangular tessellation scheme for* SO(3)*, which keeps the independence between the samples along different Euler angles. In terms of computational complexity, the separation of variable approach has the same computational complexity as the factoring of rotation approach. However, the separation of variable approach needs to compute Wigner-d functions for all values of $\vartheta$ but only requires a two dimensional FFT, whereas the factoring of rotation approach only requires the evaluation of Wigner-d function for $\pi/2$ but requires a three dimensional FFT. Since both approaches have the same complexity, we use the factoring of rotation in our implementation of the fast algorithm.*

**Remark 6.6** *If we want to analyze the signal $f$ with multiple window functions, then we do not need to recalculate the spherical harmonic transform of the modulated signal $\overline{f}\, Y_\ell^m$, which accounts for the $O(L_f^3 L_h^2)$ factor in the overall complexity. Once it is computed, the SLSHT distribution can be computed in $O(L_f^2 L_h^4)$ time for each window function of the same band-limit using the proposed efficient implementation.*

Our proposed formulation and efficient implementation can be further optimized in the case of a steerable window function. Steerable functions have an azimuthal harmonic band-limit in $m$ that is less than the band-limit in $\ell$ (see [16,28] for further details about steerability on the sphere). In this case, the $L_f^2 L_h^4$ factor contributing to the overall asymptotic complexity of the fast algorithm is reduced to $L_f^2 L_h^3$. Furthermore, we may then compute the directional SLSHT for any continuous $\omega \in [0, 2\pi)$ from a small number of basis orientations (due to the linearity of the SLSHT).

If the signal and window function are real, the computational time can be further reduced by considering the conjugate symmetry relation of the spherical harmonic coefficients. Furthermore, in this setting, the SLSHT distribution components also satisfy the conjugate symmetry property

$$g(\rho; \ell, -m) = (-1)^m \, \overline{g(\rho; \ell, m)} \tag{6.18}$$

and we do not need to compute the SLSHT distribution components of negative orders.

## 6.4 Window Localization in Spatial and Spectral Domains

The directional SLSHT distribution is the spherical harmonic transform of the product of two functions, the signal $f$ and the rotated window function $h$ and we must be careful in interpreting the directional SLSHT distribution in the sense that we do not mistake using the signal to study the window because there is no distinction mathematically. The window function should be chosen such that it provides spatial localization in some spatial region around the north pole (origin). Since we have considered a band-limited window function, the window function cannot be perfectly localized in the spatial domain due to the uncertainty principle on the sphere [90]. However, it can be optimally localized by maximizing the energy concentration of the window function in the desired directional region [27].

The interpretation of the directional SLSHT distribution depends on the chosen window function. The window function with maximum localization in some defined asymmetric region provides directional localization and thus reveals directional

features in the spatio-spectral domain. The more directional the window function, the more directional features it can reveal in the spatio-spectral domain but this tends to increase the maximum spherical harmonic degree $L_h$. Recall that the maximum degree of the directional SLSHT distribution components is given by $L_g = L_f + L_h$. Thus, when the signal is expressed in the spatio-spectral domain its spectral extent is extended by $L_h$, which results in spectral leakage. Therefore, we want the window function to be simultaneously maximally localized in some spatial region $\mathcal{R} \subset \mathbb{S}^2$ and have the minimum possible band-limit which achieves the desired level of energy concentration in the spatial region $\mathcal{R}$.

Here, we propose using a band-limited eigenfunction obtained from the solution of the Slepian concentration problem [27] as a window function, concentrated in a spatially localized elliptical region around the north pole. We first parameterize the elliptical region and later analyze the resulting eigenfunctions from the perspective of the uncertainty principle on the sphere [90]. We note that the choice of the asymmetric region as an elliptical region is only one possibility and the analysis can be extended to other asymmetric regions such as strip regions around the north pole [86].

### 6.4.1 Parametrization of Window Function

We consider a band-limited window function of maximum spherical harmonic degree $L_h$, which is spatially concentrated in the elliptical region on the sphere with major axis along the $x$-axis, and thus is orientated along the $x$-axis. The elliptical region can be parameterized using the focus colatitude $\theta_\mathrm{c}$ of the ellipse along the positive $x$-axis and the arc length $a$ of the semi-major axis:

$$\mathcal{R}_{(\theta_\mathrm{c},a)} \triangleq \big\{(\theta,\phi) : \triangle_s\big((\theta,\phi),(\theta_\mathrm{c},0)\big) + \triangle_s\big((\theta,\phi),(\theta_\mathrm{c},\pi)\big) \leq 2a\big\}, \tag{6.19}$$

where $0 \leq \theta_\mathrm{c} \leq a \leq \pi/2$. Here $\triangle_s\big((\theta,\phi),(\theta',\phi')\big) = \arccos\big(\sin\theta\sin\theta'\cos(\phi-\phi') + \cos\theta\cos\theta'\big)$ denotes the angular distance between two points $(\theta,\phi)$ and $(\theta',\phi')$ on the sphere. We note that the elliptical region defined in (6.19) takes into account the angular distances and should not be confused with the projection of an ellipse in the tangent space into $\mathbb{S}^2$.

**Remark 6.7** *For a given focus $\theta_c$, the region becomes more directional as the arc length $a$ approaches $\theta_c$ from $\pi/2$. For $a = \pi/2$, the region becomes azimuthally*

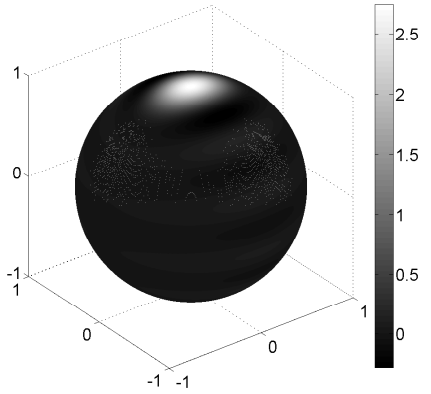


(a)

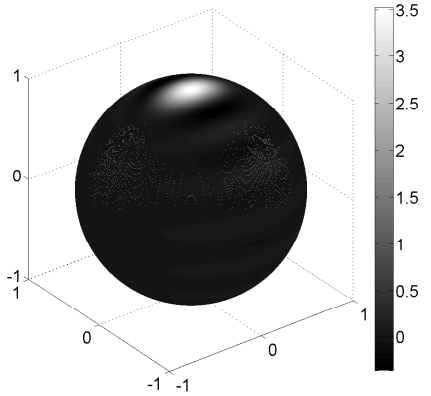


(b)

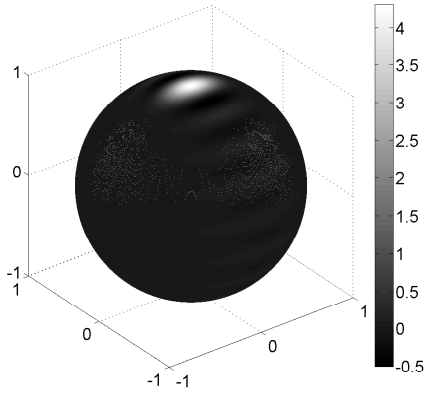


(c)

Figure 6.1: Band-limited eigenfunction windows $h$ on the sphere with 90% spatial concentration in an elliptical region $\mathcal{R}_{(\theta_c,a)}$ of focus $\theta_c = \pi/6$ and major axis: (a) $a = \pi/6 + \pi/80$, (b) $a = \pi/6 + \pi/120$ and (c) $a = \pi/6 + \pi/240$.

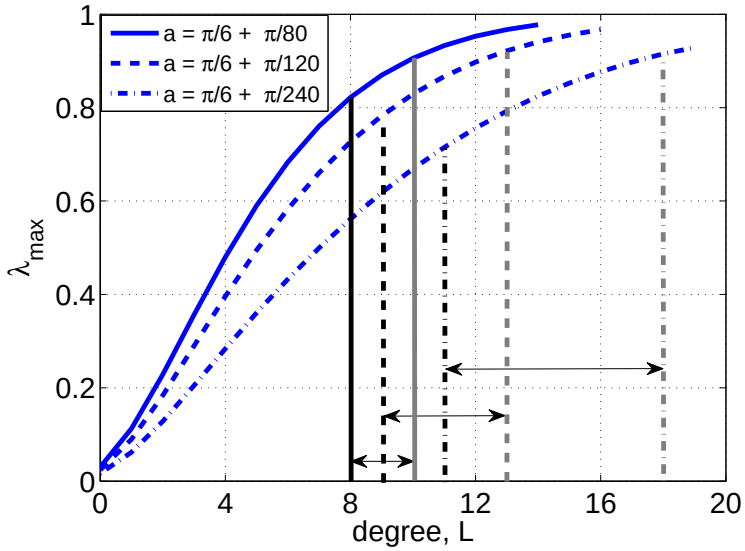


Figure 6.2: The maximum eigenvalue $\lambda_{\max}$ corresponding to the eigenfunction $h$, obtained as a solution of Slepian concentration problem on the sphere, with spherical harmonic band-limit $L$ for spatial concentration in an elliptical region of focus $\theta_c = \pi/6$ and major axis $a$ as indicated. Black vertical lines indicate the bound on the band-limit $B_h$ given by (6.20) and the gray vertical lines indicate the actual $L_h$ which ensures 90% concentration in an elliptical region.

*symmetric, i.e., we recover the polar cap of central angle $\pi/2$. Also, when $\theta_c = 0$, the region becomes azimuthally symmetric (polar cap) of central angle $a$.*

### 6.4.2 Slepian Concentration Problem

As a result of the Slepian concentration problem [27, 86] to find the band-limited function with bandwidth $L_h$ and maximal spatial concentration in an elliptical region $\mathcal{R}_{(\theta_c,a)}$, we obtain $(L_h+1)^2$ eigenfunctions. Due to the symmetry of the elliptical region about the $x$-$y$ plane, the eigenfunctions are real valued [86]. The eigenvalue associated with each eigenfunction serves as a measure of the energy concentration in the spatial region. Here we consider the use of the band-limited eigenfunction with maximum energy concentration in the elliptical region for given band-limit $L_h$ and refer to such an eigenfunction as the eigenfunction window. If $A$ denotes the area of the elliptical region, it is shown [27, 86] that most of the eigenvalues lie either near zero or unity for both symmetric and asymmetric regions and the sum of all eigenvalues, referred as an equivalent of the Shannon number [27], is equal to $N_0 = A(L_h+1)^2/(4\pi)$. Also, it is shown empirically

in [1] that there exist no more than $N_0 - 1$ spatially concentrated eigenfunctions with significant energy concentration. By noting these developments and empirical results, and considering that $L_h$ must be chosen so that we obtain at least one eigenfunction that is spatially concentrated in the elliptical region, we recover the following empirical lower bound for $L_h$:

$$L_h \gtrsim B_h \;=\; 2\left\lceil \sqrt{\frac{2\pi}{A}} \right\rceil - 1,\; A = \int_{\mathcal{R}_{(\theta_c,a)}} ds(\hat{\boldsymbol{x}}), \tag{6.20}$$

where $\lceil\,(\cdot)\,\rceil$ denotes the integer ceiling function (this bound follows directly from $N_0 \gtrsim 2$). We analyze this bound later in this section.

Let $\lambda_{\max}$ denote the eigenvalue associated with the most spatially concentrated eigenfunction. By finding the minimum value of $L_h$ which ensures that $\lambda_{\max}$ is greater than or equal to the desired energy concentration, an eigenfunction window $h(\hat{\boldsymbol{x}})$ with desired energy concentration in the elliptical region and minimum possible band-limit $L_h$ can be obtained. Thus, the focus of an elliptical region $\theta_c$, arc length of semi-major axis $a$ and maximum spectral degree $L_h$ fully parameterize the eigenfunction window. As an illustration, the three eigenfunction windows having 90% spatial concentration in the elliptical regions $\mathcal{R}_{(\theta_c,a)}$ with focus $\theta_c = \pi/6$ and $a \in \{\pi/6 + \pi/240,\, \pi/6 + \pi/120,\, \pi/6 + \pi/80\}$ and respective maximum spherical harmonic degree $L_h \in \{18,\, 14,\, 11\}$ are shown in Fig. 6.1. For these elliptical regions, in Fig. 6.2 we show $\lambda_{\max}$ versus spherical harmonic band-limit $L$ denoting the band-limit of the most concentrated eigenfunction window, where we note the difference in $L_h$ and the bound $B_h$ for the desired concentration level. For a desired concentration level of 90%, we observe that the spherical harmonic degree $L_h$ which ensures $\lambda_{\max} \geq 0.9$ deviates further from the bound $B_h$ given by (6.20) as the concentration region becomes more directional (as expected since the bound does not incorporate the level of directionality of the region).

### 6.4.3 Analysis of Eigenfunction Window Concentrated in Elliptical Region

#### 6.4.3.1 Directionality

For the use of the eigenfunction window in obtaining the directional SLSHT distribution, the directionality of the eigenfunction window must be a key criterion in

selecting the eigenfunction window for the identification of localized features of a signal in the spatio-spectral domain. We use the definition of the auto-correlation function on the sphere as a measure of the directionality of the eigenfunction window [16, 29]. The auto-correlation function is defined as the inner product of the eigenfunction window with its version rotated around the $z$-axis:

$$C_h(\varsigma) \;=\; \langle D_{\rho_1} h,\, h \rangle\,, \quad \rho_1 = (0, 0, \varsigma),\, \varsigma \in [0, \frac{\pi}{2}], \tag{6.21}$$

which can be expressed in the harmonic domain as

$$C_h(\varsigma) \;=\; \sum_{\ell=0}^{L_h} \sum_{m=-\ell}^{\ell} e^{im\varsigma} |\big(h\big)_\ell^m|^2. \tag{6.22}$$

Due to the symmetry of the elliptical region and the eigenfunction window about the major axis ($x$-axis) and minor axis ($y$-axis), we have considered $\varsigma$ in the range of 0 to $\pi/2$.

For the eigenfunction windows presented in the previous subsection, the auto-correlation function for each window is shown in Fig. 6.3, which indicates that $C_h(\varsigma)$ decays more rapidly from unity at $\varsigma = 0$ for more directional windows and therefore, the peakedness of $C_h(\varsigma)$ quantifies the ability of the window function to spatially localize the directional features of a signal.

#### 6.4.3.2 Spatial and Spectral Localization

Here we study the spatial and spectral localization of eigenfunction windows from the perspective of the uncertainty principle on the sphere [78, 90], according to which, the function cannot be simultaneously localized in both the spatial and spectral domains. The following inequality specifies the uncertainty principle for unit energy functions defined on the sphere, which relates the trade-off between the spatial and spectral localization of a function:

$$\frac{\sigma_{\mathrm{S}}}{\sqrt{1 - \sigma_{\mathrm{S}}^2}} \cdot \sigma_{\mathrm{L}} \geq 1, \tag{6.23}$$

where $\sigma_{\mathrm{S}}$ and $\sigma_{\mathrm{L}}$ denote the variance of the band-limited unit energy eigenfunction window in the spatial domain and spectral domain respectively and are defined

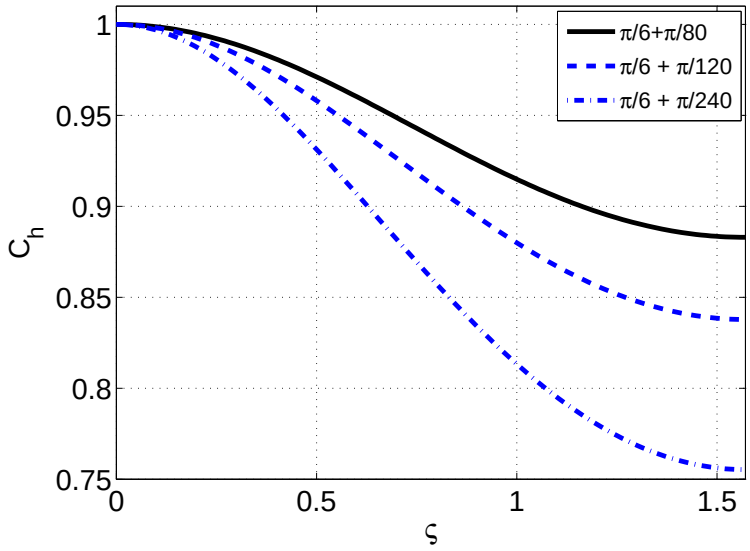


Figure 6.3: Auto-correlation function $C_h(\varsigma)$ as described in (6.21) for eigenfunction windows $h$ with spatial concentration in an elliptical region of focus $\theta_c = \pi/6$ and major axis $a$ as indicated.

as [78]

$$\sigma_{\mathrm{S}}^2 = 1 - \left( \frac{1}{2} \int_{\mathbb{S}^2} \sin(2\theta) \left| h(\theta, \phi) \right|^2 d\theta d\phi \right)^2 \tag{6.24}$$

and

$$\sigma_{\mathrm{L}}^2 = \sum_{\ell=0}^{L_h} \ell(\ell+1) \sum_{m=-\ell}^{\ell} |h_\ell^m|^2. \tag{6.25}$$

Due to the consideration of unit energy functions, $0 \leq \sigma_S \leq 1$. We note that smaller variance indicates better localization of the window function. The variance in the spatial and spectral domains and the uncertainty product for eigenfunctions concentrated in an elliptical region of focus $\pi/6$ and major-axis of different values are shown in Fig. 6.4. As expected, the variance in the spatial domain decreases as the region becomes more directional, whereas the variance in the spectral domain increases because $L_h$ increases. We also note that the uncertainty product increases as the region becomes more directional.

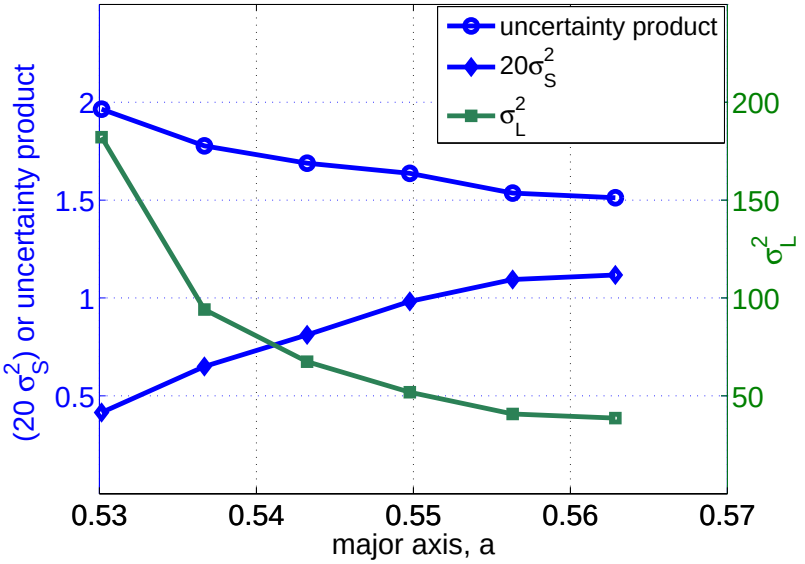


Figure 6.4: Spatial variance ($20\sigma_S^2$), spectral variance ($\sigma_L^2$) and uncertainty product, as described in (6.23), (6.24) and (6.25), are shown for eigenfunctions with spatial concentration in an elliptical region of focus $\theta_c = \pi/6$ and major axis $a$ as indicated.

## 6.5 Results

In this section, we first demonstrate the numerical validation and computation time of our algorithms to evaluate the directional SLSHT components. Later, we provide an example to illustrate the capability of the directional SLSHT, showing that it probes out the directional features of signals in the spatio-spectral domain. The implementation of the our algorithms is carried out in `MATLAB`, using the `MATLAB` interface of the `SSHT`[3] package (the core algorithms of which are written in `C` and which also uses the `FFTW`[4] package to compute Fourier transforms) to efficiently compute forward and inverse spherical harmonic transforms [41].

### 6.5.1 Numerical Validation and Computation Time

In order to evaluate the numerical accuracy and the computation time, we carry out the following numerical experiment. We use the band-limited function $h$ for spatial localization with band-limit $L_h = 18$ and spatial localization in the region $\mathcal{R}_{(\pi/6,\pi/6+\pi/240)}$. We generate band-limited test signals with band-limits $18 \leq L_f \leq 130$ by generating spherical harmonic coefficients with real and imaginary parts

[3] `http://www.jasonmcewen.org/`
[4] `http://www.fftw.org/`

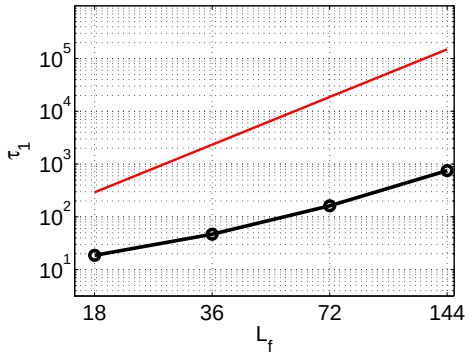


(a) Computation time to evaluate $(\overline{f}Y_\ell^m)_p^q$

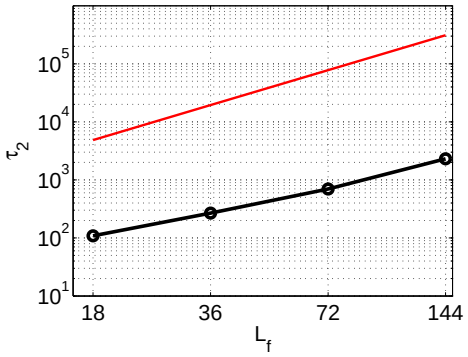


(b) Computation time to evaluate all SLSHT distribution components given $(\overline{f}Y_\ell^m)_p^q$

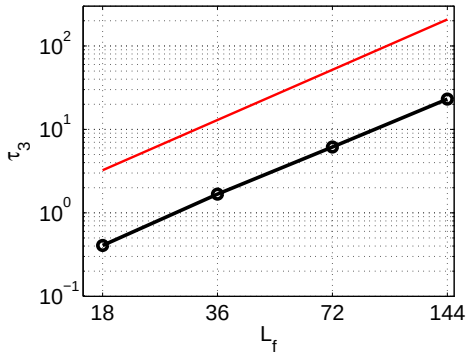


(c) Inverse transform computation time

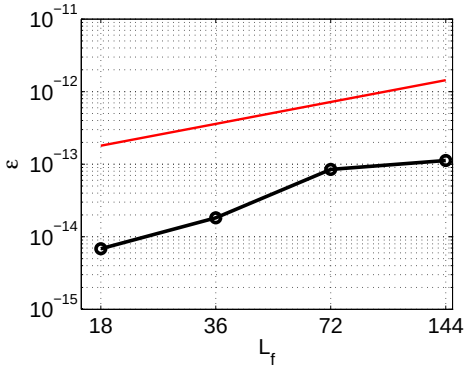


(d) Numerical validation

Figure 6.5: Numerical validation and computation time of the proposed algorithms. Computation time in seconds: (a) $\tau_1$ (b) $\tau_2$ and (c) $\tau_3$. For fixed $L_h$, $\tau_1$ evolves as $O(L_f^3)$ and both $\tau_2$ and $\tau_3$ scale as $O(L_f^2)$ as shown by the solid red lines (without markers). (d) The maximum error $\epsilon$, which empirically appears to scale as $O(L)$, as shown by the solid red line.

uniformly distributed in the interval $[0, 1]$.

For the given test signal, we measure the computation time $\tau_1$ to evaluate spherical harmonic transform of the modulated signal, i.e., $(\overline{f}Y_\ell^m)_p^q$ for $p \leq L_h$, $q \leq |p|$ and for all $\ell \leq L_f + L_h$, $m \leq |\ell|$, using the method presented in Section 6.3.2. Given the spherical harmonic transform of the modulated signal, we then measure the computation time $\tau_2$ to compute all directional SLSHT distribution components $g(\rho; \ell, m)$ for $\ell \leq L_f + L_h$ and $m \leq |\ell|$ using our fast algorithm presented in Section 6.3.2, where we compute the Wigner-$d$ functions on-the-fly for the argument $\pi/2$ by using the recursion of Trapani [88]. We also record the computation time $\tau_3$ to recover a signal from its SLSHT distribution components. All numerical experiments are performed using `MATLAB` running on a 2.4 GHz Intel Xeon proces-

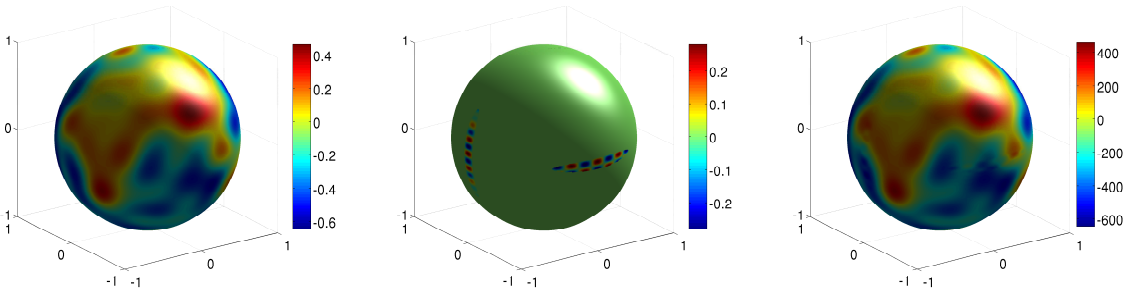


(a) $f_1$ (b) $f_2$ (c) $f$

Figure 6.6: (a) Spectrally truncated unit energy normalized Earth topographic map $f_1$ and (b) signal $f_2$ composed of higher degree spherical harmonics localized in elliptical regions. (c) Weighted sum of $f_1$ and $f_2$ as defined in (6.27).

sor with 64 GB of RAM and the results are averaged over ten test signals. The computation time $\tau_1$ and $\tau_2$ are plotted against the band-limit $L_f$ of the test signal in Fig. 6.5a and Fig. 6.5b, which respectively evolve as $O(L_f^3)$ and $O(L_f^2)$ for fixed $L_h$ and thus corroborate the theoretical complexity. The computation time $\tau_3$ for the inverse directional SLSHT is plotted in Fig. 6.5c, which scales as $O(L_f^2)$ for fixed $L_h$, again supporting the theoretical complexity.

We reconstruct the original signal from its SLSHT distribution components using (6.6) and (6.3), in order to assess the numerical accuracy of our algorithms by measuring the maximum absolute error between the original spherical harmonic coefficients of the test signal and the reconstructed values. The maximum absolute error is plotted in Fig. 6.5d for different band-limits $L_f$, which illustrates that our algorithms achieve very good numerical accuracy with numerical errors at the level of floating point precision.

### 6.5.2 Directional SLSHT Illustration

In this subsection, we provide examples to illustrate the capability of the proposed transform to reveal the localized contribution of spectral contents and probe directional features in the spatio-spectral domain.

#### 6.5.2.1 Example 1 - Synthetic Data Set

We first construct a signal having localized contribution of higher degree spectral contents and then analyze the signal using proposed directional SLSHT. Let signal $f_1$ be the spectrally truncated, unit energy normalized Earth topographic map with band-limit $L_{f_1} = 30$, which is obtained by using spherical harmonic model of topography of Earth and is shown in Fig. 6.6a. Also consider the signal $f_2$

composed of higher degree spherical harmonics localized in two non-overlapping elliptical regions with different orientation. We obtain such a signal $f_2$ by spectrally truncating the following signal $\tilde{f}_2$ with in the band-limit $L_{f_2} = 128$,

$$\tilde{f}_2(\hat{\boldsymbol{x}}) = \begin{cases} \sum_{\ell=40}^{45} \left( Y_\ell^{20}(\hat{\boldsymbol{x}}) + Y_\ell^{-20}(\hat{\boldsymbol{x}}) \right) & \hat{\boldsymbol{x}} \in \mathcal{R} = \mathcal{R}_1 \cup \mathcal{R}_1 \\ 0 & \hat{\boldsymbol{x}} \in \mathbb{S}^2 \setminus \mathcal{R}, \end{cases} \tag{6.26}$$

where $\mathcal{R}_1$ and $\mathcal{R}_2$ are the elliptical regions of the form $\mathcal{R}_{(\pi/6,\pi/6+\pi/240)}$, respectively rotated by $(\pi/2, \pi/2, 0) \in \mathrm{SO}(3)$ and $(3\pi/2, \pi/2, \pi/2) \in \mathrm{SO}(3)$. The unit energy normalized signal $f_2$ is shown in Fig. 6.6b. We note that the regions $\mathcal{R}_1$ and $\mathcal{R}_2$ have orientation along colatitude and longitude respectively.

We analyze the following synthetic signal using the proposed transform

$$f(\hat{\boldsymbol{x}}) = 10^3 \times \left( \frac{f_1(\hat{\boldsymbol{x}})}{\|f_1\|} + \frac{f_2(\hat{\boldsymbol{x}})}{4\|f_2\|} \right), \tag{6.27}$$

which can be considered as a sum of a low frequency signal and a high frequency localized signal. The signal $f$ is shown in Fig. 6.6c, where it can be observed that the information cannot be obtained about the presence of higher degree spherical harmonics localized in different directional regions. Furthermore, the spherical harmonic coefficients provide details about the presence of higher degree spherical harmonics in the signal, but do not reveal any information about the localized contribution of higher degree spherical harmonics.

If we analyze the signal by employing the SLSHT using an azimuthally symmetric window function, the presence of localized contributions of higher degree spectral contents can be determined in the spatio-spectral domain as we illustrated in Chapter 4. However, the presence of directional features cannot be extracted. Here, we illustrate that the use of the directional SLSHT enables the identification of directional features in the spatio-spectral domain, which is due to the consideration of an asymmetric window function for spatial localization.

We obtain the directional SLSHT distribution components $g(\rho; \ell, m)$ of the signal $f$ using the band-limited eigenfunction window $h$ with $L_h = 18$ and 90% concentration in the spatial domain in an elliptical region $\mathcal{R}_{(\pi/6,\pi/6+\pi/240)}$. The magnitude of the SLSHT distribution components $g(\rho; \ell, m)$ for order $m = 20$ and for degrees $\ell \in \{41, 43, 45\}$ are shown in Fig. 6.7 for Euler angle (a) $\gamma = 0$ and (b)

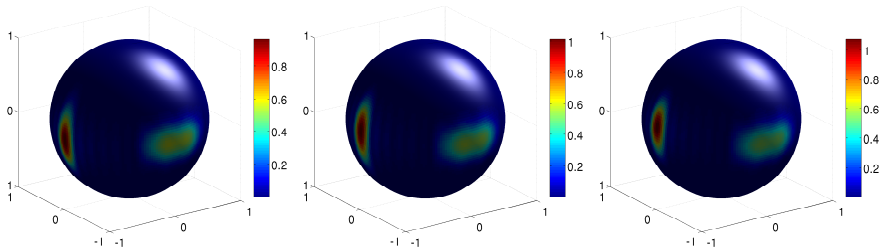

(a)

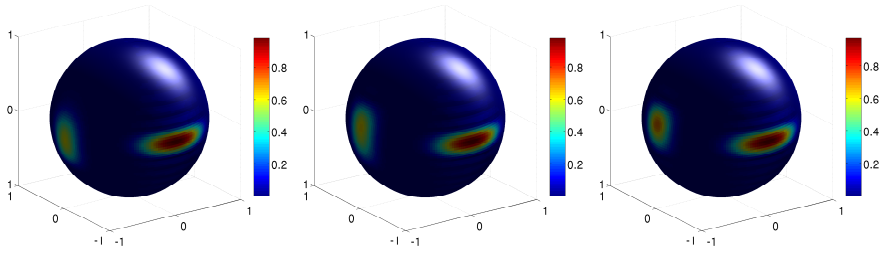

(b)

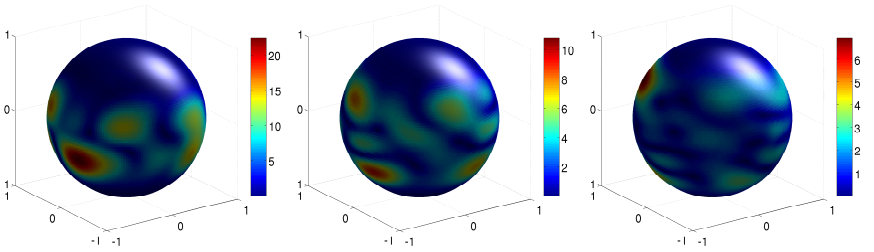

(c)

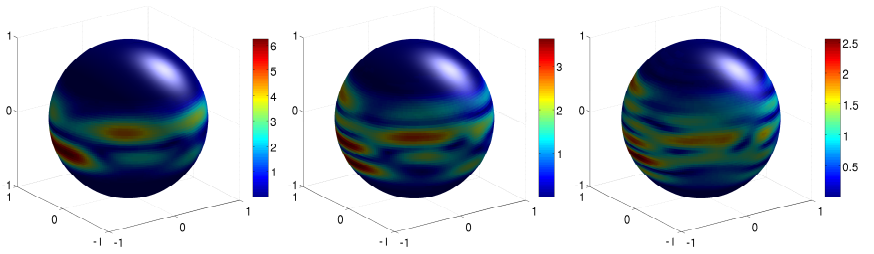

(d)

Figure 6.7: Magnitude of the components of the directional SLSHT distribution of the synthetic signal shown in Fig. 6.6c. For fixed orientation $\gamma$ of the window function around the $z$-axis, the distribution components $g(\rho; \ell, m)$ are mapped on the sphere using $\rho = (\phi, \theta, \gamma)$ for order $m = 20$. The components are shown for degrees $\ell \in \{41, 43, 45\}$ and for orientations (a) $\gamma = 0$ and (b) $\gamma \approx \pi/2$ of the window function around the $z$-axis, and the components are shown for degrees $\ell \in \{21, 23, 25\}$ and for orientation (c) $\gamma = 0$ and (d) $\gamma \approx \pi/2$. Top left: $g(\rho; 41, 20)$, top right: $g(\rho; 45, 20)$.

$\gamma = 100\pi/201 \approx \pi/2$, and for degrees $\ell \in \{21, 23, 25\}$, the components are shown for (c) $\gamma = 0$ and (d) $\gamma \approx \pi/2$. Since the elliptical region is oriented along the

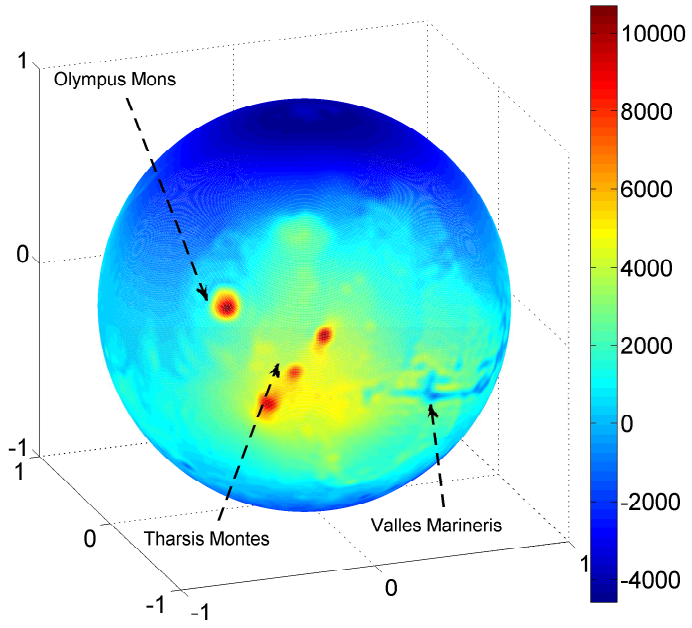


Figure 6.8: Mars signal in the spatial domain. The grand canyon Valles Marineris and the mountainous regions of Tharsis Montes and Olympus Mons are indicated.

$x$-axis, the window with orientation $\gamma = 0$ provides localization along colatitude and the window with orientation $\gamma \approx \pi/2$ provides localization along longitude. It can be observed that the localized contribution of higher degree directional spectral contents is extracted in spatio-spectral domain. The localized higher degree directional features along the orientation $\gamma = 0$ and $\gamma \approx \pi/2$ are revealed in the spatio-spectral domain as shown in Fig. 6.7a and Fig. 6.7b respectively, which are not visible in lower degree distribution components as shown in Fig. 6.7c and Fig. 6.7d.

As demonstrated, the proposed directional SLSHT is capable of probing localized directional spectral content. We further illustrate the capability of our proposed transform by analyzing the Mars topographic map in the spatio-spectral domain.

#### 6.5.2.2 Example 2 - Mars Data Set

We consider the Mars topographic map (height above geoid) as a signal on the sphere, which is obtained by using the spherical harmonic model of the topography

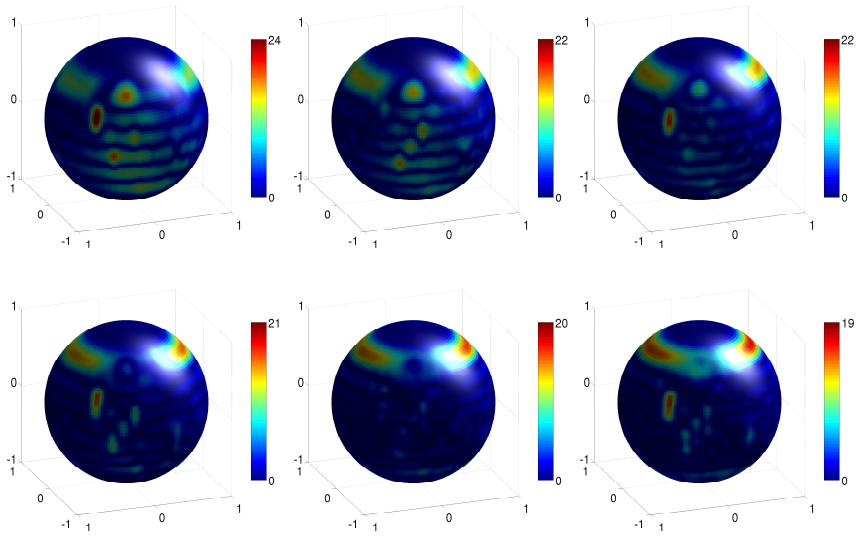

(a)

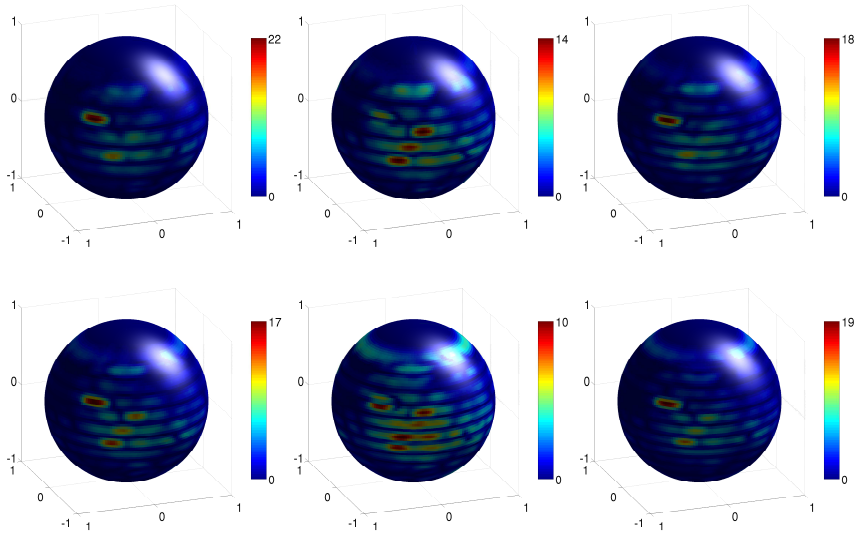

(b)

Figure 6.9: Magnitude of the components of the directional SLSHT distribution of the Mars signal obtained using the eigenfunction window concentrated in an elliptical region of focus $\theta_c = \pi/12$ and major axis $a = 7\pi/12$. For fixed orientation $\omega$, the distribution components $g(\rho; \ell, m)$ are mapped on the sphere using $\rho = (\phi, \theta, \omega)$ for order $m = 15$ and degree $20 \leq \ell \leq 25$. The components are shown for orientation (a) $\omega = 0$ and (b) $\omega \approx \pi/2$ of the window function around the $z$-axis. Top left: $g(\rho; 20, 15)$, top right: $g(\rho; 22, 15)$.

of Mars[5]. The Mars topographic map is shown in Fig. 6.8 in the spatial domain, where the grand canyon Valles Marineris and the mountainous regions of Tharsis

[5] `http://www.ipgp.fr/~wieczor/SH/`

Montes and Olympus Mons are shown, indicating the presence of high frequency contents. We note that the mountainous regions are non-directional features of the Mars map, whereas the grand canyon serves as a directional feature with direction oriented along a line of approximate constant latitude. The spherical harmonic coefficients provide details about the presence of higher degree spherical harmonics in the signal, but do not reveal any information about the localized contribution of higher degree spherical harmonics, meaning that the spherical harmonic coefficients do not directly enlighten the information about the the spatial localization of spectral contents.

We obtain the directional SLSHT distribution components $g(\rho;\ell,m)$ of the Mars map $f$ using the band-limited eigenfunction window $h$ with $L_h = 60$ and 90% concentration in the spatial domain in an elliptical region $\mathcal{R}_{(\pi/12,7\pi/12)}$. The magnitude of the SLSHT distribution components $g(\rho;\ell,m)$ for order $m = 15$ and degrees $20 \leq \ell \leq 25$ and $50 \leq \ell \leq 55$ are shown in Fig. 6.9 and Fig. 6.10 respectively, where the components in the panels are for Euler angles (a) $\omega = 0$ and (b) $\omega = 100\pi/201 \approx \pi/2$. Since the elliptical region is oriented along the $x$-axis, the window with orientation $\omega = 0$ provides localization along colatitude and the window with orientation $\omega \approx \pi/2$ provides localization along longitude. It is evident that using orientation of the window $\omega \approx \pi/2$ probes the information about the grand canyon Valles Marineris (directional feature) along longitude in the spatio-spectral domain. The localized contribution of higher degree spherical harmonics towards the mountainous region can also be observed in Fig. 6.9 for degree $20 \leq \ell \leq 25$ and both $\omega = 0$ and $\omega = \pi/2$. However, there is not significant contribution of spherical harmonics of degree $50 \leq \ell \leq 55$ towards the mountainous region as indicated in Fig. 6.10a where $\omega = 0$, but the localization of the directional features along the orientation $\omega \approx \pi/2$ are revealed in the spatio-spectral domain as shown in Fig. 6.10b. Due to the ability of the directional SLSHT to reveal the localized contribution of spectral contents and the directional or oriented features in the spatio-spectral domain, it can be useful in many applications where the signal on the sphere is localized in position and orientation.

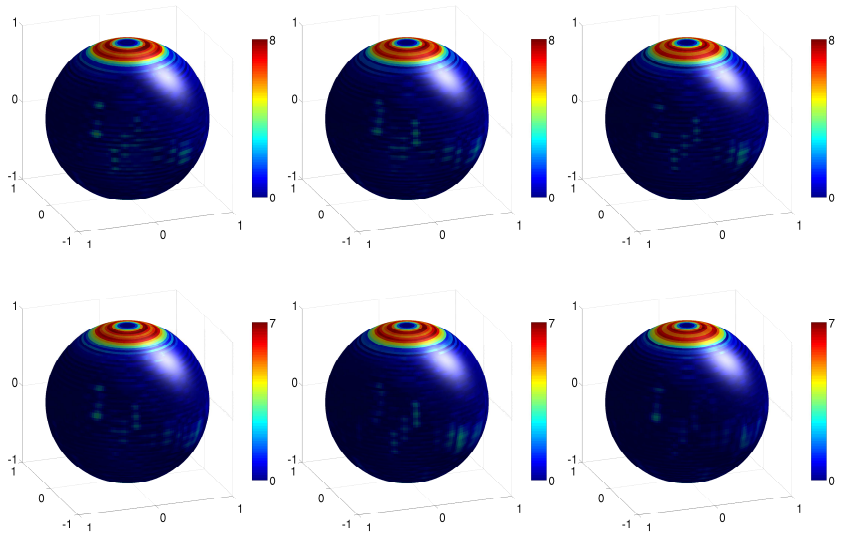

(a)

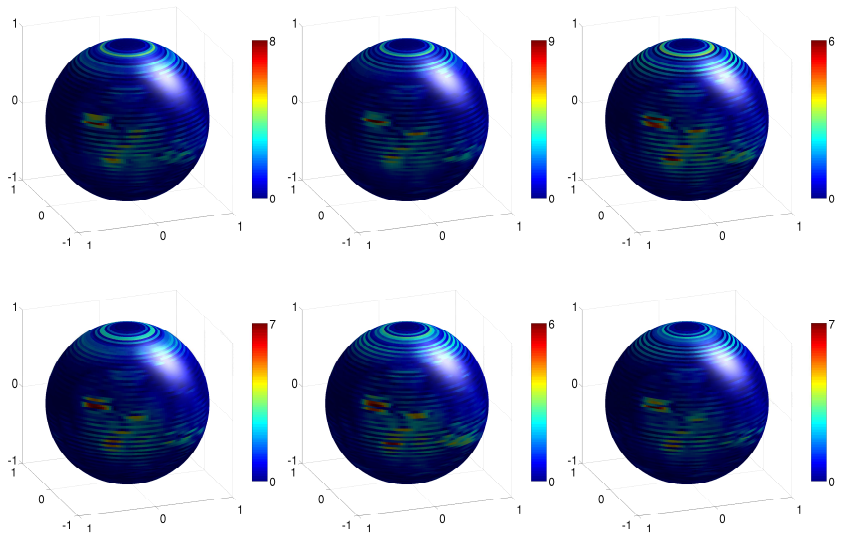

(b)

Figure 6.10: Magnitude of the components of the directional SLSHT distribution of the Mars signal obtained using the eigenfunction window concentrated in an elliptical region of focus $\theta_c = \pi/12$ and major axis $a = 7\pi/12$. For fixed orientation $\omega$, the distribution components $g(\rho; \ell, m)$ are mapped on the sphere using $\rho = (\phi, \theta, \omega)$ for order $m = 15$ and degree $50 \leq \ell \leq 55$. The components are shown for orientation (a) $\omega = 0$ and (b) $\omega \approx \pi/2$ of the window function around $z$-axis. Top left: $g(\rho; 50, 15)$, top right: $g(\rho; 52, 15)$.

## 6.6 Summary of Contributions

In this chapter, we have presented the directional SLSHT to project a signal on the sphere onto its joint spatio-spectral domain as a directional SLSHT distribution.

The directional SLSHT has been defined as localized spherical harmonic transform, where we have proposed the use of an azimuthally asymmetric window function to obtain SO(3) spatial localization, which enables the transform to resolve directional features in the spatio-spectral domain. The contributions made in this chapter are as follows.

Addressing Q8 posed in Section 1.2.1:

- Extending the SLSHT distribution formulated in Chapter 4, here, we have presented directional SLSHT to obtain such a spatio-spectral representation that reveals the localized contribution of directional features in the spatio-spectral domain. We have also provided the harmonic analysis of directional SLSHT and presented an inversion relation to synthesize the original signal from its directional SLSHT distribution.

- We have analyzed the band-limited window function obtained from the Slepian concentration problem on the sphere, with nominal concentration in an elliptical region around the north pole.

- We provided an illustration which highlighted the capability of the directional SLSHT to reveal directional features in the spatio-spectral domain.

Addressing Q9 posed in Section 1.2.1:

- We have developed a fast algorithm for the efficient computation of the directional SLSHT distribution of a signal. The computational complexity of the proposed fast algorithm to evaluate SLSHT distribution of a signal with band-limit $L_f$ using window function with band-limit $L_h$ is $O(L_f^3 L_h^2 + L_f^2 L_h^4)$ as compared to the complexity of direct evaluation, which is $O(L_f^4 L_h^3)$.

- We have also studied the numerical accuracy and the speed of our fast algorithm and shown that the simulation results corroborate theoretically evaluated computational complexities.

# Chapter 7

# Conclusions and Future Research Directions

In this chapter we summarize the general conclusions drawn from this thesis. The summary of specific contributions can be found at the end of each chapter and are not repeated here. We also outline some future research directions arising from this work.

## 7.1 Conclusions

This thesis has been primarily concerned with the development of new signal processing techniques and the extension of existing theories to analyze signals defined on the sphere.

First, in Chapter 3, we have considered the problem to define and formulate convolution on the sphere in a manner that serves as direct analog of the Euclidean domain convolution. In contrast to the existing definitions of convolution, we have formulated convolution on the sphere which is commutative in nature, admits anisotropic filter and produces an output that remains on the sphere.

In the second part of the thesis, from Chapter 4 to Chapter 6, we focussed on analysis of signals on the sphere in a joint spatio-spectral domain. Analogous to the STFT in time-frequency analysis, we developed the SLSHT, composed of spatial windowing followed by a spherical harmonic transform, to obtain the spatio-spectral representation of the signal. It has been shown that the spatio-spectral representation, herein, referred to as the SLSHT distribution represents the spatially varying spectral contents and therefore reveals information about the local-

ization of spectral contents which cannot be directly obtained from the spectral domain representation of a signal. Since the SLSHT distribution relies on a window function for spatial localization, different window functions have been studied from the perspective of the uncertainty principle. Noting that the eigenfunction obtained from the Slepian concentration problem on the sphere attains the lower bound imposed by uncertainty principle, we have proposed to use this eigenfunction as window function in obtaining SLSHT distribution of a signal. New uncertainty principles, which relate the concentration of a signal in spatial and spectral domain, have also been derived.

Earlier, in Chapter 4, we used azimuthally symmetric window functions for spatial localization in order to parameterize the SLSHT distribution on $\mathbb{S}^2$. Later, we extended the development of the SLSHT in Chapter 6, where an azimuthally asymmetric window function is used for spatial localization and the spatio-spectral representation is referred to as the directional SLSHT distribution. The use of an asymmetric window function enables the SLSHT to also reveal localization of *directional* features in the spatio-spectral domain. Due to the fact the rotation is fully characterized by the consideration of all three Euler angles, the asymmetric window provides SO(3) spatial localization and therefore the directional SLSHT distribution is parameterized on SO(3) instead of $\mathbb{S}^2$. Since the data-sets on the sphere may be of large size, and the SLSHT distribution of a signal must be computed for each spatial position and for each spectral component, we have developed fast algorithms for efficient computation of the SLSHT distribution.

The spatially localized spherical harmonic transform (SLSHT) distribution, representing the spatially-varying spectrum of a signal on the unit sphere, presents a mechanism to transform, modify and filter the signal in the joint spatio-spectral domain to realize spatially varying spectral filtering. As in the time-frequency analogy, such a transformation in the spatio-spectral domain can lead to a modified distribution that is not the SLSHT distribution of a physically valid spatial signal. Therefore, we formulated and solved an optimization problem to find the closest physically valid signal to the modified SLHT distribution. We illustrated two types of transformation to the SLSHT distribution, multiplicative modification and convolutive modification, both being instances of a general linear integral operator. It has been shown that the proposed framework enables the processing of signals in the joint spatio-spectral domain in a way that cannot be accomplished separately

in either spatial or spectral domain.

## 7.2 Future Research Directions

A number of interesting future research directions arise from the work presented in this thesis.

- The capability of the SLSHT distribution to reveal localized contribution of spectral contents depends on the window function being used for spatial localization. Considering that there exists a localization trade-off for a window function in the spatial and spectral domains, the choice of window function affects the resulting SLSHT distribution. Use of the same window function to achieve localization for all spatial positions may not be adequate to find what spectral components exist at different spatial positions. Lower spatial resolution window should be used in the region of lower degree spectral components. Higher spatial resolution window must be employed in the region that contains localized higher degree spectral components in order to distinguish spatially varying spectral components at different spatial positions. Therefore, there is a need to investigate the use of different resolution window functions at different spatial positions to achieve localization, such that the resolution of the window function adapts to the characteristics of the signal being analyzed. An analogous problem is well known in time-frequency analysis [99–101], where it has been shown that, according to several different measures of performance, the optimal window function for STFT depends on the signal being analyzed.

- In this thesis, we have studied the SLSHT distribution as spatio-spectral representation of signals on the sphere. The SLSHT has been formulated in analogy with the STFT in time-frequency analysis. There exist more sophisticated, different types of time-frequency distributions in the literature with different properties [65]. Potentially, these existing techniques need to extended and tailored for signals on the sphere. For example, the ambiguity function for signals on the sphere formulated in [102] can be used to develop a general class of spatio-spectral distributions for signals on the sphere similar to the Cohen class of time-frequency distributions [64, 65].

- In Chapter 5, we presented a framework for transformation of signals in the spatio-spectral domain. There are natural generalizations of the proposed framework. The technique we developed to recover a spectral response of a valid signal on the unit sphere from a modified SLSHT distribution is not limited to linear transformations in the spatio-spectral domain. Since there exist efficient computational techniques to *exactly* evaluate the spherical harmonic transform of the the band-limited signals [31, 41], we have considered the signal in the spectral domain in the proposed mathematical developments and formulations. We consider the development of efficient computational techniques to do signal processing in spatio-spectral domain an open problem for further work.

- The problem of optimal filtering on the sphere has been investigated in [25, 103] and applied in [104] for the detection of bubble collision signatures in WMAP 7-year observations [82]. Following the explorations and research on the filtering of Euclidean signals in the time-frequency domain using STFT [105], the proposed SLSHT distribution can be used to formulate the optimal filtering in the joint spatio-spectral domain for signals on the sphere.

# Appendix A

## A.1 Proof of Theorem 5.1 (Least Squares Solution)

We take the derivative of the total error $E$ in (5.8) with respect to the $u$-th element of $\boldsymbol{d}$, $\big(d\big)_u$, and set it to zero

$$\frac{\partial E}{\partial \big(d\big)_u} = \int_{\mathbb{S}^2} \sum_{n=0}^{N_g} \frac{\partial \big|e(\hat{\boldsymbol{x}}; n)\big|^2}{\partial \big(d\big)_u} \, ds(\hat{\boldsymbol{x}}) = 0.$$

Now using $e(\hat{\boldsymbol{x}}; n) \triangleq v(\hat{\boldsymbol{x}}; n) - \Psi_{n,:}(\hat{\boldsymbol{x}})\boldsymbol{d} = v(\hat{\boldsymbol{x}}; n) - \sum_{u=0}^{N_f} \Psi_{n,u}(\hat{\boldsymbol{x}})\big(d\big)_u$ and rearranging the terms results in

$$\int_{\mathbb{S}^2} \sum_{n=0}^{N_g} \sum_{u'=0}^{N_f} \overline{\Psi_{n,u}(\hat{\boldsymbol{x}})} \Psi_{n,u'}(\hat{\boldsymbol{x}}) \big(d\big)_{u'} \, ds(\hat{\boldsymbol{x}}) = \int_{\mathbb{S}^2} \sum_{n=0}^{N_g} \overline{\Psi_{n,u}(\hat{\boldsymbol{x}})} v(\hat{\boldsymbol{x}}; n) \, ds(\hat{\boldsymbol{x}}),$$

which can be written in matrix form as

$$\underbrace{\Big( \int_{\mathbb{S}^2} \boldsymbol{\Psi}^H(\hat{\boldsymbol{x}}) \, \boldsymbol{\Psi}(\hat{\boldsymbol{x}}) \, ds(\hat{\boldsymbol{x}}) \Big)}_{\boldsymbol{\mathcal{M}}} \boldsymbol{d} = \int_{\mathbb{S}^2} \boldsymbol{\Psi}^H(\hat{\boldsymbol{x}}) \boldsymbol{v}(\hat{\boldsymbol{x}}) \, ds(\hat{\boldsymbol{x}}), \tag{A.1}$$

from which (5.10) becomes clear. Now, let us examine the entries of $\boldsymbol{\mathcal{M}}$ in more detail

$$\mathcal{M}_{u,u'} = \sum_{n=0}^{N_g} \int_{\mathbb{S}^2} \overline{\psi_{n,u}(\hat{\boldsymbol{x}})} \, \psi_{n,u'}(\hat{\boldsymbol{x}}) \, ds(\hat{\boldsymbol{x}}). \tag{A.2}$$

Upon using the definition of the elements of $\mathbf{\Psi}$ in (4.12), we obtain

$$\mathcal{M}_{u,u'} = \sum_{n=0}^{N_g} \sum_{r=0}^{N_h} \sum_{r'=0}^{N_h} \overline{T(u;r;n)}\, T(u';r';n) \int_{\mathbb{S}^2} \overline{\big(h\big)_r(\hat{\boldsymbol{x}})} \big(h\big)_{r'}(\hat{\boldsymbol{x}})\, ds(\hat{\boldsymbol{x}}),$$

which can be simplified using (2.31) and employing the orthonormal property of spherical harmonics

$$\mathcal{M}_{u,u'} = \sum_{n=0}^{N_g} \sum_{p=0}^{L_h} \sum_{q=-p}^{p} \frac{4\pi}{2p+1} \big|\big(h\big)_p^0\big|^2\, \overline{T(u;r;n)}\, T(u';r;n),$$

where the mapping $(p,q) \leftrightarrow r$ has been used. Now using $\overline{T(u;r;n)} = T(u;r;n)$, the additional mapping $(s',t') \leftrightarrow u'$ and (2.24) we arrive at

$$\mathcal{M}_{u,u'} = \sum_{\ell=0}^{L_g} \sum_{p=0}^{L_h} (2\ell+1)\, \sqrt{(2s+1)(2s'+1)} \big|\big(h\big)_p^0\big|^2 \begin{pmatrix} s & p & \ell \\ 0 & 0 & 0 \end{pmatrix} \begin{pmatrix} s' & p & \ell \\ 0 & 0 & 0 \end{pmatrix} \sum_{m=-\ell}^{\ell} \sum_{q=-p}^{p} \begin{pmatrix} s & p & \ell \\ t & q & -m \end{pmatrix} \begin{pmatrix} s' & p & \ell \\ t' & q & -m \end{pmatrix}.$$

Now we invoke the following orthogonality relation of Wigner-3$j$ symbols [106],

$$(2s+1) \sum_{m=-\ell}^{\ell} \sum_{q=-p}^{p} \begin{pmatrix} s & p & \ell \\ t & q & -m \end{pmatrix} \begin{pmatrix} s' & p & \ell \\ t' & q & -m \end{pmatrix} = \delta_{s,s'}\, \delta_{t,t'}, \tag{A.3}$$

to conclude that $\mathcal{M}_{u,u'}$ is only non-zero when $s = s'$ and $t = t'$ or when $u = u'$, that is,

$$\mathcal{M}_{u,u} = \sum_{\ell=0}^{L_g} \sum_{p=0}^{L_h} (2\ell+1) \big|\big(h\big)_p^0\big|^2 \begin{pmatrix} s & p & \ell \\ 0 & 0 & 0 \end{pmatrix}^2 = \sum_{p=0}^{L_h} \big|\big(h\big)_p^0\big|^2, \tag{A.4}$$

where the following identity of Wigner-3$j$ symbols is employed in obtaining the second equality [106]

$$\sum_{\ell=0}^{L_g} (2\ell+1) \begin{pmatrix} s & p & \ell \\ 0 & 0 & 0 \end{pmatrix}^2 = 1, \quad 0 \le p \le L_h,\ 0 \le s \le L_f. \tag{A.5}$$

We note here that the entries of the matrix $\boldsymbol{\mathcal{M}}$ given by (A.4) also appeared in [1, 58] as the sum of the rows of the coupling matrix (see [58] for details). With the entries of the matrix $\boldsymbol{\mathcal{M}}$ in (A.4), $\boldsymbol{\mathcal{M}}$ becomes identity matrix scaled by the

energy of the window function defined in (5.11) and Theorem 5.1 is proved.

■

## A.2 Proof of Lemmas 5.1-5.3

**Proof of Lemma 5.1**

From the definition of MMD in (5.16) and using the inversion relation presented in Theorem 4.1, we conclude that the $n$-th component of $\boldsymbol{d}$ can be obtained as

$$\big(d\big)_n = \frac{1}{\sqrt{4\pi}\big(h\big)_0^0} \int_{\mathbb{S}^2} g(\hat{\boldsymbol{x}}; n)\, z(\hat{\boldsymbol{x}}; n)\, ds(\hat{\boldsymbol{x}}).$$

Using the spherical harmonic expansion $z(\hat{\boldsymbol{x}}; n) = \sum_{c=0}^{N_{z_n}} \big(z_n\big)_c Y_c(\hat{\boldsymbol{x}})$, the SLSHT distribution formulation in (4.7) and the orthogonality relation of spherical harmonics, we obtain

$$\big(d\big)_n = \frac{1}{\sqrt{4\pi}\big(h\big)_0^0} \sum_{u=0}^{N_f} \big(f\big)_u \sum_{r=0}^{\min(N_h, N_{z_n})} \sqrt{\frac{4\pi}{2p+1}}\, \big(h\big)_p^0 \big(z_n\big)_r\, T(u; r; n), \quad (p, q) \leftrightarrow r. \tag{A.6}$$

Now according to (3.7),

$$\big(w_n\big)_r \triangleq \sqrt{\frac{4\pi}{2p+1}}\, \big(h\big)_p^0 \big(z_n\big)_r, \quad (p, q) \leftrightarrow r \tag{A.7}$$

can be understood as the spherical harmonic coefficient of the convolution output between $z(\hat{\boldsymbol{x}}; n)$ and the azimuthally symmetric window function $h(\hat{\boldsymbol{x}})$. Hence, we can express $\big(d\big)_n$ in (A.6) as

$$\big(d\big)_n = \frac{1}{\sqrt{4\pi}\big(h\big)_0} \sum_{u=0}^{N_f} \big(f\big)_u \sum_{r=0}^{\min(N_h, N_{z_n})} \big(w_n\big)_r\, T(u; r; n). \tag{A.8}$$

Now using the expression for $T(u; r; n)$ on the right hand side of (2.23), $f(\hat{\boldsymbol{x}}) = \sum_{u=0}^{N_f} \big(f\big)_u Y_u(\hat{\boldsymbol{x}})$, and $w_n(\hat{\boldsymbol{x}}) = \sum_{u=0}^{N_f} \big(w_n\big)_r Y_r(\hat{\boldsymbol{x}})$ we obtain the stated result in Lemma 5.1.

**Proof of Lemma 5.2**

Proof of Lemma 5.2 is easy. First, according to (5.17) and (4.10)

$$\boldsymbol{v}(\hat{\boldsymbol{x}}) = \boldsymbol{z}(\hat{\boldsymbol{x}}) \odot \boldsymbol{g}(\hat{\boldsymbol{x}}) = \boldsymbol{z}(\hat{\boldsymbol{x}}) \odot \big(\boldsymbol{\Psi}(\hat{\boldsymbol{x}})\boldsymbol{f}\big) = \big(\mathrm{diag}\big(\boldsymbol{z}(\hat{\boldsymbol{x}})\big)\boldsymbol{\Psi}(\hat{\boldsymbol{x}})\big)\boldsymbol{f}. \tag{A.9}$$

Therefore, according to Theorem 4.1 we can write the the spectral response of signal $d(\hat{\boldsymbol{x}})$, $\boldsymbol{d}$, corresponding to $\boldsymbol{v}(\hat{\boldsymbol{x}})$ as

$$\boldsymbol{d} = \frac{1}{K}\int_{\mathbb{S}^2} \boldsymbol{v}(\hat{\boldsymbol{x}})\, ds(\hat{\boldsymbol{x}}) = \Big(\frac{1}{K}\int_{\mathbb{S}^2} \big(\mathrm{diag}\big(\boldsymbol{z}(\hat{\boldsymbol{x}})\big)\boldsymbol{\Psi}(\hat{\boldsymbol{x}})\big)\, ds(\hat{\boldsymbol{x}})\Big)\boldsymbol{f}.$$

By comparison with (5.12) we conclude (5.20).

Equation (5.21) follows from using (4.6), (4.12), $z(\hat{\boldsymbol{x}};u) = \sum_{c=0}^{N_{z_u}} \big(z_u\big)_c Y_c(\hat{\boldsymbol{x}})$, and orthogonality relation of spherical harmonics. This was also implied in (A.7) and (A.8) in the proof of Lemma 5.1.

**Proof of Lemma 5.3**

We first use (5.15) in (5.13) and the the sifting property of Dirac delta function to arrive at (5.22). For obtaining the entries of $\boldsymbol{\Upsilon}$, we proceed as follows. From (4.6) and (4.12), we know that

$$\psi^H_{u,n}(\hat{\boldsymbol{x}}) = \overline{\psi_{n,u}(\hat{\boldsymbol{x}})} = \sum_{r=0}^{N_h} \sqrt{\frac{4\pi}{2p+1}}\, Y_r(\hat{\boldsymbol{x}})\,\overline{(h)^0_p}\,\overline{T(u;r;n)}, \quad (p,q)\leftrightarrow r, \tag{A.10}$$

$$\psi_{n,u'}(\hat{\boldsymbol{x}}) = \sum_{r'=0}^{N_h} \sqrt{\frac{4\pi}{2p'+1}}\,\overline{Y_{r'}(\hat{\boldsymbol{x}})}\,(h)^0_{p'} T(u';r';n), \quad (p',q')\leftrightarrow r'. \tag{A.11}$$

Upon using the above, $z(\hat{\boldsymbol{x}};n) = \sum_{c=0}^{N_{z_n}} \big(z_n\big)_c Y_c(\hat{\boldsymbol{x}})$ in (5.22), we obtain

$$\begin{aligned}\Upsilon_{u,u'} = \frac{1}{\mathcal{E}} \sum_{n=0}^{N_g}\sum_{r=0}^{N_h}\sum_{r'=0}^{N_h}\sum_{c=0}^{N_{z_n}} &\frac{4\pi}{\sqrt{(2p+1)(2p'+1)}}\overline{(h)^0_p}(h)^0_{p'}\big(z_n\big)_c \\ &\times \overline{T(u;r;n)}\, T(u';r';n)\int_{\mathbb{S}^2} Y_r(\hat{\boldsymbol{x}})Y_c(\hat{\boldsymbol{x}})\overline{Y_{r'}(\hat{\boldsymbol{x}})}\, ds(\hat{\boldsymbol{x}}).\end{aligned} \tag{A.12}$$

Finally, recalling $\overline{T(u;r;n)} = T(u;r;n)$ and the definition (2.23) for the integral in (A.12), we obtain

$$\begin{aligned}\Upsilon_{u,u'} = \frac{1}{\mathcal{E}} \sum_{n=0}^{N_g}\sum_{r=0}^{N_h}\sum_{r'=0}^{N_h}\sum_{c=0}^{N_{z_n}} &\frac{4\pi}{\sqrt{(2p+1)(2p'+1)}}\overline{(h)^0_p}(h)^0_{p'}\big(z_n\big)_c \\ &\times T(u;r;n)\, T(u';r';n)\, T(r;c;r'),\end{aligned} \tag{A.13}$$

which is identical to (5.23).

# Bibliography


[1] M. A. Wieczorek and F. J. Simons, "Localized spectral analysis on the sphere," *Geophys. J. Int.*, vol. 162, no. 3, pp. 655–675, May 2005.

[2] M. K. Chung, K. J. Worsley, B. M. Nacewicz, K. M. Dalton, and R. J. Davidson, "General multivariate linear modeling of surface shapes using surfstat," *NeuroImage*, vol. 53, no. 2, pp. 491–505, 2010.

[3] P. Yu, P. E. Grant, Q. Yuan, H. Xiao, F. Segonne, R. Pienaar, E. Busa, J. Pacheco, N. Makris, R. L. Buckner, P. Golland, and B. Fischl, "Cortical surface shape analysis based on spherical wavelets," *IEEE Trans. Med. Imag.*, vol. 26, no. 4, pp. 582–597, Apr. 2007.

[4] M. Simons, S. C. Solomon, and B. H. Hager, "Localization of gravity and topography: constraints on the tectonics and mantle dynamics of Venus," *Geophys. J. Int.*, vol. 131, no. 1, pp. 24–44, Oct. 1997.

[5] P. Audet, "Directional wavelet analysis on the sphere: Application to gravity and topography of the terrestrial planets," *J. Geophys. Res.*, vol. 116, Feb. 2011.

[6] R. Ng, R. Ramamoorthi, and P. Hanrahan, "Triple product wavelet integrals for all-frequency relighting," *ACM Trans. Graph.*, vol. 23, no. 3, pp. 477–487, Aug. 2004.

[7] P. Schröder and W. Sweldens, "Spherical wavelets: Efficiently representing functions on a sphere," in *Wavelets in the Geosciences*, Roland Klees and Roger Haagmans, Eds., vol. 90 of *Lecture Notes in Earth Sciences*, pp. 158–188. Springer, Berlin Heidelberg, 2000, (Reprinted from Computer Graphics Proceedings, 1995, 161-172, ACM Siggraph.).

[8] C. H. Brechbühler, G. Gerig, and O. Kübler, "Parametrization of closed surfaces for 3-D shape description," *Computer Vision and Image Understanding*, vol. 61, no. 2, pp. 154–170, Mar. 1995.

[9] C. Han, B. Sun, R. Ramamoorthi, and E. Grinspun, "Frequency domain normal map filtering," *ACM Trans. on Graphics*, vol. 26, no. 3, pp. 28:1–28:12, July 2007.

[10] D. Colton and R. Kress, *Inverse Acoustic and Electromagnetic Scattering Theory*, Springer-Verlag, Berlin, second edition, 1998.

[11] Charmaine Armitage and Benjamin D. Wandelt, "Deconvolution mapmaking for cosmic microwave background observations," *Phys. Rev. D*, vol. 70, no. 12, pp. 123007:1–123007:7, Dec. 2004.

[12] K.-W. Ng, "Full-sky correlation functions for CMB experiments with asymmetric window functions," *Phys. Rev. D*, vol. 71, no. 8, pp. 083009:1–083009:9, Apr. 2005.

[13] J. D. McEwen, P. Vielva, Y. Wiaux, R. B. Barreiro, L. Cayón, M. P. Hobson, A. N. Lasenby, E. Martínez-González, and J. L. Sanz, "Cosmological applications of a wavelet analysis on the sphere," *J. Fourier Anal. and Appl.*, vol. 13, no. 4, pp. 495–510, Aug. 2007.

[14] J. D. McEwen, M. P. Hobson, A. N. Lasenby, and D. J. Mortlock, "A high-significance detection of non-Gaussianity in the Wilkinson Microwave Anisotropy Probe 1-yr data using directional spherical wavelets," *Mon. Not. R. Astron. Soc.*, vol. 359, no. 4, pp. 1583–1596, 2005.

[15] J.-L. Starck, Y. Moudden, P. Abrial, and M. Nguyen, "Wavelets, ridgelets and curvelets on the sphere," *Astron. & Astrophys.*, vol. 446, no. 3, pp. 1191–1204, Feb. 2006.

[16] Y. Wiaux, L. Jacques, and P. Vandergheynst, "Correspondence principle between spherical and Euclidean wavelets," *Astrophys. J.*, vol. 632, no. 1, pp. 15–28, Oct. 2005.

[17] D. N. Spergel, R. Bean, O. Doré, M. R. Nolta, C. L. Bennett, J. Dunkley, G. Hinshaw, N. Jarosik, E. Komatsu, L. Page, H. V. Peiris, L. Verde,

M. Halpern, R. S. Hill, A. Kogut, M. Limon, S. S. Meyer, N. Odegard, G. S. Tucker, J. L. Weiland, E. Wollack, and E. L. Wright, "Three-year Wilkinson Microwave Anisotropy Probe (WMAP) observations: Implications for cosmology," *The Astrophysical Journal Supplement Series*, vol. 170, no. 2, pp. 377–408, 2007.

[18] D. B. Ward, R. A. Kennedy, and R. C. Williamson, "Theory and design of broadband sensor arrays with frequency invariant far-field beam patterns," *J. Acoust. Soc. Am.*, vol. 97, no. 2, pp. 1023–1034, Feb. 1995.

[19] T. S. Pollock, T. D. Abhayapala, and R. A. Kennedy, "Introducing space into MIMO capacity calculations," *J. Telecommun. Syst.*, vol. 24, no. 2, pp. 415–436, Oct. 2003.

[20] M. A. Wieczorek and F. J. Simons, "Minimum variance multitaper spectral estimation on the sphere," *J. Fourier Anal. Appl.*, vol. 13, no. 6, pp. 665–692, 2007.

[21] J.-P. Antoine and P. Vandergheynst, "Wavelets on the 2-sphere: A group-theoretical approach," *Appl. Comput. Harmon. Anal.*, vol. 7, no. 3, pp. 262–291, 1999.

[22] D. Marinucci, D. Pietrobon, A. Balbi, P. Baldi, P. Cabella, G. Kerkyacharian, P. Natoli, D. Picard, and N. Vittorio, "Spherical needlets for cosmic microwave background data analysis," *Mon. Not. R. Astron. Soc.*, vol. 383, no. 2, pp. 539–545, 2008.

[23] J. D. McEwen, M. P. Hobson, and A. N. Lasenby, "A directional continuous wavelet transform on the sphere," *Arxiv preprint astro-ph/0609159*, 2006.

[24] J. D. McEwen, M. P. Hobson, D. J. Mortlock, and A. N. Lasenby, "Fast directional continuous spherical wavelet transform algorithms," *IEEE Trans. Signal Process.*, vol. 55, no. 2, pp. 520–529, Feb. 2007.

[25] J. D. McEwen, M. P. Hobson, and A. N. Lasenby, "Optimal filters on the sphere," *IEEE Trans. Signal Process.*, vol. 56, no. 8, pp. 3813–3823, Aug. 2008.

[26] R. Kakarala and P. Ogunbona, "A phase-sensitive approach to filtering on the sphere," *IEEE Trans. Signal Process.*, vol. 60, no. 12, pp. 6330–6339, Dec. 2012.

[27] F. J. Simons, F. A. Dahlen, and M. A. Wieczorek, "Spatiospectral concentration on a sphere," *SIAM Rev.*, vol. 48, no. 3, pp. 504–536, 2006.

[28] Y. Wiaux, L. Jacques, P. Vielva, and P. Vandergheynst, "Fast directional correlation on the sphere with steerable filters," *Astrophys. J.*, vol. 652, no. 1, pp. 820–832, Nov. 2006.

[29] Y. Wiaux, J. D. McEwen, P. Vandergheynst, and O. Blanc, "Exact reconstruction with directional wavelets on the sphere," *Mon. Not. R. Astron. Soc.*, vol. 388, no. 2, pp. 770–788, 2008.

[30] B. T. T. Yeo, W. Ou, and P. Golland, "On the construction of invertible filter banks on the 2-sphere," *IEEE Trans. Image Process.*, vol. 17, no. 3, pp. 283–300, Mar. 2008.

[31] J. R. Driscoll and D. M. Healy, Jr., "Computing Fourier transforms and convolutions on the 2-sphere," *Adv. Appl. Math.*, vol. 15, no. 2, pp. 202–250, June 1994.

[32] R. A. Kennedy, T. A. Lamahewa, and L. Wei, "On azimuthally symmetric 2-sphere convolution," *Digital Signal Processing*, vol. 5, no. 11, pp. 660–666, Sept. 2011.

[33] P. Sadeghi, R. A. Kennedy, and Z. Khalid, "Commutative anisotropic convolution on the 2-sphere," *IEEE Trans. Signal Process.*, vol. 60, no. 12, pp. 6697–6703, Dec. 2012.

[34] Z. Khalid, S. Durrani, R. A. Kennedy, and P. Sadeghi, "On the construction of low-pass filters on the unit sphere," in *Proc. IEEE Int. Conf. Acoust., Speech, Signal Process., ICASSP'2011*, Prague, Czech Republic, May 2011, pp. 4356–4359.

[35] D. Slepian and H. O. Pollak, "Prolate spheroidal wave functions, Fourier analysis and uncertainity-I," *Bell Syst. Techn. J.*, vol. 40, pp. 43–63, Jan. 1961.

[36] H. J. Landau and H. O. Pollak, "Prolate spheroidal wave functions, Fourier analysis and uncertainity-II," *Bell System Tech J.*, vol. 40, pp. 65–84, Jan. 1961.

[37] H. J. Landau and H. O. Pollak, "Prolate spheroidal wave functions, Fourier analysis and uncertainity-III: The dimension of the space of essentially time- and band-limited signals," *Bell System Tech J.*, vol. 41, pp. 1295–1336, 1962.

[38] D. Slepian, "Fourier analysis and uncertainty-IV: extensions to many dimensions; generalized prolate spheroidal functions," *Bell Syst. Tech. J*, vol. 43, pp. 3009–3057, 1964.

[39] A. Albertella, F. Sansò, and N. Sneeuw, "Band-limited functions on a bounded spherical domain: the Slepian problem on the sphere," *J. Geodesy*, vol. 73, no. 9, pp. 436–447, June 1999.

[40] J. J. Sakurai, *Modern Quantum Mechanics*, Addison Wesley Publishing Company, Inc., Reading, MA, 2nd edition, 1994.

[41] J. D. McEwen and Y. Wiaux, "A novel sampling theorem on the sphere," *IEEE Trans. Signal Process.*, vol. 59, no. 12, pp. 5876–5887, Dec. 2011.

[42] G. Warner, *Harmonic Analysis on Semi-Simple Lie Groups II*, NY: Springer, 2nd edition, 1972.

[43] R. Camporesi, "Harmonic analysis and propagators on homogeneous spaces," *Physics Reports*, vol. 196, pp. 1–134, Nov. 1990.

[44] J.-P. Antoine and P. Vandergheynst, "Wavelets on the $n$-sphere and related manifolds," *J. Math. Phys.*, vol. 39, pp. 3987, 1998.

[45] B. D. Wandelt and K. M. Górski, "Fast convolution on the sphere," *Phys. Rev. D*, vol. 63, no. 12, pp. 123002, May 2001.

[46] M. Tegmark, D. H. Hartmann, M. S. Briggs, and C. A. Meegan, "The angular power spectrum of BATSE 3B gamma-ray burst," *Astrophysical J.*, vol. 468, pp. 214–224, Sep. 1996.

[47] K.-I. Seon, "Smoothing of all-sky survey map with Fisher-Von Mises function," *J. Korean Phys. Soc.*, vol. 48, no. 3, pp. 331–334, Mar. 2006.

[48] I. Dokmanić and D. Petrinović, "Convolution on the $n$-sphere with application to PDF modeling," *IEEE Trans. Signal Process.*, vol. 58, no. 3, pp. 1157–1170, Mar. 2010.

[49] J.-P. Antoine, L. Demanet, L. Jacques, and P. Vandergheynst, "Wavelets on the sphere: implementation and approximations," *Appl. Comp. Harm. Anal.*, vol. 13, no. 3, pp. 177–200, 2002.

[50] L. Demanet and P. Vandergheynst, "Directional wavelets on the sphere," Tech. Rep., Technical Report R-2001-2, Signal Processing Laboratory, Lausanne, 2001.

[51] I. Bogdanova, P. Vandergheynst, J.-P. Antoine, L. Jacques, and M. Morvidone, "Stereographic wavelet frames on the sphere," *Appl. Comp. Harm. Anal.*, vol. 19, no. 2, pp. 223–252, 2005.

[52] R. B. Barreiro, M. P. Hobson, A. N. Lasenby, A. J. Banday, K. M. Górski, and G. Hinshaw, "Testing the Gaussianity of the COBE DMR data with spherical wavelets," *Mon. Not. R. Astron. Soc.*, vol. 318, pp. 475–481, Oct. 2000.

[53] D. Pietrobon, A. Amblard, A. Balbi, P. Cabella, A. Cooray, and D. Marinucci, "Needlet detection of features in the WMAP CMB sky and the impact on anisotropies and hemispherical asymmetries," *Phys. Rev. D*, vol. 78, no. 10, pp. 103504, Nov. 2008.

[54] J. Schmitt, J.-L. Starck, J. M. Casandjian, J. Fadili, and I. Grenier, "Poisson denoising on the sphere: application to the Fermi gamma ray space telescope," *Astron. & Astrophys.*, vol. 517, pp. A26, July 2010.

[55] P. Vielva, E. Martínez-González, R. B. Barreiro, J. L. Sanz, and L. Cayón, "Detection of non-Gaussianity in the WMAP 1-year data using spherical wavelets," *Astrophys. J.*, vol. 609, pp. 22–34, 2004.

[56] F. J. Simons, I. Loris, G. Nolet, I. C. Daubechies, S. Voronin, P. A. Vetter, J. Charlty, and C. Vonesch, "Solving or resolving global tomographic models with spherical wavelets, and the scale and sparsity of seismic heterogeneity," *Geophys. J. Int.*, vol. 187, pp. 969–988, 2011.

[57] F. J. Simons, I. Loris, E. Brevdo, and I. C. Daubechies, "Wavelets and wavelet-like transforms on the sphere and their application to geophysical data inversion," in *Wavelets and Sparsity XIV*. 2011, vol. 81380, p. 81380X, SPIE.

[58] F. A. Dahlen and F. J. Simons, "Spectral estimation on a sphere in geophysics and cosmology," *Geophys. J. Int.*, vol. 174, pp. 774–807, 2008.

[59] J. Flanagan, *Speech Analysis Synthesis and Perception*, NY: Springer, 2nd edition, 1972.

[60] J. B. Allen and L. R. Rabiner, "A unified approach to short-time Fourier analysis and synthesis," *Proceedings of the IEEE*, vol. 65, no. 11, pp. 1558–1564, Nov. 1977.

[61] J. B. Allen, "Applications of the short time Fourier transform to speech processing and spectral analysis," in *Proc. of IEEE International Conference on Acoustics, Speech, and Signal Processing, ICASSP '82*, May 1982, vol. 7, pp. 1012–1015.

[62] D. L. Jones and R. G. Baraniuk, "A simple scheme for adapting time-frequency representations," *IEEE Trans. Signal Process.*, vol. 42, no. 12, pp. 3530–3535, Dec. 1994.

[63] D. L. Jones and T. W. Parks, "A high resolution data-adaptive time-frequency representation," *IEEE Trans. Acoust., Speech, Signal Process.*, vol. 38, no. 12, pp. 2127–2135, Dec. 1990.

[64] L. Cohen, *Time-frequency analysis: Theory and applications*, Prentice-Hall, Inc., 1995.

[65] L. Cohen, "Time-frequency distributions−a review," *Proc. IEEE*, vol. 77, no. 7, pp. 941–981, July 1989.

[66] R. L. Allen and D. W. Mills, *Signal Analysis: Time, Frequency, Scale and Structure*, IEEE Press, Piscataway, NJ, 2004.

[67] B. Boashash, *Time frequency signal analysis and processing: a comprehensive reference*, Elsevier, UK, 2003.

[68] J. Zhong and Y. Huang, "Time-frequency representation based on an adaptive short-time Fourier transform," *IEEE Trans. Signal Process.*, vol. 58, no. 10, pp. 5118–5128, Oct. 2010.

[69] L. Durak and O. Arikan, "Short-time Fourier transform: two fundamental properties and an optimal implementation," *IEEE Trans. Signal Process.*, vol. 51, no. 5, pp. 1231–1242, May 2003.

[70] R. Tao, Y. Li, and Y. Wang, "Short-time fractional Fourier transform and its applications," *IEEE Trans. Signal Process.*, vol. 58, no. 5, pp. 2568–2580, May 2010.

[71] K. Skrapas, G. Boultadakis, A. Karakasiliotis, and P. Frangos, "Time - frequency analysis of radar signals for ISAR applications," in *Proceedings of 2nd International Conference on Recent Advances in Space Technologies, 2005.*, June 2005, pp. 699–703.

[72] M. L. Kramer and D. L. Jones, "Improved time-frequency filtering using an STFT analysis-modification-synthesis method," in *Proc. IEEE-SP Int. Symp. Time-Freq., Time-Scale Anal., 1994.*, Oct. 1994, pp. 264–267.

[73] L. Cohen, "Time frequency filtering," in *Proc. IEEE Int. Conf. Acoust., Speech, Signal Process., ICASSP'1988*, Apr. 1988, pp. 2212–2215.

[74] B. E. A. Saleh and N. S. Subotik, "Time-variant filtering of signals in the mixed time-frequency domain," *IEEE Trans. Acoust., Speech, Signal Process.*, vol. 33, no. 6, pp. 1479–1485, Dec. 1985.

[75] T. A. C. M. Classen and W. F. G. Mecklenbrauker, "The Wigner distribution-a tool for time-frequency signal analysis; Part I," *Philips J. Res*, vol. 35, pp. 217–250, 1980.

[76] G. F. Boudreaux-Bartels and F. Hlawatsch, "References for the short-time Fourier transform, Gabor expansion, wavelet transform, Wigner distribution, ambiguity function, and other time-frequency and time-scale signal representations," Tech. Rep., Technical Report 0492-0001, University of Rhode Island, Electrical Eng. Dept., Kingston, RI, 1992.

[77] T. Bülow, "Spherical diffusion for 3D surface smoothing," *IEEE Trans. Pattern Anal. Mach. Intell.*, vol. 26, no. 12, pp. 1650–1654, Dec. 2004.

[78] F. J. Narcowich and J. D. Ward, "Nonstationary wavelets on the $m$-sphere for scattered data," *Appl. Comput. Harmon. Anal.*, vol. 3, no. 4, pp. 324–336, Oct. 1996.

[79] G. Boudreaux-Bartels and T. Parks, "Time-varying filtering and signal estimation using Wigner distribution synthesis techniques," *IEEE Trans. Acoust., Speech, Signal Process.*, vol. 34, no. 3, pp. 442–451, June 1986.

[80] F. Hlawatsch, W. Kozek, and W. Krattenthaler, "Time-frequency subspaces and their application to time-varying filtering," in *Proc. IEEE Int. Conf. Acoust., Speech, Signal Process., ICASSP'1990*, Apr. 1990, vol. 3, pp. 1607–1610.

[81] W. Kozek and F. Hlawatsch, "A comparative study of linear and nonlinear time-frequency filters," in *Proc. IEEE-SP Int. Symp. Time-Freq., Time-Scale Anal., 1992.*, Oct. 1992, pp. 163–166.

[82] N. Jarosik, C. L. Bennett, J. Dunkley, B. Gold, M. R. Greason, M. Halpern, R. S. Hill, G. Hinshaw, A. Kogut, E. Komatsu, D. Larson, M. Limon, S. S. Meyer, M. R. Nolta, N. Odegard, L. Page, K. M. Smith, D.N. Spergel, G. S. Tucker, J. L. Weiland, E. Wollack, and E. L. Wright, "Seven-year Wilkinson Microwave Anisotropy Probe (WMAP) observations: Sky maps, systematic errors, and basic results," *Astrophys. J.*, vol. 192, no. 2, pp. 1–14, 2011.

[83] Planck collaboration, "ESA Planck blue book," Tech. Rep. ESA-SCI(2005)1, ESA, 2005.

[84] T. Risbo, "Fourier transform summation of Legendre series and D-functions," *J. Geodesy*, vol. 70, pp. 383–396, 1996.

[85] R. A. Kennedy and P. Sadeghi, *Hilbert Space Methods in Signal Processing*, Cambridge University Press, New York, NY, 2012.

[86] Z. Khalid, S. Durrani, R. A. Kennedy, and P. Sadeghi, "Revisiting Slepian concentration problem on the sphere for azimuthally non-symmetric regions," in *5th International Conference on Signal Processing and Communication Systems, ICSPCS'2011*, Honolulu, HI, Dec. 2011, p. 7.

[87] D. A. Varshalovich, A. N. Moskalev, and V. K. Khersonskii, *Quantum Theory of Angular Momentum*, World Scientific, 1988.

[88] S. Trapani and J. Navaza, "Calculation of spherical harmonics and Wigner $d$ functions by FFT. applications to fast rotational matching in molecular replacement and implementation into *amore*," *Acta Cryst. A*, vol. 62, no. 4, pp. 262–269, July 2006.

[89] R. N. Czerwinski and D. L. Jones, "Adaptive short-time Fourier analysis," *IEEE Signal Process. Lett.*, vol. 4, no. 2, pp. 42–45, Feb. 1997.

[90] W. Freeden and V. Michel, "Constructive approximation and numerical methods in geodetic research today – an attempt at a categorization based on an uncertainty principle," *J. Geodesy*, vol. 73, no. 9, pp. 452–465, 1999.

[91] F. J. Harris, "On the use of windows for harmonic analysis with the discrete Fourier transform," *Proc. IEEE*, vol. 66, no. 1, pp. 51–83, Jan. 1978.

[92] D. Donoho and P. Stark, "Uncertainty principles and signal recovery," *SIAM J. Appl. Math.*, vol. 49, pp. 906–931, June 1989.

[93] E. J. Candes, J. Romberg, and T. Tao, "Robust uncertainty principles: exact signal reconstruction from highly incomplete frequency information," *IEEE Transactions on Information Theory*, vol. 52, no. 2, pp. 489–509, Feb. 2006.

[94] V. K. Goyal, A. K. Fletcher, and S. Rangan, "Compressive sampling and lossy compression," *IEEE Signal Processing Magazine*, vol. 25, no. 2, pp. 48–56, March 2008.

[95] R. A. Kennedy, W. Zhang, and T. D. Abhayapala, "Spherical harmonic analysis and model-limited extrapolation on the sphere: Integral equation formulation," in *Proc. 2nd International Conference on Signal Processing and Communication Systems*, Dec. 2008, pp. 1–6.

[96] M. Schechter, *Principles of functional analysis*, American Mathematical Society, 2nd edition, 2002.

[97] W. Krattenthaler and F. Hlawatsch, "Time-frequency design and processing of signals via smoothed Wigner distributions," *IEEE Trans. Signal Process.*, vol. 41, no. 1, pp. 278–287, Jan. 1993.

[98] D. W. Jepsen, E. F. Haugh, and J. O. Hirschfelder, "The integral of the associated Legendre function," in *Proc. Natl. Acad. Sci. USA.*, Sept. 1955, vol. 41, pp. 645–647.

[99] G. Jones and B. Boashash, "Window matching in the time-frequency plane and the adaptive spectrogram," in *Proceedings of the IEEE-SP International Symposium Time-Frequency and Time-Scale Analysis, 1992*, Oct. 1992, pp. 87–90.

[100] R. G. Baraniuk and D. L. Jones, "A signal-dependent time-frequency representation: optimal kernel design," *IEEE Trans. Signal Process.*, vol. 41, no. 4, pp. 1589–1602, Apr. 1993.

[101] G. Jones and B. Boashash, "Generalized instantaneous parameters and window matching in the time-frequency plane," *IEEE Trans. Signal Process.*, vol. 45, no. 5, pp. 1264–1275, May 1997.

[102] Z. Khalid, S. Durrani, P. Sadeghi, and R. A. Kennedy, "Ambiguity function and Wigner distribution on the sphere," in *Proc. IEEE Int. Conf. Acoust., Speech, Signal Process., ICASSP'2012*, Kyoto, Japan, Mar. 2011.

[103] R. Arora and H. Parthasarathy, "Optimal estimation and detection in homogeneous spaces," *IEEE Trans. Signal Process.*, vol. 58, no. 5, pp. 2623–2635, May 2010.

[104] J. D. McEwen, S. M. Feeney, M. C. Johnson, and H. V. Peiris, "Optimal filters for detecting cosmic bubble collisions," *Phys. Rev. D.*, vol. 85, no. 10, pp. 103502, 2012.

[105] F. Hlawatsch, G. Matz, H. Kirchauer, and W. Kozek, "Time-frequency formulation, design, and implementation of time-varying optimal filters for signal estimation," *IEEE Trans. Signal Process.*, vol. 48, no. 5, pp. 1417–1432, May 2000.

[106] L. C. Biedenharn and J. D. Louck, *Angular Momentum in Quantum Physics: Theory and Application*, Addison Wesley, Reading, MA, 1981.